Rockefeller University
Digital Commons @ RU

Student Theses and Dissertations

2019

Spontaneity and Precision in the Drosophila Central Nervous System

Bennett Ferris

Follow this and additional works at: https://digitalcommons.rockefeller.edu/student_theses_and_dissertations

 Part of the Life Sciences Commons

Recommended Citation

Ferris, Bennett, "Spontaneity and Precision in the Drosophila Central Nervous System" (2019). *Student Theses and Dissertations*. 504.
https://digitalcommons.rockefeller.edu/student_theses_and_dissertations/504

This Thesis is brought to you for free and open access by Digital Commons @ RU. It has been accepted for inclusion in Student Theses and Dissertations by an authorized administrator of Digital Commons @ RU. For more information, please contact nilovao@rockefeller.edu.

SPONTANEITY AND PRECISION IN THE *DROSOPHILA* CENTRAL NERVOUS SYSTEM

A Thesis Presented to the Faculty of

The Rockefeller University

in Partial Fulfillment of the Requirements for

the degree of Doctor of Philosophy

by

Bennett Ferris

June 2019

© Copyright by Bennett Ferris 2019

SPONTANEITY AND PRECISION IN THE *DROSOPHILA* CENTRAL NERVOUS SYSTEM

Bennett Ferris, Ph.D.

The Rockefeller University 2019

Many organisms that can locomote change their navigational strategies depending upon behavioral context. During foraging or exploration, for instance, many animals navigate by interspersing straight runs with turns whose direction and frequency may originate, at least at times, from largely stochastic processes. Conversely, during goal-directed navigation, animals may use stored heading and distance signals to travel efficiently to a desired location. This thesis explores the circuitry underlying these disparate navigational strategies in *Drosophila*.

I first show that normal synaptic transmission in a genetically specified population of neurons is necessary for one to observe an appreciable rate of spontaneous flight turns in *Drosophila*, but synaptic transmission in these same neurons is dispensable for the execution of two types of visually evoked turns. I then describe experiments on a population of neurons whose coordinated activity is thought to represent the fly's heading angle during walking. Specifically, I show that angular resolution of the heading estimate carried by this population of neurons is at most 5.625º, and may be even finer. Furthermore, it is known that the neurons that carry this

heading signal can update their heading estimate either in reference to a visual landmark or, when such a landmark is absent, in reference to the animal's rotational body movements. I end the thesis by demonstrating that, when a fly stands still, the visual and non-visual estimates of the fly's heading angle are not always aligned and can in fact deviate by many tens of degrees. The functional purpose of this discrepancy remains unclear, but this difference might provide insight into how a heading system can store an angular memory in complete darkness, without significant drift, for many minutes.

Acknowledgments

To my parents, for giving me access to the best possible education, and for teaching me that the classes were the least important part; for giving me confidence in myself, and also teaching me the importance of hard work; for instilling in me the values of a scientist (perhaps without meaning to): thank you.

Before I ever got to Rockefeller I had the immense privilege of learning science from a cavalcade of inspired teachers. To Lisa Baldwin, Abraham Rutchick, Christopher Seto, and Jason Sello: thank you for showing me how to think creatively and thank you for all of your thoughtful advice.

To Maimon lab members past and present: Without your questions, criticisms, encouragement, and discussion my thesis would have been very much the poorer. Thanks to Jonathan Hirokawa and Kristopher Fonselius for technical support, Arun Chakravorty for generating fly stocks, and Atsuko Adachi for her extensive help with immunohistochemistry and fly genetics. Thanks to Jonathan Green for sharing fly stocks and code and introducing me to the NP0212 project. Thanks to Cheng Lyu for generously sharing intellectual space in the E-PG resolution topic and for numerous helpful discussions. Thanks to Itzel Ishida and Vikram Vijayan for building and helping me navigate the closed loop configuration I used in chapter 3 of this thesis. I also owe a particular debt of gratitude to Vikram Vijayan, whose unceasing commentary from the desk across from mine has always lightened my mood – and has often helped my project. To the entire Maimon Lab, I wish you all the best in your quest to solve brain.

To my friends: thank you for your unquantifiable emotional support. To my friends in the Rockefeller community, in particular Stephen Serene: thank you for teaching me how to think like a biologist in your spare time.

To my Summer Neuroscience Program co-directors, Raffi Cohn, Laura Seeholzer, Aylesse Sordillo, Annie Handler, and Amy Dunn: thank you co-directing this wonderful education program with me, and for teaching me how to teach. To the students: thank you for your enthusiasm and curiosity. It always gave me a boost.

Thanks to the Anderson lab, the Clandinin Lab, the Ruta lab, and Nilay Yapici for fly stocks. Thanks to Anne von Philipsborn for both fly stocks and lending expertise on the neuroanatomy of the thoracic ganglion. I would like to thank Jonathan Victor for his perspective concerning the E-PG resolution question. I wish to thank my committee, Shai Shaham, Cori Bargmann, and Vanessa Ruta for their valuable suggestions and help.

To Gaby: I could thank you for helping me become a better writer, speaker, thinker, tinkerer, and tetherer of flies to small plastic plates, but mostly I want to thank you for the immense patience you showed while I slowly learned to do those things. This thesis has benefited immeasurably from your far-reaching creativity and your attention to the smallest detail. Thank you for being my advisor.

Table of Contents

List of Figures

Chapter 1 | Introduction

Animals behave in unpredictable ways. A wide range of organisms can initiate spontaneous behavior that displays profound variability, despite similar environmental input. Inbred, isogenic *Drosophila* exhibit fly-to-fly variability in turning behavior in a Y-shaped maze (Buchanon, Kain, and de Bivort 2015). Rats, in a competitive task in which they cannot guess their opponent's behavior, switch to a stochastic behavioral mode to decrease their own predictability (Tervo *et al.* 2014). Juvenile zebra finches early in song acquisition warble out noisy, random-seeming first drafts (Ölveczky, Andalman, and Fee 2005). Babbling babies produce extremely variable sounds, some of which are not found in the language spoken by their parents (Jakobson 1968). Across organisms, randomness pervades. While it is possible that each of these motor acts represents a feed-forward response to an environmental stimulus, it is also possible that they represent the outputs of neural circuits whose functional role is to generate spontaneous behavior.

Damage to an animal's nervous system can sometimes degrade spontaneous locomotor activity while sparing motor systems more generally. In one natural example, the jewel wasp *Ampulex compressa*, which hunts the cockroach *Periplaneta americana* as live food for their larvae, captures its quarry by injecting venom into precise locations in the cockroach's central nervous system (Williams 1942). The wasp's venom induces a hypokinetic state, blocking spontaneous walking without paralyzing the cockroach (Gal and Libersat 2008; Fouad, Rathmayer, and Libersat 1996). In humans,

neurological disease can degrade spontaneous behavior specifically. Activity in mammalian cortico-basal-ganglia loops has been implicated in internal initiation processes that are likely dispensable for more reflexive actions (Carli, Evenden, and Robbins 1985; Alexander, De Long, and Strick 1986). When components of these circuits are degraded in Parkinson's Disease, patients' ability to initiate actions is impaired (Janovic 2008), whereas reflexive actions are spared (Janovic 2008; Terao *et al.* 2013).

In the laboratory, it is possible to identify circuits whose neurophysiology is related to variable behavior, and to validate these regions' importance for those behaviors by inactivating them. Brain regions specialized for generating babbling in songbirds (Ölveczky, Andalman, and Fee 2005) and for exploratory behavior in zebrafish (Dunn *et al.* 2016) have been identified physiologically, and lesions or inactivation of these regions disrupt the generation of these variable behaviors. In nematodes, repeated presentations of the same odor stimulus to an immobilized worm inactivates a network of three interneurons that promote reversals, but the network is inactivated only probabilistically. Inhibiting synaptic transmission in one of these interneurons *increases* the reliability of the circuit, so that the three interneurons are dependably hyperpolarized by the odor stimulus. Perhaps these neurons' stochasticity in the intact circuit is not a bug, but is instead a feature of this chemosensory neural circuit (Gordus *et al.* 2015).

Foraging is a behavior in which unpredictability can reliably be found. In the absence of food-related cues, many organisms forage by interspersing a series of

straight runs of variable length with sharp reorientations at times drawn from power law or exponential distributions (Berg and Brown 1972; Bertrand *et al.* 2007; Sims *et al.* 2008; Roberts *et al.* 2016). A navigational strategy governed by stochasticity may appear to be borne out of total confusion. However, in a variety of organisms, the distribution of run lengths in these seemingly random foraging routes have been argued to approximate the optimally efficient distributions for discovering randomly distributed resources (Bertrand *et al.* 2007; Sims *et al.* 2008).

When scientists first tracked the trajectories of freely flying flies, they noted that their paths were composed of segments of straight flight interspersed with rapid rotations, which were dubbed *saccades* (Collett and Land 1975). The purpose of a straight-run-and-saccade locomotor strategy is still not settled, although one influential idea is that insects navigate with rapid turns so as to restrict the amount of time that their retinal image is blurred during locomotion (Collett and Land 1975).

The free flight trajectories of the fruit fly *Drosophila melanogaster* bear superficial similarities to those of the foraging animals described above; the lengths of straight runs between saccades may be, at least at times, drawn from a power law distribution (Reynolds and Frye 2007). Spontaneous saccades may help flies search efficiently for randomly distributed resources when no obvious sensory stimulus is available to guide them (Reynolds and Frye 2007).

Are these saccades *bona fide* spontaneous actions? Even a uniform cylindrical arena is not devoid of sensory stimuli; flying flies avoid crashing into the wall, and some of the seemingly random saccades flies make in free flight may ultimately be shown to

have some relationship to the time history of sensory experience (Censi *et al.* 2013; Mongeau and Frye 2017). However, visual stimuli may be controlled, and vestibular stimuli removed, by gluing flies in place such that they cannot rotate or translate but may still flap their wings, a preparation known as “tethered flight” (Heisenberg and Wolf 1979).

In the tethered flight paradigm, flies’ intention to turn was historically inferred from measuring the actual yaw torque produced by attempted steering movements (Heisenberg and Wolf 1979). Recently it has become more common to track the amplitude of the left and right wing-strokes with a photodiode or camera. The difference between the left and right wingbeat amplitude is correlated to the fly’s yaw torque (Tammero, Frye, and Dickinson 2004), and so this value is also used to infer the fly’s steering intention.

Flies’ fictive turning responses in the tethered flight situation often mirror what flies actually do when they are permitted to fly freely. In free flight, flies turn away from the center of an expanding dark spot, a visual simulation of an impending collision (Muijres *et al.* 2014). In tethered flight, flies also steer their wings away from these visual stimuli (Tammero and Dickinson 2002b). In free flight, flies fly toward tall, vertically oriented dark objects and steer clear of objects with smaller aspect ratios, which may represent potential predators (Maimon, Straw, and Dickinson 2008). In tethered flight, if one configures the setup such that flies may use their wing steering movements to control the angular position of a visual stimulus, they steer their wings such that they orient toward tall, dark stripes and orient away from squatter stimuli with

lower aspect ratios (Maimon, Straw, and Dickinson 2008). In both tethered and free flight, flies steer to the left when panoramic optic flow rotates to the left, and vice versa, a behavior known as the optomotor response (Götz 1968, Stowers *et al.* 2017).

In free flight, flies pepper their flight trajectories with spontaneous saccades (Reynolds and Frye 2007). An analogous behavior is observed in tethered flight. Flies flying before a stationary visual scene perform frequent, sharp wing-steering movements, which most likely represent saccadic attempts to turn left or right (Heisenberg and Wolf 1979). Like others (Heisenberg and Wolf 1979; Lindsay, Sustar, and Dickinson 2017), I will refer to these attempted turns in tethered flight as *saccades*.

It should be noted that the fly's sensory environment does contribute to the rate of spontaneous saccades in tethered flight. The initial paper describing spontaneous saccades in rigidly tethered *Drosophila* notes that the rate of spontaneous saccades decreases markedly when flies fly in total darkness (Heisenberg and Wolf, 1979). However, with a uniform bright screen – a simple condition with light, yet providing no obvious time-varying input – flies perform saccades to the left and right at a rate of ~0.5 Hz and these turns are not tied closely in time to any obvious external stimulus one can measure, which is the basis by which I and others operationally define them as spontaneous (Heisenberg and Wolf 1979; Maye *et al.* 2007; Kim, Fitzgerald, and Maimon 2015).

In addition to spontaneous saccades, tethered, flying flies perform a suite of visually guided flight behaviors. In chapter two of this thesis, I will two discuss two types of visually evoked flight turns that can be operationally separated from spontaneous

ones. One class, loom-evoked saccades, are rapid steering maneuvers away from the center of a rapidly expanding disc that simulates an object that is on a collision course with the fly (Tammero and Dickinson 2002b; Muijres *et al.* 2014). The kinematics of loom-evoked saccades are subtly different from those of spontaneous turns in free flight, but both involve a roll of the body followed by a counter-roll and a rotation about the yaw axis (Muijres *et al.* 2014; Muijres *et al.* 2015). Another class of visually evoked turns, optomotor responses, are syn-directional steering responses to rotational, wide-field, optic flow. Optomotor responses are thought to help flies keep a straight flight trajectory.

Spontaneous saccades, loom-evoked saccades, and optomotor responses represent three easily measurable and well-controlled steering maneuvers on the tether, which allowed me to ask a fundamental question regarding motor behavior. Namely, are spontaneous flight turns dissociable from these types of visually evoked flight turns, beyond the trivial fact that the latter require vision? In chapter two of this thesis, I will present evidence that the *Drosophila* nervous system contains a genetically specified population of neurons whose activity is necessary for the generation of spontaneous saccades in tethered flight, but which are dispensable for reflexive responses to visual stimuli.

Exploratory behavior is useful when an organism has no strong cues to follow. But scientists have also been fascinated by the biological mechanisms that allow cells and organisms to locomote to a specific location. Surprisingly, certain navigational tasks do not require any storage of any explicitly spatial information. Nematode worms (Ward

1973), leukocytes (Boyden Jr. 1962), and even bacteria (Berg and Brown 1972) navigate up concentration gradients toward a chemoattractant by performing a “biased random walk”. In such a navigational strategy, the animal or cell intersperses runs of linear travel with random reorientations at random times. However, the animal or cell can change the rate of these random turns such that the distance between turns increases as the organisms or cells travel up the chemoattractant’s concentration gradient and the distance between turns decreases as they travel down it. The resultant trajectories can be variable from individual to individual, but this strategy reliably biases trajectories toward regions of high concentration of chemoattractant (Block, Segall, and Berg 1982; Pierce-Shimomura, Morse, and Lockery 1999; Tranquillo, Laufenburger, and Zigmond 1988).

While a biased random walk strategy will eventually get a cell or organism to a local maximum in the concentration of a chemoattractant, the trajectory will likely be tortuous and inefficient. Moreover, this navigational strategy will not be of much use if sensory cues associated with the destination cannot be directly sensed. These problems can be circumvented if an organism could somehow estimate the direction it is facing relative to its destination and how far away from the destination it might be.

How do nervous systems build a sense of direction? In vertebrates, the first physiological evidence of neuronal representation of an animal’s heading came in form of extracellular recordings of Head Direction (HD) neurons in the rat Postsubiculum (PoS) (Ranck 1984; Taube, Muller, and Ranck 1990a; Taube, Muller, and Ranck 1990b). When cells in this region are recorded extracellularly while a rat explores a

circular arena, individual neurons' firing rates vary as a function of the direction the animal is facing, peaking at a certain azimuthal angle (the cell's "preferred direction"). This cellular correlate of heading angle is persistent; when the animal's head is pointed in an HD cell's preferred direction, the HD cell's firing rate exhibits little adaptation (Taube and Muller 1998). While no single HD cell unambiguously encodes the animal's facing direction, one can extract a good estimate of this variable by taking a circular mean of a group of HD cells' preferred directions weighted by their firing rates. In other words, HD cells' population activity represents the animal's head direction (Redish, Elga, and Touretzky 1996). HD cells have since been recorded in many other brain regions, including the anterodorsal nuclei of the thalamus (Taube 1995), and the lateral mammalary nuclei (Stackman & Taube 1998), as well as in other mammals such as bats and non-human primates (Finkelstein *et al.* 2015; Robertson *et al.* 1999).

Vestibular input is a key modulator of the mammalian head direction signal. HD cell firing rate can be updated by self-motion cues when the animal turns its head, but also when the animal is passively rotated (Taube, Muller, and Ranck 1990b). In addition to self-motion-related cues, HD cells are also tuned to the position of visual stimuli. In many cases, rotating the position of a visual landmark (such as a cue card on a side wall of the arena) causes HD neurons' preferred directions to rotate (Taube, Muller, and Ranck 1990b). Whereas positional stimuli anchor HD tuning to an external reference, these stimuli are not required for HD cells to update their heading estimate, which can occur even in complete darkness, by integrating the animal's own movements. HD cells

still maintain a preferred direction when the lights are turned off, although the preferred direction does drift over time (Mizumori and Williams 1993), as one might expect for any signal whose value is being updated only by the integration of small rate-of-change inputs. Whereas visual stimuli are dispensable for HD neurons to maintain a preferred direction, vestibular information is absolutely required. Lesioning the vestibular system abolishes HD tuning, even when lights are on and the animal has access to positional stimuli to which a preferred direction is normally yoked (Stackman and Taube 1997).

While a functioning vestibular system is necessary for mammalian HD cell tuning, it appears that this tuning is not maintained solely by integrating rotations measured by the vestibular system. In rats, HD cells sometimes shift their preferred direction when they are allowed to walk from one experimental chamber to another, but these shifts are larger when rats are carried between chambers (Stackman *et al.* 2003; Taube 2007). Optic flow is also capable of rotating HD cells' preferred firing direction (Arleo *et al.* 2013). These results are consistent with a model in which the mammalian head direction system takes multiple inputs into account – vestibular cues, positional visual information, optic-flow visual information, as well as proprioceptive signals and/or efference copies of motor commands – to update the heading angle estimate (Taube 2007).

An influential model for explaining the origin of head direction tuning and how this signal can be updated by self-motion cues was outlined by Skaggs *et al.* in 1995. In the model, HD neurons are arranged in a ring, such that neurons with similar preferred directions are near one another in the ring. Model HD neurons excite their neighbors

and inhibit neurons further away on the ring. If the strength of excitation and inhibition are properly tuned, this will ensure that only one “bump” of activity can ever exist on the ring of HD cells at any given time; any competitor bumps are quashed by the inhibition arising from the first bump. This bump can rotate around the ring when driven to do so by two populations of cells: left-shifting and right-shifting “rotation neurons”. These rotation neuron populations are tuned to both the animal’s head direction and vestibular cues: left-shifting rotation neurons are excited by vestibular information related to left turns, and right-shifting rotation neurons are excited by vestibular information related to right turns. Rotation neurons and HD neurons with the same preferred direction mutually excite one another, but the connections are slightly offset: left-shifting rotation neurons excite the HD neurons whose preferred direction is slightly to the left of their own, and the converse is true for right-shifting rotation neurons (Skaggs *et al.* 1995). Neurons with this dual tuning to both head direction and angular velocity have been recorded in the lateral mammalary nuclei (Stackman and Taube 1998), and lesioning the lateral mammalary nuclei disrupts HD cell tuning in the anterior dorsal nucleus of the thalamus (Blair and Sharp 1998; Bassett *et al*. 2007). When distant visual landmarks are available, these visual cues have strong effects on the responses of HD neurons. Specifically, in the model, HD neurons’ responses to the positions of visual landmarks are mediated by “visual neurons”, where each such neuron is activated by stimuli appearing in a local receptive field about the yaw axis; that is, when a visual cue is located at one specific angle with respect to the animal’s head (Skaggs *et al.* 1995). The

influence of the visual neurons is typically strong, and can override the integrating inputs to position the activity bump at specific angles along the ring.

How does the mammalian brain use its head-direction signal to guide behavior? Although no circuit connecting mammalian HD cells to behavioral output has yet been described, HD tuning has been shown to be correlated with spatial behavior in navigational tasks. In a task wherein rats entered an arm of a radial maze to retrieve a reward, shifting of HD cells' preferred directions was associated with error trials (Dudchenko and Taube 1997). Rats can be trained to forage for a food pellet on a featureless platform and, upon finding the food, to take the most direct route back to their starting point. During the foraging phase of this task, optogenetic inhibition of inputs to the dorsal tegmental nucleus, where vestibular inputs to HD neurons reside (Taube 2007), causes the rats to take inaccurate homing trajectories (Butler *et al.* 2017). But the effects of disrupting head direction tuning are perhaps more complex than any one silencing experiment can encapsulate. To explain further, I first need to briefly describe two other classes of cells whose spiking rates correlate with spatial variables in mammals.

In the hippocampus, neurons called "place cells" fire action potentials when an animal occupies a specific location in a given context (O'Keefe and Dostrovsky 1971). Like HD cell tuning curves, place cell firing fields rotate with the rotation of a visual cue, in concert with the concomitant rotation of HD neuron preferred directions (Bostock, Muller, and Kubie 1991; Yoganarasimha and Knierim 2005) and place fields are maintained when the lights are turned off (Quirk, Muller, and Kubie 1990). In the Medial

Entorhinal Cortex (MEC), the firing rates of neurons known as “grid cells” are strongly modulated by the distance an animal has walked along an axis. (Moser, Rowland, and Moser 2015). As a rat explores an arena, these cells fire in a regular spatial pattern such that the firing fields of individual grid cells often form a regular hexagonal lattice. Similar to place cells and head direction cells, the angular orientations of grid cells’ firing fields remain fixed relative to external visual cues, and the spatial properties of these firing fields are preserved as the animal walks in the dark (Hafting *et al.* 2005).

In comparison to the specific two-dimensional-positional signal carried by place cells or the distance-along-an-oriented-axis signal carried by grid cells, HD cells provide the mammalian brain a simpler signal; azimuthal head direction always falls on a single, wrapped dimension. Evidence suggests that information from HD cells feeds into place and grid cells. A shift in the preferred firing direction of a head direction cell relative to the external environment is accompanied by an equivalent rotation of place cell firing fields (Knierem *et al.* 1995). Disrupting the activity of the HD network decreases the specificity of place cell firing fields in certain conditions (Harland *et al.*, 2017), and also impairs the spatial autocorrelation of grid cell firing fields (Winter, Clark, and Taube 2015). In this sense, HD cells appear to be a foundational spatial-cognition cell type upon which other spatial signals rely.

Many place cells reside in the hippocampus and thus it has been theorized that the mammalian hippocampus is a “cognitive map” which imparts an innate ability to learn the Euclidean geometry of relevant locations and relate these locations to one another (O’Keefe and Nadel, 1978). This theory is buttressed by evidence showing that

lesioning the hippocampi disrupts an animal's ability to learn and recall explicitly spatial relationships in a variety of animals and paradigms (Kaada, Rasmussen, and Kveim 1961; Nadel 1968; Milner, Corkin, and Tueber 1968; Eichenbaum, Stewart, and Morris 1990). While the specific mechanisms by which HD cells control behavior are not completely clear, head direction tuning underlies the spatial tuning of cells that make up and project to the hippocampus, a structure that is necessary for many navigational behaviors.

What about animals without a hippocampus? Are they totally lost? Or do their brains contain some other map-like or vectorial representation of space? While their brains contain many fewer neurons than those of their mammalian counterparts, the navigational feats of insects are no less astounding. Specifically, many insects seem to keep track of their position relative to a salient location by adding up how far they have traveled in each direction from it, a process known as "path integration".

Desert ants of the genus *Cataglyphis* are particularly adept path integrators. These ants scavenge for food on hot, featureless salt flats on the outskirts of the desert. While their outbound paths are tortuous, the ants are capable of walking hundreds of meters directly back to their nest in a relatively straight line (Muller and Wehner 1988). The ants calculate their distance and direction from home by counting their steps relative to the position of the sun and the e-vector orientation of polarized light in the sky (Sommer and Wehner 2005; Wehner and Müller 2006; Wittlinger, Wehner, and Wolf 2006).

Honey bees display evidence of spatial memory as well. Worker bees that find a food source fly back and forth between this location and the hive (Von Frisch 1967). Upon re-entering the hive, successful foragers often perform a “waggle dance”. We know that these bees can store the angle of a food source relative to the position of the sun because the dance’s angle with respect to the vertical communicates the angle of the food source relative to the sun to the worker’s hive-mates (Von Frisch 1967), who thereupon fly in the direction indicated by the dance (Riley *et al.* 2005).

Monarch butterflies migrate up to 3600 km every fall from the United States to their overwintering grounds in central Mexico (Brower 1996). The butterflies retain a straight heading during flight by orientating with respect to a time-compensated sun compass (Mouritsen and Frost 2002) and with respect to the e-vector orientation of polarized light (Reppert, Zhu, and White 2004). Intriguingly, none of the animals that perform this migration have ever made the trip before (Brower 1996). This behavior demonstrates the butterfly’s ability to navigate with a stored heading relative to an environmental stimulus (the position of the sun, which changes over the course of the day), a heading angle which the animal is capable of storing for the duration of its 75 day journey (Brower 1996).

A recent study argues that even the humble fruit fly, *Drosophila melanogaster*, path integrates over shorter distances. When flies are permitted to walk freely around an arena 1.7 cm in diameter, after discovering a small drop of food, they leave and return to the location multiple times, and their trajectories hew closer to the location of the food drop per distance walked than is predicted by a direction-agnostic model of

random search. Flies can perform this spatially oriented search behavior in the dark, and they do not need functional pheromone-secreting cells or olfactory cues from the food to do so. Thus, these data argue that *Drosophila* can perform path integration by keeping an internal tally of their heading angles and distance travelled to know where they are relative to the food drop during this task (Kim and Dickinson 2017).

The navigational capabilities of insects suggests that their brains contain representations of angular heading. Indeed, electrophysiological recordings in many insects have uncovered neurons with HD-like tuning to navigationally relevant visual stimuli. In the locust, neurons have been identified that are tuned to the e-vector angle of polarized light (Heinze and Homberg 2007), and in the Monarch butterfly, neurons have been identified which are tuned to the e-vector angles of polarized light and/or the azimuthal position of a bright, unpolarized light spot (Heinze and Reppert 2011). Other HD-like cells, such as those recorded in the cockroach, have been shown to update their heading signal in reference to the facing direction of the animal (Varga and Ritzmann 2016). One feature that the above cell populations have in common is that they all innervate a region of the arthropod brain known as the central complex.

The central complex comprises a set of central, multi-layered, multi-columned neuropils that are conserved across arthropods (Homberg 2008). The structured neuropils in this region include a multi-glomerular, handlebar-shaped region called the

protocerebral bridge, a layered and columnated central body which, in *Drosophila,* is called the fan-shaped body, and a toroidal neuropil called the ellipsoid body[1].

In *Drosophila*, multiple lines of perturbational evidence point toward the central complex as an important locus of locomotor control. *Drosophila* genetic mutants in whose brains the structure of the central complex is distorted exhibit disrupted walking and flight behavior (Strauss and Heisenberg 1993, Ilius, Wolf, and Heisenberg 1994). Perturbing the activity of neurons that innervate central complex neuropils disrupts navigational behaviors as well. A set of neurons called “ring neurons”, each of whose axons project around the entire ellipsoid body, seem to be particularly important for visually-guided navigational tasks. In a “detour paradigm”, a fly is allowed to walk freely around a circular arena surrounded by a panoramic, computer-controlled, LED display. Two vertical dark stripes directly across from one another are shown on the display and flies tend to walk back and forth between them (Götz 1980). When both stripes are removed and immediately replaced by a distractor (a single vertical, dark stripe 90º away from the initial two), the fly turns and walks toward this distractor. One second later, the distractor is removed. Although there are no stripes on the arena, the fly tends to walk in the direction it had been traveling before the distractor appeared, suggesting that it had maintained an angular memory of that heading angle (Strauss and Pichler

[1] In other arthropods, the homologous structure to the fan-shaped body is called the “central body upper” and the homologous structure to the ellipsoid body is often linear, as opposed to toroidal, and is called the “central body lower”.

1998). This angular orientation memory depends upon the activity of ring neurons (Neuser *et al.* 2008).

Flies also display spatial memory capabilities in a modified Morris Water Maze task. In the task, flies are permitted to walk around an arena, again bounded by a cylindrical LED panoramic display, showing a complex visual scene. Most of the floor is heated to a temperature that flies find aversive, but there is a single ~1" diameter cool zone on the floor whose position relative to the surrounding visual scene remains fixed. The visual scene and the cool zone are rotated in tandem every few minutes. At first, flies search around the entire arena for the cool spot. Over time, the flies' paths toward the cool spot become increasingly direct, as evidenced by shorter search times and more efficient trajectories to find the cool spot. If the visual scene and cool zone position are not rotated in tandem, but rather at a varying, random angle relative to one another, the flies trajectories to the cool spot do not get as directed over time, arguing that flies learn to associate aspects of the visual panorama with the location of the cool zone. This form of learning is abolished when ring neurons are inhibited (Ofstad, Zuker, and Reiser 2011).

In addition to being necessary for visually guided navigational behaviors, many ring neurons show physiological responses to localized visual stimuli. Specifically, when one images $[Ca^{2+}]$ in ring neuron dendrites, one observes strong visual responses to small bars in specific locations around the animal and these responses are tuned to the angular orientation of the small bar (Seelig and Jayaraman 2013). Both characteristics

suggests that ring neurons may play a role in detecting the angular position of navigationally relevant landmarks (Seelig and Jayaraman 2013).

Among the neurons to which ring neurons are functionally connected (Franconville, Beron, and Jayaraman 2018) is a population of cells called “E-PGs”. The abbreviation “E-PG” indicates that each neuron’s dendrites arborize in the **E**llipsoid Body, and that the neuron’s axons project to both the **P**rotocerebral Bridge and the **G**all (Figure 1.1a-c). E-PG physiology is reminiscent of that of HD neurons. A typical experiment to demonstrate this fact places a fly on an air-cushioned ball in angular closed-loop control of a visual landmark (such as a bright bar). When the fly turns left, the bar rotates right, and vice versa, allowing the fly to control the angular location of the bar on the screen with her own behaviors. During such an experiment, if one images calcium signals from E-PG cells in the ellipsoid body, one observes a single “bump” of calcium, and this activity bump rotates around the ellipsoid body in concert with the changing angular position of the landmark on the screen. Individual E-PG neurons are tuned to the angular position of this landmark, and the fly’s virtual heading direction (equivalent to the angular location of the landmark on the panoramic screen) can be easily extracted from E-PG population activity based on visual inspection or a simple algorithm to find the peak location of activity around the ellipsoid body (Seelig and Jayaraman 2015).

Figure 1.1 | Fluidity and stability in the E-PG heading signal

(a) Central complex in the *Drosophila* brain. (**b**) Cartoon of a single E-PG neuron, with dendrites in the ellipsoid body and terminal boutons in the protocerebral bridge and Gall. (**c**) Schematic of wiring diagram of E-PGs in the ellipsoid body and protocerebral bridge. Colors indicate sub-regions innervated by individual neurons (from Turner-Evans and Jayaraman 2016). (**d**) Imaging neural activity in a fly walking on an air-cushioned ball in closed loop control of a bright bar displayed on an LED arena. (**e, f**) Two example recordings of E-PG neurons of the same fly walking in closed loop. The first column shows the fluorescent activity in each glomerulus over time. The second column shows the bar angle and phase angle overlaid, 0º indicating the bar is directly in front of the fly. The E-PG phase is offset by a constant value so that the phase and bar position overlap. Gray vertical bars indicate where the bar is behind the fly. The third column shows the fly's forward rotation on the ball. In (**e**) the E-PG phase tracks the position of the bar as the fly walks. In (**f**) the E-PG activity persists and the phase of the E-PG signal maintains a constant value as the fly stands still for more than 40 seconds.

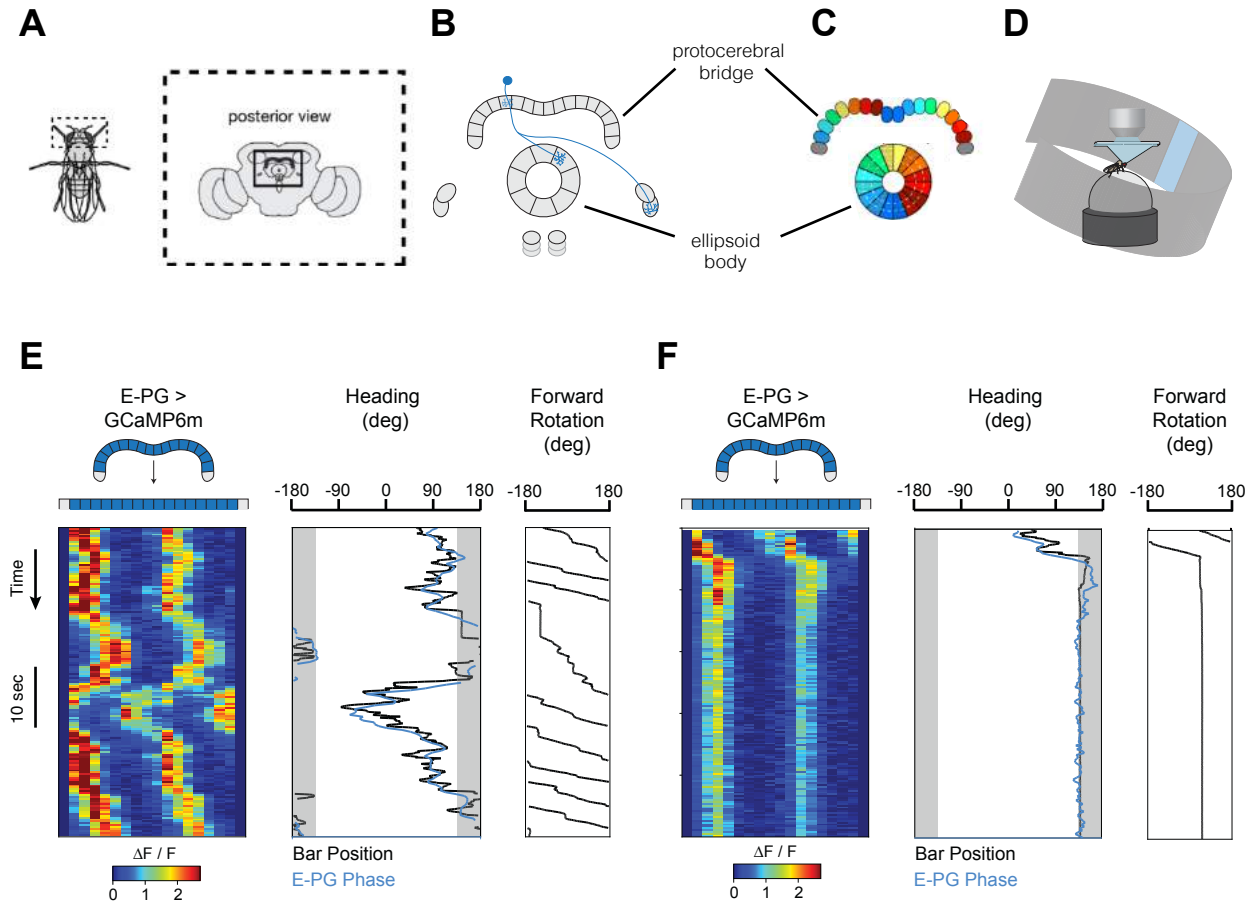
A
posterior view
B
protocerebral bridge
ellipsoid body
C
D
E
E-PG > GCaMP6m
Heading (deg)
Forward Rotation (deg)
-180 -90 0 90 180
-180 180
Time
10 sec
ΔF / F
0 1 2
Bar Position
E-PG Phase
F
E-PG > GCaMP6m
Heading (deg)
Forward Rotation (deg)
-180 -90 0 90 180
-180 180
ΔF / F
0 1 2
Bar Position
E-PG Phase

Several aspects of the E-PG activity bump suggest that it may function to encode the fly's heading angle in the world. First, just as a fly can only ever be facing one direction, the E-PG population calcium signal is confined to a single “bump” of calcium activity in the ellipsoid body. Second, just as a heading signal must update as the animal turns, the E-PG activity bump position around the ellipsoid body updates as the fly rotates. Third, just as an ideal heading system would be able to encode an animal’s heading in a variety of environments, so too does the E-PG bump encode the fly’s heading relative to a variety of visual scenes. The E-PG bump is not retinotopic; both complex and simple visual scenes elicit a single bump of E-PG activity in the ellipsoid body. Indeed, when flies walk in closed loop control of the angular position of a single bright vertical bar, different animals exhibit different offsets between the angular positions of the landmark and the activity bump (Seelig and Jayaraman 2015), consistent with the notion that the activity bump represents the abstract concept of the fly’s heading, as opposed to any given landmark’s absolute position. Fourth, just as many heading signals can be updated solely by the animal’s own movements, the E-PG bump persists and continues to update in the correct direction when the fly walks in complete darkness (Seelig and Jayaraman 2015). Finally, barring any unexpected rotations of the visual scene, an ideal heading estimate would continue to indicate the same angle as long as an animal stood still. Just so, when the fly stands still in the dark, the E-PG calcium bump stays in the same location for tens of seconds to minutes (for as long as has been measured) when flies stand still (Seelig and Jayaraman 2015). Note that the E-PG activity bump updates in the dark even though the fly is tethered. In

this situation, the fly's rotations on the ball are not accompanied by a vestibular signal of the turn. In contrast, rat HD neurons require vestibular input to maintain their tuning (Stackman and Taube 1997). The fly central complex must therefore integrate proprioceptive signals from the animal's legs in order to update the E-PG heading signal[2].

The anatomy of E-PG neurons makes it possible to image this heading signal in E-PG axon terminals in the protocerebral bridge. E-PG cells are columnar; there is a consistent mapping between the 1 of 16 wedges of the ellipsoid body in which an individual E-PG neuron arborizes and the 1 of 18 glomeruli of the protocerebral bridge to which it projects (Figure 1.1b-c) (Wolff, Iyer, and Rubin 2015), such that if E-PGs in adjacent tiles of the ellipsoid body were to become active, E-PGs in the adjacent glomeruli of the protocerebral bridge would also. E-PGs in adjacent wedges of the ellipsoid body project to opposite sides of the protocerebral bridge (Wolff, Iyer, and Rubin 2015). Based upon E-PG anatomy and their observed physiology in the ellipsoid body, one might predict that E-PGs have two activity bumps in the protocerebral bridge: one on the left bridge, and one on the right.

[2] In principle, E-PG neurons could update in the dark in response to efference copies of motor commands, as well as proprioception. Cross-correlations between E-PG activity and behavior have shown that the E-PG bump position changes hundreds of ms *after* the animal behaves. This is also true for other central complex neurons whose activity represents the fly's heading (Green *et al.* 2017, Turner-Evans *et al.* 2017). While functionally it is possible for a brain signal to be updated by a late corollary discharge, for succinctness I will refer to these idiothetic cues that rotate these heading estimates as "proprioceptive".

Indeed, when one images E-PG calcium activity in the protocerebral bridge via 2-photon excitation of GCaMP while the fly walks on an air-cushioned ball (Figure 1.1d), one observes two to three bumps of calcium activity with a periodicity of 8 protocerebral bridge glomeruli. These peaks of calcium activity rotate in concert, moving to the left when the when the fly turns right on the ball, and vice versa (Figures 1.1e-f)[3] (Green *et al.* 2017, Turner-Evans *et al.* 2017). As these calcium activity peaks are periodic, their position can be estimated by taking a Fourier transform of the 18-element vector of calcium activity along the bridge – where every element of the vector represents the calcium activity of a single glomerulus – and extracting the phase of the Fourier component at 8 glomeruli (Green *et al*. 2017, see Methods). This *phase* (i.e. the position of these peaks in the bridge) tracks the virtual heading of the fly (Figures 1.1e-f)[4]

Recent evidence demonstrates for the first time that E-PG activity helps flies to perform navigational tasks. For example, normal physiological signaling in E-PG neurons is required, in both flight and walking, for a dispersal behavior called “menotaxis” or "arbitrary angle fixation", wherein an animal walks for an extended period of time at an arbitrary, fixed angle with respect to a visual landmark (Giraldo *et al.* 2018;

---

[3] When the calcium bump sits at the most ventral part of the ellipsoid body, the E-PG activity in the protocerebral bridge is spread across both ends of the structure and very middle, such that there are three activity bumps in the bridge instead of two. While this may look like a further bifurcation of the heading signal, it is really just a wrapping artifact that comes from representing a circular feature on the linear structure of the bridge.

[4] Although there are 2-3 bumps of E-PG calcium activity in the protocerebral bridge, these bumps remain eight glomeruli apart from one another and rotate in unison. It is on this basis that we describe the multiple-bump signal as a periodic signal characterizable by a single phase.

Green *et al.* 2018). Moreover, in walking menotaxis, E-PGs have been interpreted to serve as a *current heading* signal in a *current-vs.-goal-heading* comparison, to guide the fly's turning and forward speed. In summary, multiple lines of correlational and perturbational evidence suggest that the phase of the periodic bumps of calcium activity in E-PG neurons represents a fly's current heading, and that this heading estimate is used to guide locomotion in navigational tasks.

A natural constraint on the usefulness of the E-PG signal for guiding behavior is the angular precision of the signal. How precise is the E-PG heading estimate? The answer to this question may depend upon the sensory context in which the fly finds itself. If sensory cues informative about the fly's angular heading are available, the E-PGs can inherit their heading estimate from the relevant sensory neurons. For instance, if the sun is visible and if the E-PGs have stored a mapping between the azimuthal position of the sun and the anatomical position of the activity bump, then the E-PGs can carry a relatively precise heading signal as defined by their visual inputs. In this case, the angular resolution of the E-PG heading estimate might be the same as the angular resolution with which the relevant visually sensitive neurons can signal the angular position of visual cues.

However, what happens if the sky is overcast and all relevant celestial cues, like the sun, are unavailable? In this case – simulated by complete darkness in the imaging experiments – empirical evidence has shown that E-PGs still carry a heading estimate and that this estimate is stored and updated via intrinsic dynamics and assessments of self-movement of the animal (Seelig and Jayaraman 2015). How do neural systems that

signal heading, like E-PG neurons, store an angular variable in the absence of positional cues and what is the angular resolution of the E-PG heading estimate in darkness?

HD neurons, including E-PGs, seem to represent the navigational variable of heading direction via their population activity (Redish, Elga, and Touretzky 1996; Zhang 1996). To explain how populations of neurons can persistently store a variable, computational neuroscientists have modeled these and other neuronal circuits as "attractor networks". In a network of *N* nodes, it is possible to use a single point to represent the network's state (i.e. the activity of all of the nodes) in an *N*-dimensional space (or in some state-space with reduced dimensionality). In an attractor network, the nodes are connected such that, if the network state resides in a "basin of attraction", the network state gravitates toward a stable state, also known as an "attractor state" (Knierim and Zhang 2012).

The simplest type of attractor network is a "point-attractor", in which the network possesses a single equilibrium state. However, an attractor network can have more than one attractor state. In 1982, John Hopfield modeled a highly interconnected network of neurons with random synaptic weights, which, given a set of random initial states would, over time, converge to one of a small set of stable states. Importantly, the system showed a bias toward relaxing to the stable state most similar to the starting state, as though the network state had been attracted to that nearby stable point (Hopfield 1982).

Attractor states may be discontinuously scattered around the state-space. But, if the weights of the network are carefully tuned, these attractor states may be arranged in a continuum (Knierim and Zhang 2012). This configuration of stable states might be useful for a network whose role was to calculate and store a value that falls on such a continuum. The orbital position of the eye represents just such a value. Many vertebrates move their eyes by interspersing long periods of stable gaze with quick, saccadic eye movements. Between saccades, the animal's eye position along one axis falls on a continuum between some minimum and maximum value, and this position is temporarily stored. Neurons in the goldfish hindbrain integrate eye-velocity signals to generate a persistent firing rate that correlates with the animal's eye position (Aksay *et al.* 2000) and these neurons' activity controls the eye's position (Aksay *et al.* 2007). If one plots the firing rate of one of these velocity-to-position integrating neurons against a second such neuron, these points fall along a line. Put another way, the activity states of velocity-to-position integrating neurons form a line through state space, and the activity of these neurons has been modeled as a "line-attractor" (Seung 1996; Seung *et al.* 2000) – although it should be noted that further research has elaborated upon this model, suggesting that the velocity-to-position integrating neurons of the goldfish and zebrafish can be modeled as a multi-dimensional attractor (Aksay *et al.* 2003; Miri *et al.* 2011).

Line attractors can represent the value of some variable between two boundaries. But what if the variable an animal needs to compute is circular, such as the orientation of an edge? Such variables are capably represented by "ring attractor"

network models. In ring attractor networks, only a small subset of cells are ever stably active at a time, but this active pool of cells can gradually and stably change over time. The active pool of cells is said to carry a "bump" of activity around the network. Ring attractor networks have the additional property that if the activity bump moves smoothly across the whole population along a single dimension, the first set of neurons eventually become active again. These networks are called ring attractors because one can imagine arranging the cells, functionally, in a ring – even if they are not anatomically arranged as such in the brain – where the activity bump travels smoothly around the ring.

Neurons in mammalian V1 that preferentially respond to edges with a specific orientation have been modeled as a ring attractor. In principle, orientation tuning in these neurons might be the product of feed-forward visual input. However, a purely feed-forward model of orientation tuning predicts certain features that are not observed in real V1 neurons, such as a relationship between the width of a V1 neuron's orientation tuning curve and the stimulus contrast. However, when an interaction term is introduced between V1 model neurons such that they weakly excite other V1 neurons with similar orientation tuning and inhibit V1 neurons tuned to a perpendicular orientation, this brings the model's behavior more in line with experimental observations (Ben-Yishai, Bar-Or, and Sompolinsky 1995). If one were to arrange these model neurons in a circle such that the neurons' angular positions matched their preferred orientation, and then rotated an edge in these model neurons' receptive fields while

tracking the neurons' activity, one would observe a bell-shaped bump of activity rotating around this ring (Ben-Yishai, Bar-Or, and Sompolinsky 1995).

Head direction neurons have also been modeled as ring attractor networks that integrate angular velocity to rotate the activity bump (Skaggs *et al.* 1995; Redish, Elga, and Touretzky 1996; Zhang 1996). In these models, the uniqueness of the head direction signal is maintained by short-range excitation and long-range inhibition; HD neurons excite other HD neurons with similar preferred directions and inhibit those with preferred directions opposite their own (Zhang 1996). When an animal is facing in an HD neuron's preferred direction, persistent activity maintained by recurrent excitation from other HD neurons with the same preferred direction (Redish, Elga, and Touretzky 1996).

Direct evidence that the mammalian head direction signal is maintained by ring attractor dynamics, as opposed to purely feed-forward signals, is beginning to accumulate. In rats, when multiple HD neurons are simultaneously recorded, these neurons have the same temporal correlation structure when the animal is awake as they do when the animal is asleep, when feed-forward inputs should not be present (Peyrache *et al.* 2015).

Evidence has recently emerged that *Drosophila* E-PG neurons, whose physiology is analogous to that of vertebrate HD neurons, can be modeled by a ring attractor. Kim *et al.* simultaneously imaged the E-PG activity bump and used optogenetics to activate E-PGs innervating a portion of the ellipsoid body away from the calcium bump. Ring attractor models predict that, at any given time, there should only

be one activity bump (Skaggs *et al.* 1995; Redish, Elga, and Touretzky 1996; Zhang 1996). In simulations, injecting current into HD neurons far away from the bump center cause the bump to slide or jump to the stimulated location (Zhang 1996). Correspondingly, exogenous activation of E-PG neurons off of the bump center generated a new bump at the stimulated location *and* degraded the original activity bump (Kim *et al.* 2017). This was taken as direct evidence that the E-PGs maintain a heading signal via a ring attractor network.

If the E-PGs' population-level calcium-bump estimate of the fly's heading angle can be modeled as a ring attractor, what can this tell us about the system's angular resolution? While many continuous attractor networks are idealized as possessing an infinite number of attractor states, in reality the maximum number of stationary states in an attractor network is the number of nodes in that network (Seung *et al.* 2000). Mammals possess such a large number of HD neurons that the ring attractor they comprise may be regarded as quasi-continuous. In small-brained animals such as *Drosophila*, however, anatomical considerations related to the small number of neurons become important.

The precision of the E-PG ring attractor is likely to be limited by the number of cells. Is it possible to determine the number of "nodes" in the E-PG ring attractor network based on anatomy alone? The answer is not totally clear; it depends on the level of anatomical organization one considers most important (neuropil compartment, cell, neurite, single synapse, etc.). Still, bearing this caveat in mind, one might estimate the E-PG's angular resolution to fall between 5º and 45º based on the known anatomy.

A single E-PG axon projects to one of 8 glomeruli in one half of the protocerebral bridge, and the cell's boutons always fill this entire sub-region. Together, these 8 glomeruli represent all of azimuthal space with double coverage (on the left and right protocerebral bridge), corresponding to 45º encoded by each glomerulus. Single E-PG neurons' dendrites are restricted to "wedges" of the ellipsoid body occupying 1/16th of the region's volume (22.5º per wedge). Some E-PGs' dendrites are restricted to a "demi-wedge" occupying 1/32nd of the EB's volume (11.25º per demi-wedge). Cell counts for the number of E-PG neurons labeled in a GAL4 line can vary between 36 and 68 neurons (Wolff, Iyer, and Rubin 2015; Giraldo *et al.* 2018). If the smallest unit of angular resolution is not any anatomical sub-region of the Ellipsoid Body, but is instead the individual E-PG neuron, then the E-PG neurons' estimate of heading direction could be precise to 5º in some flies. While even this estimate may seem somewhat low resolution, it is worth noting that the angle subtended by a single lens in the *Drosophila* eye – and thus the resolution of any visual positional information signal upon which the fly might base its angular orientation estimate – is itself around 5º (Heisenberg and Wolf 1984). If each node in the network is a set of synapses, rather than a single neuron, then the resolution could be better yet.

At first blush it might seem that an attractor network with more nodes, and therefore higher angular resolution, is inherently superior to one with fewer. However, continuous attractor networks appear to exhibit a kind of precision-accuracy tradeoff. To explain why this might be the case, it is helpful to describe the attractor network as having an associated energy landscape (this is sometimes referred to as the network's

Lyapunov function) (Brody, Romo, and Kepecs 2003). In the absence of feed-forward input to the network, the network state can only flow to lower regions of the energy landscape. Attractor states are represented as local minima on this energy landscape. In a truly continuous attractor network with infinite attractor states, the minimum value of this energy function falls along a continuum. Weights must be tuned extremely precisely to keep the floor of this landscape perfectly flat; imperfections cause the system to drift to a single global energy minimum (Brody, Romo, and Kepecs 2003). In models of the goldfish velocity-to-position integrator, when the recurrent synaptic weights are purposefully reduced 10%, the model's prediction for the animal's eye position always decays toward a single null position (Seung *et al.* 2000). Even a perfectly tuned attractor network with a flat energy minimum presents potential pitfalls. Such a system would have no energy barrier between attractor states, and so noise in feed-forward circuits would cause a this truly continuous network state to drift around the attractor manifold, rendering the theoretically accurate neural representation hopelessly imprecise (Brody, Romo, and Kepecs 2003). Conversely, it has been suggested that attractor networks with fewer states might exhibit higher precision, since more noise is required for a transition to a nearby attractor state. Of course if the E-PG heading estimate were to be represented by network with few attractor states, this would have obvious implications on the potential accuracy of that estimate, as this would limit fly's ability to discriminate similar heading angles. Because anatomy does not provide a clear estimate of the number of attractor states in the E-PG network, and since computational theory does not imply an optimal number of stable states in an attractor network given a number of

potential nodes, if one wants to know the resolution of the E-PG heading estimate it seems best to just measure it empirically.

Chapter three of my thesis builds on the work of a colleague graduate student in the lab, Cheng Lyu, who set out to determine the resolution of the E-PG heading estimate. One approach Cheng took was to directly measure the distribution of residences of the E-PG phase "bump". If there are distinct stable points, one should be able to observe these as periodic hotspots in the E-PG phase residence distribution. One complication is that the GCaMP signal represents a filtered history of a neuron's electrical activity, with decay time constant in the hundreds of milliseconds for the GCaMP6 family of calcium sensors (Chen, T-W *et al.* 2013). Thus, even if the E-PG phase hypothetically rotated in discrete steps, the filtered GCaMP signal would necessarily filter these steps in space and time, thus potentially leading one to erroneously believe that the E-PG phase rotated in a more continuous fashion. Therefore, Cheng focused on measuring the angular position of E-PG phase in the brain specifically *while the fly stood still for many seconds*. During such events, the E-PG phase remains stable in the brain and the errors induced by GCaMP filtering of the underlying calcium signal are minimized or potentially eliminated.

In order to observe any potential hotspots of E-PG phase residence, one must measure the E-PG phase during thousands of standing events. In a 20 minute recording session, one can expect, in the absolute best case scenario, approximately 40 standing events by a fly, which is an insufficient number of samples to assess the shape a multi-modal distribution with up to 16 modes or more. It was therefore necessary for Cheng to

record the E-PG phases from dozens of flies in such a manner that it was possible to compare the E-PG phase signal meaningfully across flies. This cross-fly comparison is very difficult to make if one measures the E-PG phase in the ellipsoid body because the borders defining adjacent wedges and demi-wedges of the ellipsoid body are anatomically indistinct, and thus it is not possible to discern where one E-PG neuron's dendritic arbor ends and another's begins. In addition, the ellipsoid body will almost certainly be slightly rotated in the imaging plane from one preparation to the next, making registering phases across flies without adding angular noise from this technical concern nearly impossible. However, in the protocerebral bridge, the E-PG cells always innervate the exact same 16 glomeruli whose borders are separated by a small gap and thus easily defined in the same manner across preparations. The protocerebral bridge is also a linear structure (In contrast to the toroidal ellipsoid body), and so slight rotations in the preparation do not disrupt one's ability to make the same phase measurement across flies. Cheng therefore elected to measure the distribution of E-PG phases during standing events in the protocerebral bridge.

If a histogram of E-PG phases is drawn at random from a probability distribution with 16 modes, then the Fourier transform of that histogram will show a peak at 22.5º (corresponding to 360º / 16) (Figure 1.2a). Cheng compiled the histogram of E-PG phase angles during 1867 standing events in darkness and 1892 events where flies controlled the angular position of a tall vertical bar in angular closed loop. A Fourier analysis of these empirically measured histograms did not reveal measurable periodicity at 22.5º (Figures 1.2b-c). While a power spectrum peak at 22.5º could not be detected

in these data, this does not rule out the possibility that the E-PG phase may reside in 16 (or more or less) stable states because this analysis assumes that discrete stable states are consistently distributed in every fly with respect to the anatomical structure of the protocerebral bridge. This assumption may be wrong. That said, if stable states exist in the E-PG system, they cannot be detected with this method in this dataset.

Figure 1.2 l 16-stable state periodicity cannot be detected in the E-PG heading estimate in the Protocerebral Bridge.

(**a –c**) Middle: histograms of the average phase of standing events, such as the event shown in Figure 1.1f, drawn from multiple flies. 5.625º bin size. Right: power spectrum of this histogram. (**a**) Histogram drawn from a probability distribution with 16 equally spaced stable points. The power spectrum of this histogram shows a peak at 22.5º (360º/16). (**b**) Histogram drawn from 1867 standing events while the fly walked in the dark. The corresponding power spectrum shows much less power at 22.5º. (**c**) Histogram drawn from 1892 standing events while the fly walked in closed loop with a bright bar. The corresponding power spectrum shows much less power at 22.5º. Cheng Lyu collected the data, analyzed it, and generated these figures.

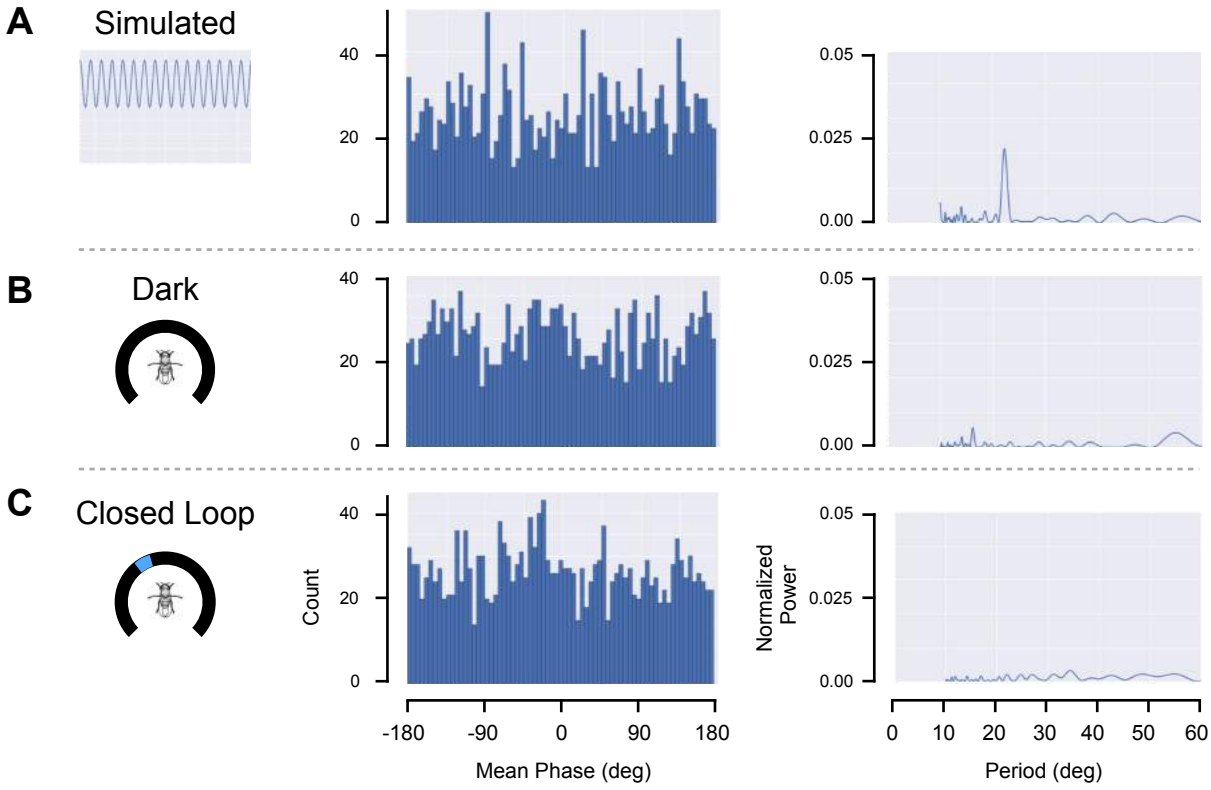
A
Simulated
B
Dark
C
Closed Loop
40
20
0
0.05
0.025
0.00
Count
Normalized Power
-180
-90
0
90
180
Mean Phase (deg)
0
10
20
30
40
50
60
Period (deg)

Building on Cheng's work, I approached the question of the E-PG heading resolution question from a new angle. When flies walk with a tall bright bar in angular closed loop, abruptly jumping the bar leads to a concomitant repositioning of the position of the E-PG bump(s), i.e., the E-PG phase, in the ellipsoid body and bridge (Seelig and Jayaraman, 2015; Green *et al*. 2018). This is analogous to the behavior of mammalian HD neurons, whose preferred directions relative to an angular landmark remain consistent when that visual landmark is rotated (Yoganarasimha and Knierim 2005). If one were to jump the tall bright bar less and less, eventually one would find an angular shift so small that one could not detect a concurrent change in the E-PG phase in the direction in which the bar was jumped. The smallest angular shift in the position of a landmark that elicits a measurable change in the E-PG phase represents the resolution with which we can detect that the E-PG phase signals the location of those landmarks. The actual resolution of the E-PG phase may be better than our measurement, but our measurement would provide an upper bound to this value. I therefore set out to determine the smallest visual perturbation to which the E-PGs bump position responds (Figure 1.3a). The answer to this question would reveal the measurable resolution of the E-PG phase to feed-forward, positional visual input.

A separate, but related question is how precisely the E-PGs can store an angular variable in the absence of visual input. It may seem as though the resolution of the E-PGs with and without visual input ought to be the same, but in fact these two values might be quite different. In a ring attractor network, in the absence of sensory inputs, the bump of activity must be centered on a particular node; if the ring attractor is idealized

as an energy landscape, bumps centered on these nodes are represented by local minimal in the energy landscape. Imagine, however, a visual stimulus whose angular position fell between two nodes. This visual stimulus might excite both of those neighboring nodes. In this situation, the activity bump stills fall on the ring, but the network state is “propped up” on a higher energy region of the energy landscape by the feed-forward input. If the visual input is removed, *the network state must relax to the nearest attractor state*. Assuming that these attractor states are evenly distributed around the ring, the maximum size of that relaxation ought to be one half the distance between attractor points – any relaxations larger than this would move past the nearest local energy minimum. The experiment devised was to repeatedly remove visual input while the fly stood still, and measure the change in E-PG phase in response. The smaller the relaxations, the higher the presumptive angular resolution of the E-PGs. (Figure 1.3b). We are very confident that there are more than 8 stable states (maximum relaxation of 22.5º) and we cannot detect periodicity in E-PG phase probability corresponding to 16 stable states (which would correspond to a maximum relaxation size of 11.25º). Maximum relaxation sizes smaller than these values would suggest that the E-PG ring attractor network is comprised of more than 8 or 16 attractor states, respectively.

Small relaxations would imply a high number of attractor states – but what about large ones? The occurrence of larger-than-expected E-PG phase relaxations would, seemingly to my best understanding, confound any attempt to explain such E-PG phase rotations as relaxing toward the nearest stable state of a ring attractor. Continuous

attractor models with asymmetric weights between nodes tend to revert to single- or multiple-point attractors (Zhang 1996, Seung *et al.* 2000). If large E-PG phase relaxations are observed but they always proceed to the same anatomical position, then we might suppose that this anatomical position represents an attractor state which is slightly lower in energy than the other attractor states in the E-PG network. If, however, large relaxations are common, and the E-PG phase does *not* always relax to the same value, it would raise the possibility that the phase to which the E-PGs relaxed indicated some other stored angular variable (Figure 1.3c), whose mechanism and function might be worth considering in future research on the E-PGs.

In chapter three of this thesis I will show that, when a fly stands still, the phase of the E-PG heading signal measurably rotates in response to a 5.625º displacement of the visual stimulus, implying that the angular resolution of the E-PGs roughly matches that of the early visual system. I will further show that, when the visual stimulus is abruptly removed, the E-PG phase routinely relaxes further than a perfectly tuned 8-state ring attractor would allow. Instead, the E-PG phase tends to relax to a nearby position that is remembered for a given standing event, but whose value can change over time, both across flies and within flies from one standing event to the next. This "latent" phase angle, unmasked only when visual stimuli are abruptly removed, may represent a second angular variable whose value can both be stably stored and flexibly updated in the E-PG attractor network.

Figure 1.3 | Determining the resolution of the E-PG heading estimate and the topology of the E-PG energy landscape.

(**a**) Rapidly jumping a visual landmark to a nearby position (blue and red bars) will always update the heading estimate if the resolution of the heading estimate to visual input is smaller than the size of the jump (bottom, left), but will not always update this estimate if the resolution is larger than the jump (bottom right). (**b**) Above: schematic of the visual stimulus. Below: unwrapped energy landscapes of two ring-attractor networks with different numbers of stable states. In a well-tuned ring attractor with symmetric weights between the nodes, the maximum size of the E-PG phase relaxation upon the removal of the visual stimulus should be half the distance between attractor states – the distance between local energy maxima and local energy minima. If a heading estimate is represented by a ring attractor network with a large number of attractor states, (left), abrupt removal of the visual stimulus (top, dashed blue rectangle) should lead to a small displacement of the heading estimate (bottom: dotted blue circle to filled blue circle). If a heading estimate is represented by a ring attractor with fewer states (right), the maximum displacement observed should be larger. (**c**) In the event that the E-PGs relax to a single point attractor, the angular position of this attractor could represent mistuning of the weights between neurons that was hard-wired in development, or the position of this point attractor could change over the course of the experiment. In the schematic, energy landscapes as a function of phase angle are represented, with colors representing the energy landscapes at different points in time. If the position of a point attractor was hardwired (left), we would not expect to observe the angular position of the energy minimum change over time. If the phase relaxed to different angular positions over the course of an experiment, that would suggest that the angular position of the energy minimum could change over time.

A

Estimating E-PG phase resolution with small jumps of a visual stimulus

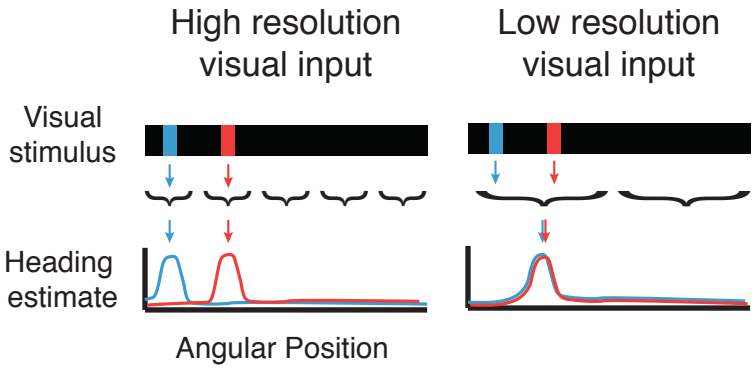

B

Estimating E-PG phase resolution by abrupt removal of the visual stimulus

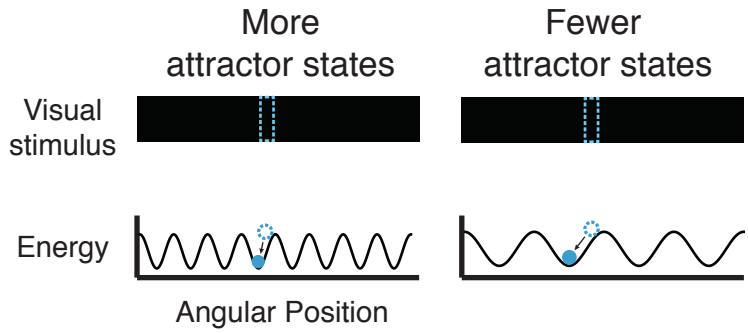

C

Determining whether a global attractor state is anatomically defined or is updated over time

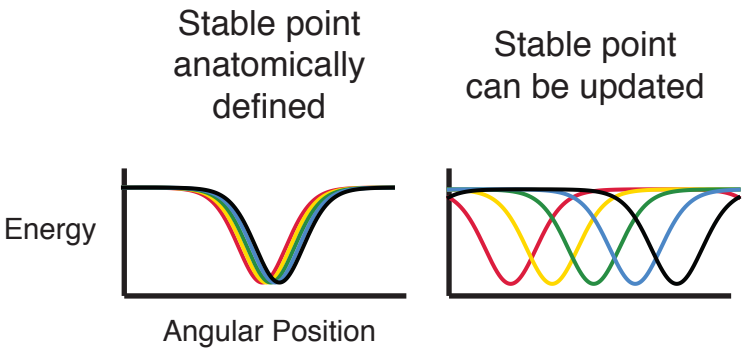

Chapter 2 | A neural population required for spontaneous flight turns

In this chapter, I will present evidence that the synaptic activity of neurons labeled by the *NP0212-GAL4* line is necessary for spontaneous flight turns, but not flight turns evoked by expansion stimuli or optic flow. I use genetically-defined subsets of the *NP0212-GAL4* line to suggest that the neurons whose inactivation causes this striking phenotype are cholinergic and reside in the thoracic ganglion.

A setup for studying spontaneous flight turning in *Drosophila*

To study spontaneous and visually evoked flight turns, we glued *Drosophila* to a custom platform (Maimon, Straw, and Dickinson 2010) and tracked their wing movements during tethered flight with a camera from below (Figures 2.1a-b). We computed the left- minus-right wingbeat angle (L–R WBA) with respect to the fly's body axis, a signal correlated with yaw torque (Tammero, Frye, and Dickinson 2004), as a measure of the fly's intention to turn. Positive deflections in L–R WBA indicate that the fly is attempting to turn right, and negative deflections indicate that the fly is attempting to turn left. We note that L–R WBA is not a perfect measure of the fly's yaw torque (let alone attempted maneuvers along other rotational axes) because it does not capture many important kinematic aspects of the wing's motion, like the angle of attack and timing of the wing flip, but it serves as a sufficient measure for our first-order purposes here: determining whether the fly is attempting any turns at all.

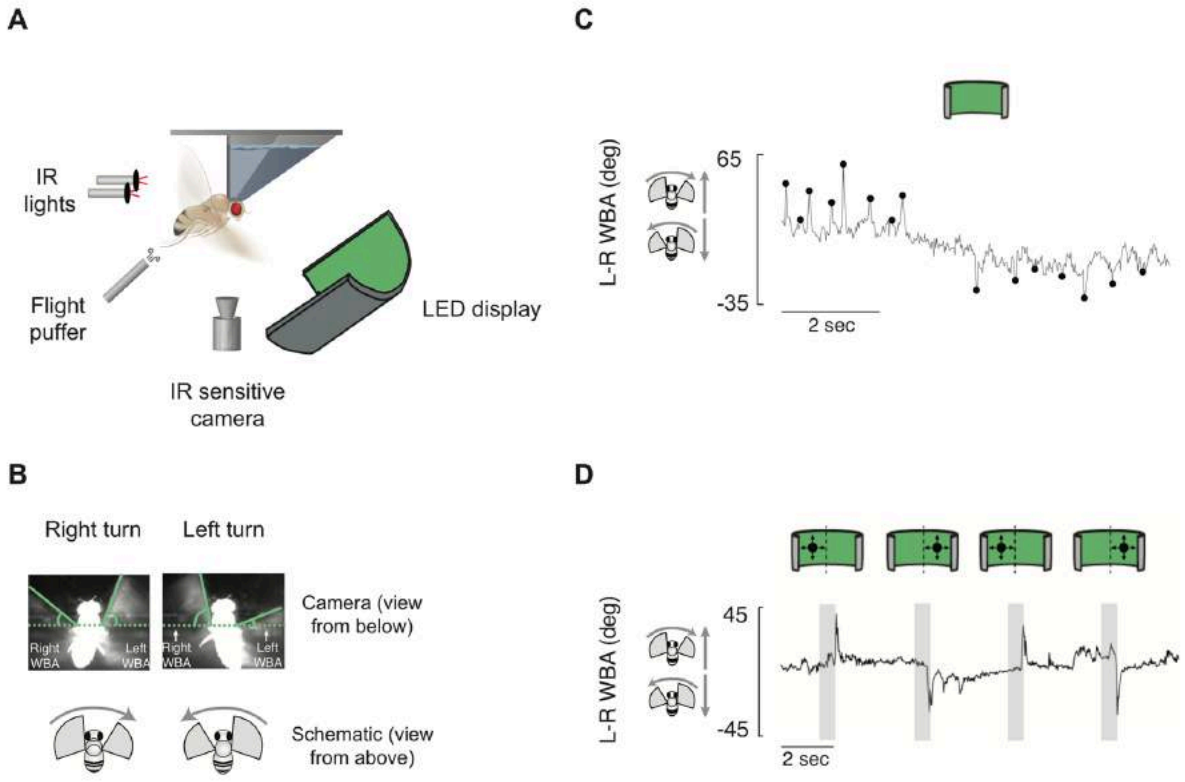

Figure 2.1 | A behavioral setup for measuring both spontaneous and visually evoked flight turns in *Drosophila*

(**a**) Experimental apparatus. (**b**) Still images showing a fly turning right and left. (**c**) An example trace of a fly flying in the context of a uniformly lit screen making spontaneous saccades. Saccades were picked algorithmically and are marked at their peaks (black dots). (**d**) An example trace shows a fly responding to loom stimuli whose center of expansion is to the left or right of the fly. Gray boxes indicate stimulus expansion.

Flies flew in front of a panoramic light-emitting diode (LED) display. With the display uniformly lit, frequent, sharp deflections of the L–R WBA signal, or saccades, are observed (Figure 2.1b) (Heisenberg and Wolf 1979). We computationally identified spontaneous saccades (black dots in Figure 2.1c) by subtracting the slow changes of L–R WBA from the raw signal and using a threshold-crossing algorithm on this baseline-subtracted signal. Rigidly tethered flies typically perform saccades in bursts of turns in one direction, followed by bursts of turns in the other direction, and so on (Heisenberg and Wolf 1979). In a more naturalistic behavioral paradigm, in which flies were attached to a thread so they were free to rotate about their yaw axis, others have observed this same propensity to execute bursts of turns in the same direction (Mayer *et al.* 1988). In a similar paradigm, in which tethered, flying flies are free to actually rotate about their yaw axis within a vertically oriented magnetic field (Bender and Dickinson 2006a), we observed the same pattern of syn-directional bursts of saccades (Figures 2.2a-d). This tendency to perform saccades in syn-directional bursts was independent of any individual fly's overall tendency to perform more left turns or right turns in both paradigms (Figures 2.2e-f).

Figure 2.2 | Rigidly and magnetically tethered flies both perform bursts of syn-directional saccades.

(**a**) Schematics of the magnetic tether (left) and rigid tether (right) setups. (**b**) Example traces of a magnetically tethered fly (left) and a rigidly tethered fly (right) flying in the context of a uniformly lit screen. Rightward saccades are marked by green dots, leftward saccades by magenta dots. Both flies were of Heisenberg Canton-S (HCS) genetic background. (**c**) Analysis pipeline for determining the likelihood of observed saccade sequences. (**d**) The fraction of syn-directional saccades in both magnetically and rigidly tethered HCS flies (black dots: n = 9 and n = 7 individual flies, respectively; red bars: means of real data) as well as in shuffled turn sequences (blue: mean and 95% confidence interval, n = 50,000 simulations of turn sequences of 9 and 7 flies, respectively). *** $p < 0.001$ as estimated by comparing the mean fraction of syn-directional saccades between real and simulated populations. In simulations, we resampled the actual saccades generated by a fly, but in a randomized order. (**e**) Flies with low or high saccade direction bias were just as likely to show runs of saccades in the same direction as the previous turn. Individual magnetically tethered flies' fraction of fraction of syn-directional saccades are plotted against their turning bias. $p > 0.2$, $r^2 = 0.22$. (**f**) Same as in (e), but for rigidly tethered flies. $p > 0.5$, $r^2 = 0.07$.

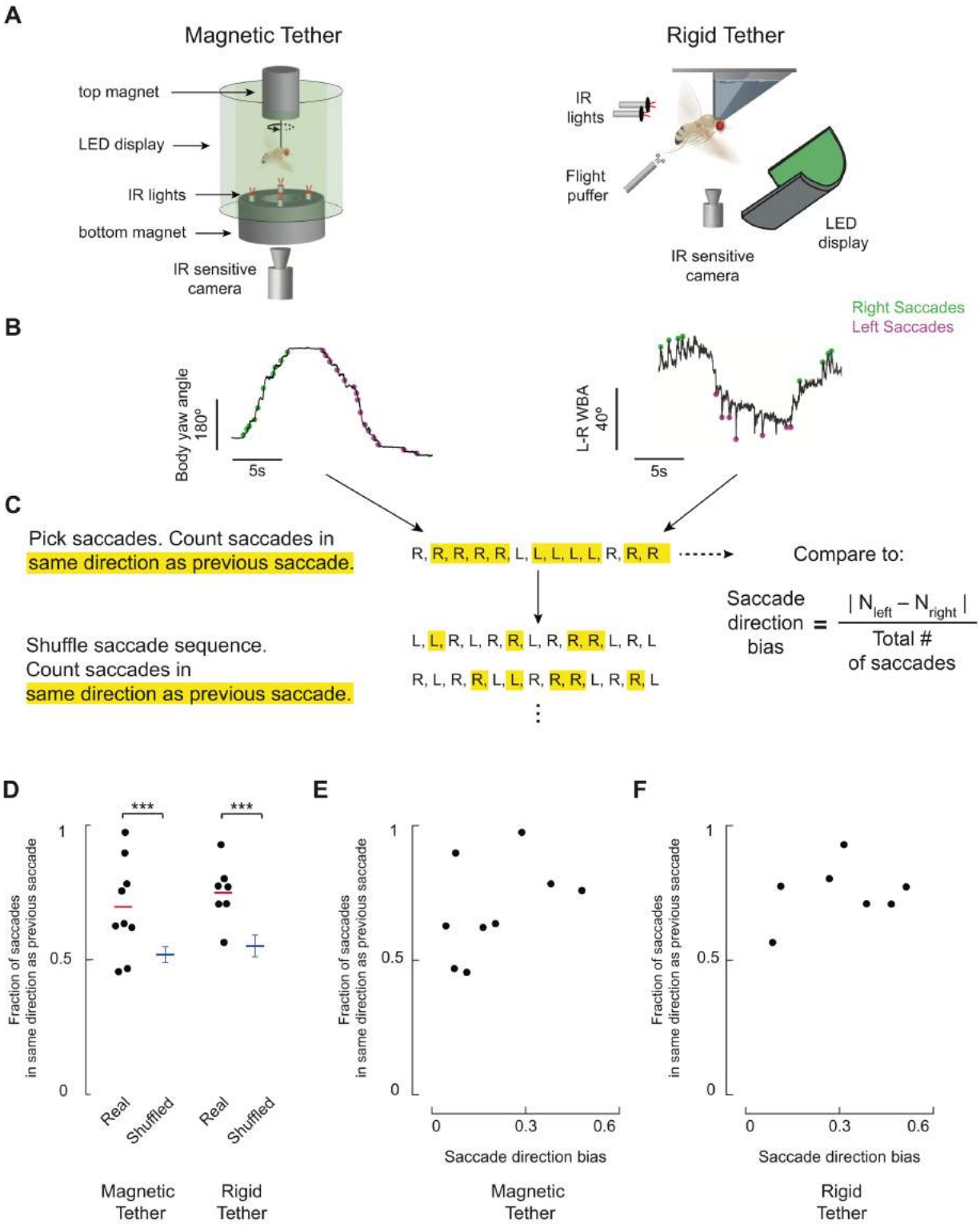
A
Magnetic Tether
top magnet
LED display
IR lights
bottom magnet
IR sensitive camera
Rigid Tether
IR lights
Flight puffer
IR sensitive camera
LED display
B
Right Saccades
Left Saccades
Body yaw angle 180°
5s
L-R WBA 40°
5s
C
Pick saccades. Count saccades in same direction as previous saccade.
R, R, R, R, R, L, L, L, L, L, R, R, R
Compare to:
Saccade direction bias = | N_left – N_right | / Total # of saccades
Shuffle saccade sequence. Count saccades in same direction as previous saccade.
L, L, R, L, R, R, L, R, R, R, L, R, L
R, L, R, R, L, L, R, R, R, L, R, R, L
D
***
***
Fraction of saccades in same direction as previous saccade
1
0.5
0
Real
Shuffled
Real
Shuffled
Magnetic Tether
Rigid Tether
E
Fraction of saccades in same direction as previous saccade
1
0.5
0
0
0.3
0.6
Saccade direction bias
Magnetic Tether
F
Fraction of saccades in same direction as previous saccade
1
0.5
0
0
0.3
0.6
Saccade direction bias
Rigid Tether

In addition to performing spontaneous saccades, *Drosophila* also perform saccades in response to looming discs in free flight (Muijres *et al.* 2014; Muijres *et al.* 2015) and while tethered (Tammero and Dickinson 2002b). When a loom stimulus appears on the right, flies typically turn left and vice versa (Figure 2.1d) (Tammero and Dickinson 2002b; Muijres *et al.* 2014). Thus, tethered flying flies perform rapid flight turns that can be operationally characterized as spontaneous or as visually evoked, allowing us to ask whether the mechanisms for executing spontaneous saccades and this sub-class of visually evoked turns are dissociable.

Normal synaptic activity in cells targeted by *NP0212-GAL4* is essential for spontaneous turns

When synaptic transmission is impaired in neurons targeted by the *NP0212-GAL4* driver line (Figure 2.3a), flies performed very few spontaneous saccades. To silence these cells, we expressed *UAS-shibire^{ts1}* (*UAS-Shi^{ts}*), a temperature-sensitive, dominant-negative allele of dynamin. Above the restrictive temperature of 29ºC, *shibire^{ts}* blocks synaptic transmission by inhibiting the recycling of synaptic vesicles (Koenig, Saito, and Ikeda 1983). We controlled the flies' temperature by passing temperature-regulated water over the flies' head and front tip of their thorax while their wings remained dry and free to perform tethered flight. We monitored the flies' saccade behavior at 19ºC, when the flies should behave normally, and at 34ºC, when *shibire^{ts}* is expected to block vesicle recycling.

Upon heating, the mean saccade rate of *NP0212-GAL4*; *UAS- Shi^{ts}* flies (NP0212 > Shi^{ts}) decreased from 24.8 ± 4.9 to 2.9 ± 1.1 turns per minute (mean ± SEM). Three out of eleven flies, including the example fly shown (Figure 2.3c, bottom row), did not saccade for as long as we kept them at 34ºC. Control flies did not show this effect upon heating (Figures 2.3b-e). Flight persisted when synaptic transmission was inhibited in neurons labeled by *NP0212- GAL4*. Indeed, NP0212 > Shi^{ts} flies significantly increased their left + right wingbeat angle (L+R WBA) (Figure 2.3f), a proxy for flight power (Dickinson, Lehmann, and Chan 1998). High wingbeat angles are unlikely to prevent turning on their own, because we observed no significant correlation between average L+R WBA and saccade rate in any of the above genotypes at either temperature (data not shown). Whereas NP0212 > Shi^{ts} flies exhibited a markedly reduced saccade *rate* compared to parental controls at 34ºC, the average *size* of each saccade, when a saccade was rarely observed, was not significantly smaller than that of saccades at 19ºC (Figure 2.4a-c). In addition, the saccade magnitude of NP0212 > Shi^{ts} flies at 34ºC was not significantly smaller than those of the *UAS-Shi^{ts}* parental controls at 34ºC, although the average saccade magnitude of NP0212 > Shi^{ts} flies was 28% smaller than that of *NP0212-GAL4* control flies at 34ºC (Figure 2.4a-c).

Saccades in tethered flight are relatively fast wing movements (~350 ms duration) that ride on top of slower fluctuations of the L–R WBA signal (Figure 2.3c; green arrows indicate start of slow left turns). In addition to the observed deficit in spontaneous saccades, NP0212 > Shi^{ts} flies also stopped making these slow turns. To isolate the slower component of the flies' wing movements, we plotted the distribution of

observed wingbeat amplitudes in a low-pass filtered L–R WBA signal, which we call L–R WBA(lpf). This low-pass-filtered signal is the floor from which we detect saccades, so by definition, it excludes the saccades we defined computationally. Different flies had different median values of L–R WBA(lpf)—i.e., they sometimes had a bias to tonically turn left or right, which may be due to slight differences in the way the flies were tethered. We therefore subtracted the median from every fly's L–R WBA(lpf) distribution so we could compare each distribution's shape. When we did so, the distributions of L–R WBA(lpf) were relatively similar across all genotypes at 19ºC (Figure 2.5a), but at 34ºC, NP0212 > Shi^{ts} flies showed L–R WBA(lpf) values that were much more tightly distributed around zero than those of parental controls (Figure 2.5b). At 19ºC, we also observed a small variance drop in NP0212 > Shi^{ts} flies compared to controls (Figure 2.5a), which may be due to a small amount of *shibire^{ts}*-mediated inhibition at 19ºC.

We also took a power spectrum of each fly's L–R WBA to determine whether inhibiting NP0212 neurons decreased the power spectral density at low frequencies. When we compared the power in each frequency band between genotypes, we found that NP0212 > Shi^{ts} L–R WBA traces at 34ºC displayed significantly less power at frequencies between 0.1 and 0.316 Hz, 0.316 and 1 Hz, 1 and 3.16 Hz, and 3.16 and 10 Hz than those of control flies flying at the same temperature. At 19ºC, this effect was not detectable (Figures 2.5c-d). By both measures described above, NP0212 > Shi^{ts} flies exhibit less slow turning at 34ºC than controls.

Figure 2.3 | Inhibiting synaptic transmission in neurons targeted by *NP0212-GAL4* largely abolishes spontaneous saccades.

(**a**) Immunofluorescence of mCD8-GFP (green) and Brp (magenta) in the brain and thoracic ganglion of a NP0212 > GFP fly. Left: maximum z projection. Right: maximum z projections of three subsets in z. The scale bars represent 100 μm. (**b**) Example L–R WBA traces of spontaneous turning behavior in NP0212 > Shi^{ts} and parental control flies at 19ºC (blue) and 34ºC (orange). (**c**) Ten-minute-long example traces. Saccades are indicated by black dots. Traces are aligned to the x axis in (d). Green arrowheads indicate the approximate onset times of five example, persistent turns to the left. (**d**) Top three sections: raster plot of saccades in NP0212 > Shi^{ts} and parental controls. Every line represents an individual fly, and each saccade is indicated by a tick. Second from bottom: the average saccade rate of each genotype, binned every 30 s. Line and shaded regions indicate mean ± SEM. Bottom: temperature traces from 5 flies from each genotype overlaid. Time zero was set to when the bath hit 26ºC. (**e**) Spontaneous saccade rate of NP0212 > Shi^{ts} flies and parental controls at 19ºC (blue) and 34ºC (orange; black bars: mean ± SEM; *$p < 0.05$; Wilcoxon signed-rank test with a Bonferroni correction; n = 10–12). (**f**) Average L+R WBA in NP0212 > Shi^{ts} and parental controls at 19ºC (blue) and 34ºC (orange; n = 10–12; black bars: mean ± SEM; *$p < 0.05$; Wilcoxon signed-rank test with a Bonferroni correction. Genotypes labeled with different letters have average L+R WBA values at 34ºC that are significantly different; $p < 0.05$; Mann-Whitney U test with Bonferroni correction)

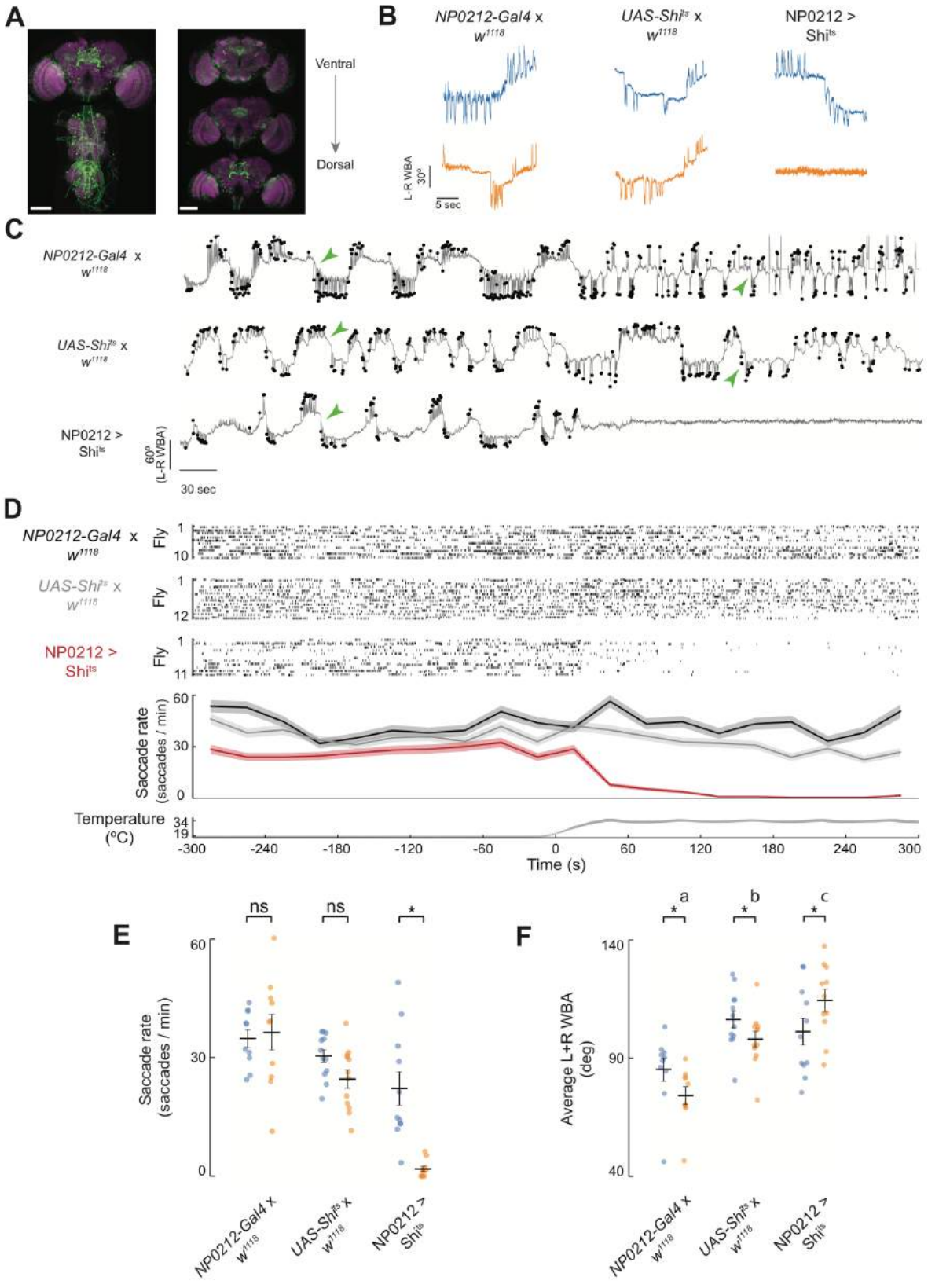
A
Ventral
Dorsal
B
NP0212-Gal4 x w1118
UAS-Shits x w1118
NP0212 > Shits
L-R WBA 30°
5 sec
C
NP0212-Gal4 x w1118
UAS-Shits x w1118
NP0212 > Shits
60° (L-R WBA)
30 sec
D
NP0212-Gal4 x w1118
UAS-Shits x w1118
NP0212 > Shits
Fly
Saccade rate (saccades / min)
Temperature (°C)
Time (s)
E
Saccade rate (saccades / min)
ns
ns
*
NP0212-Gal4 x w1118
UAS-Shits x w1118
NP0212 > Shits
F
Average L+R WBA (deg)
a
b
c
*
*
*
NP0212-Gal4 x w1118
UAS-Shits x w1118
NP0212 > Shits

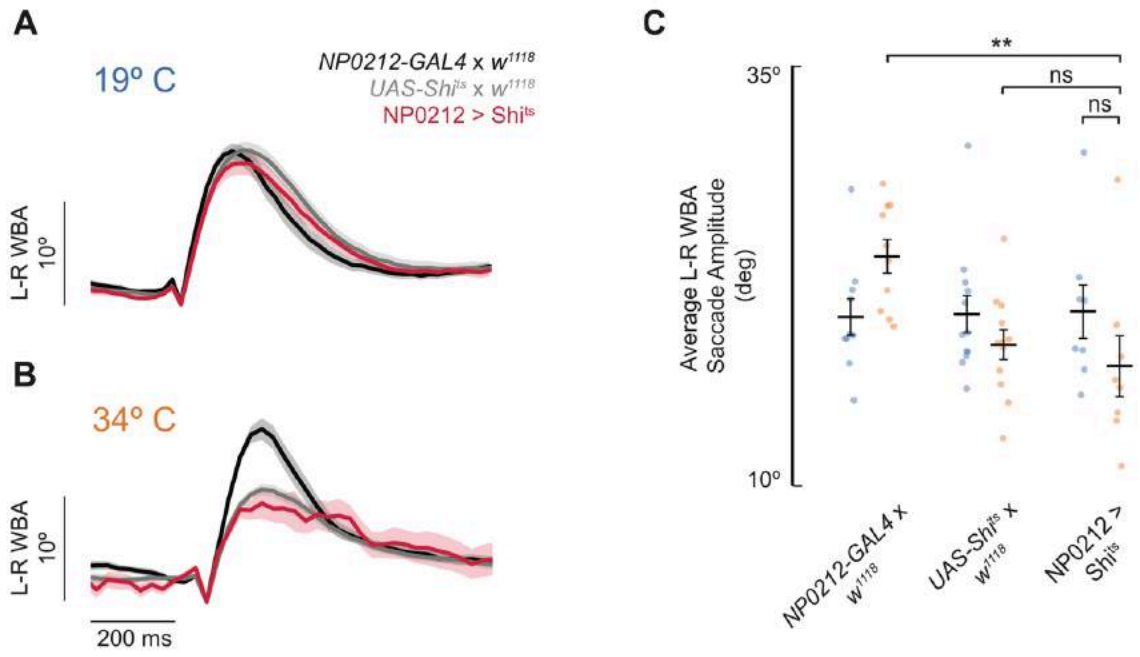

Figure 2.4 l Inhibiting synaptic transmission in neurons targeted by *NP0212-GAL4* does not significantly change the average saccade size relative to controls.

(**a**) Average saccade at 19ºC, aligned to turn onset. Line and shaded regions: mean ± SEM. (black: *NP0212-GAL4* x w^{1118}, n = 1504 turns; gray: *UAS-Shi*^{ts} x w^{1118}, n = 1600 turns; red: NP0212 > Shi^{ts}, n = 1035 turns). (**b**) Same as in (a), but at 34ºC. (black: *NP0212-GAL4* x w^{1118}, n = 1514 turns; gray: *UAS-Shi*^{ts} x w^{1118}, n = 1543 turns; red: NP0212 > Shi^{ts}, n = 108 turns). (**c**) Average saccade amplitude of NP0212 > Shi^{ts} flies and parental controls at 19ºC (blue) and 34ºC (orange) (n = 10-12, black bars: mean ± SEM. Between genotypes: ** $p < 0.01$, Wilcoxon Signed Rank Test with a Bonferroni Correction. Within genotypes a Mann-Whitney U-test with a Bonferroni Correction was employed.)

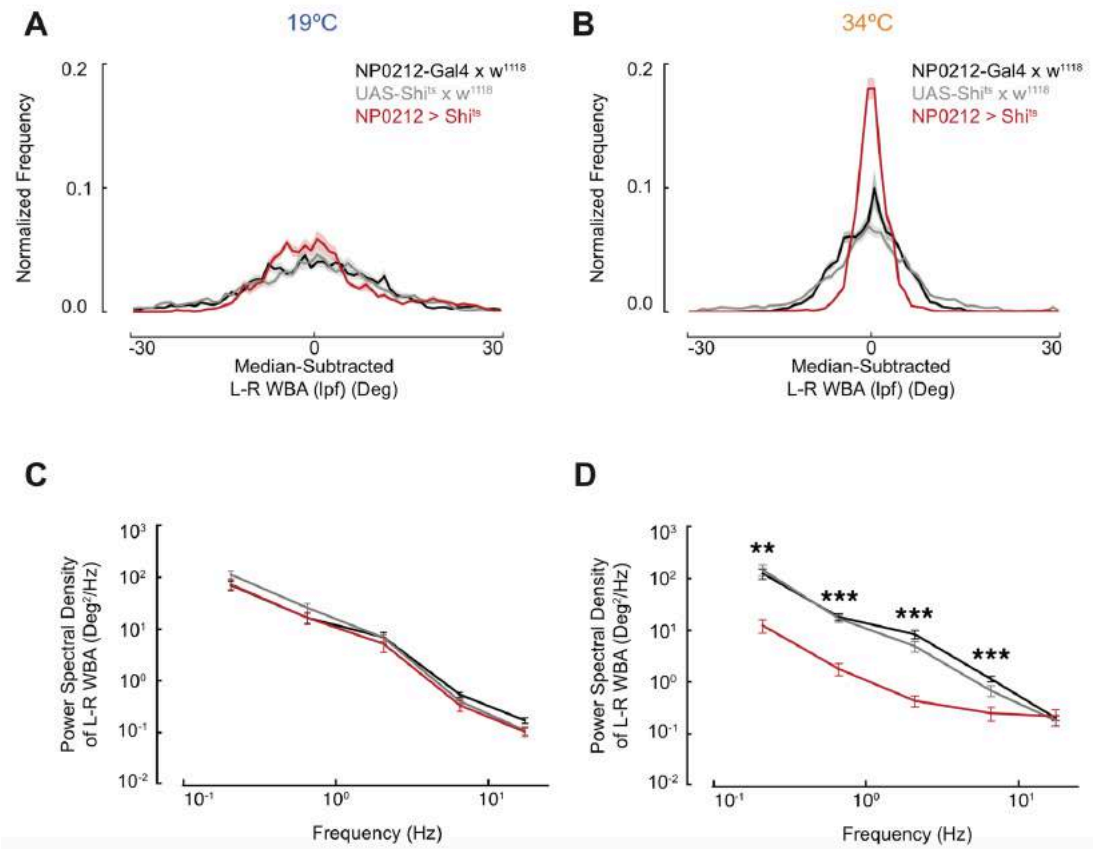

Figure 2.5 I Slow turns are abolished by inhibiting synaptic transmission in neurons targeted by *NP0212-GAL4.*

(**a**) Distribution of L–R WBA(lpf) during flight at 19ºC for NP0212 > Shi^{ts} (n = 11 flies, red) and parental controls (*NP0212-GAL4* x *w^{1118}*; n = 10; black and *UAS-Shits* x *w^{1118}*; n = 12; gray). Line and shaded region indicate mean ± SEM. (**b**) Same as (a) but at 34ºC. NP0212 > Shi^{ts} flies' L–R WBA(lpf) distributions display lower variance than both parental controls at both temperatures; $p <<< 0.001$; Levene's test of variance. (**c**) Average power spectra of the L–R WBA of NP0212 > Shi^{ts} flies (n = 11) and parental controls (*NP0212-GAL4* x *w^{1118}*; n = 10 and *UAS-Shi^{ts}* x *w1118*; n = 12, colors as above) at the 19ºC, binned between half-powers of ten. Spectra are plotted on a $\log_{10}$-$\log_{10}$ scale. Mean ± SEM. (**d**) Same as (c) but at 34ºC. Significance asterisks indicate that NP0212 > Shi^{ts} is significantly different from both parental controls; ***$p < 0.001$; **$p < 0.01$; Mann-Whitney U test.

To determine whether the suppression of spontaneous turning in NP0212 could be observed at room temperature and with a different synaptic silencing reagent, we compared the spontaneous turning rate of flies in which *NP0212-GAL4* drove expression of tetanus toxin light chain (TeTxLC-active), which blocks synaptic transmission by cleaving synaptobrevin (Sweeney *et al* 1995), to the turning rate of flies that expressed an inactive form of the protein (TeTxLC-inactive). We made an effort to restrict tetanus toxin transcription to the 24 hours immediately prior to behavioral testing by using a temperature-sensitive variant of GAL80 (*GAL80^{ts}*), an inhibitor of *GAL4* (Suster *et al.* 2004), expressed in all cells under the control of the tubulin promotor (McGuire *et al.* 2003). NP0212 > TeTxLC-active flies displayed a marked reduction in saccade rate when compared to NP0212 > TeTxLC-inactive controls (Figures 2.6a-b), corroborating the results seen with *shibire^{ts}*. Slow turning was also reduced in NP0212 > TeTxLC-active flies compared to controls (Figures 2.6c-d).

Figure 2.6 | Inhibiting synaptic transmission in neurons targeted by *NP0212-GAL4* with Tetanus Toxin Light Chain markedly reduces the rate of spontaneous saccades and slow turns.

(**a**) Example traces of flies of the indicated genotype flying under blank screen conditions. Saccades were algorithmically detected and are indicated by black dots. (**b**) Spontaneous turning rate of NP0212 > TeTxLC-active flies (red) and NP0212 > TeTxLC-inactive controls (black). (Black bars: mean ± SEM, n = 10-12, *** $p < 0.001$, Mann-Whitney U-Test). (**c**) Distribution of L–R WBA(lpf) during flight for NP0212 > TeTxLC-Active (n = 10 flies, red) and NP0212 > TeTxLC-Inactive controls (n = 12 flies, black). Shaded regions represent 95% CI, calculated by multiplying 1.96 by the SEM across flies. NP0212 > TeTxLC-Active flies display lower variance than controls, $p <<< 0.001$, Levene's test of variance. (**d**) Average power spectra of the L–R WBA of NP0212 > TeTxLC-active (n = 12) and NP0212 > TeTxLC-active controls (n = 10, colors as above), binned between half-powers of ten. Spectra are plotted on a $\log_{10}$-$\log_{10}$ scale. Mean ± SEM.

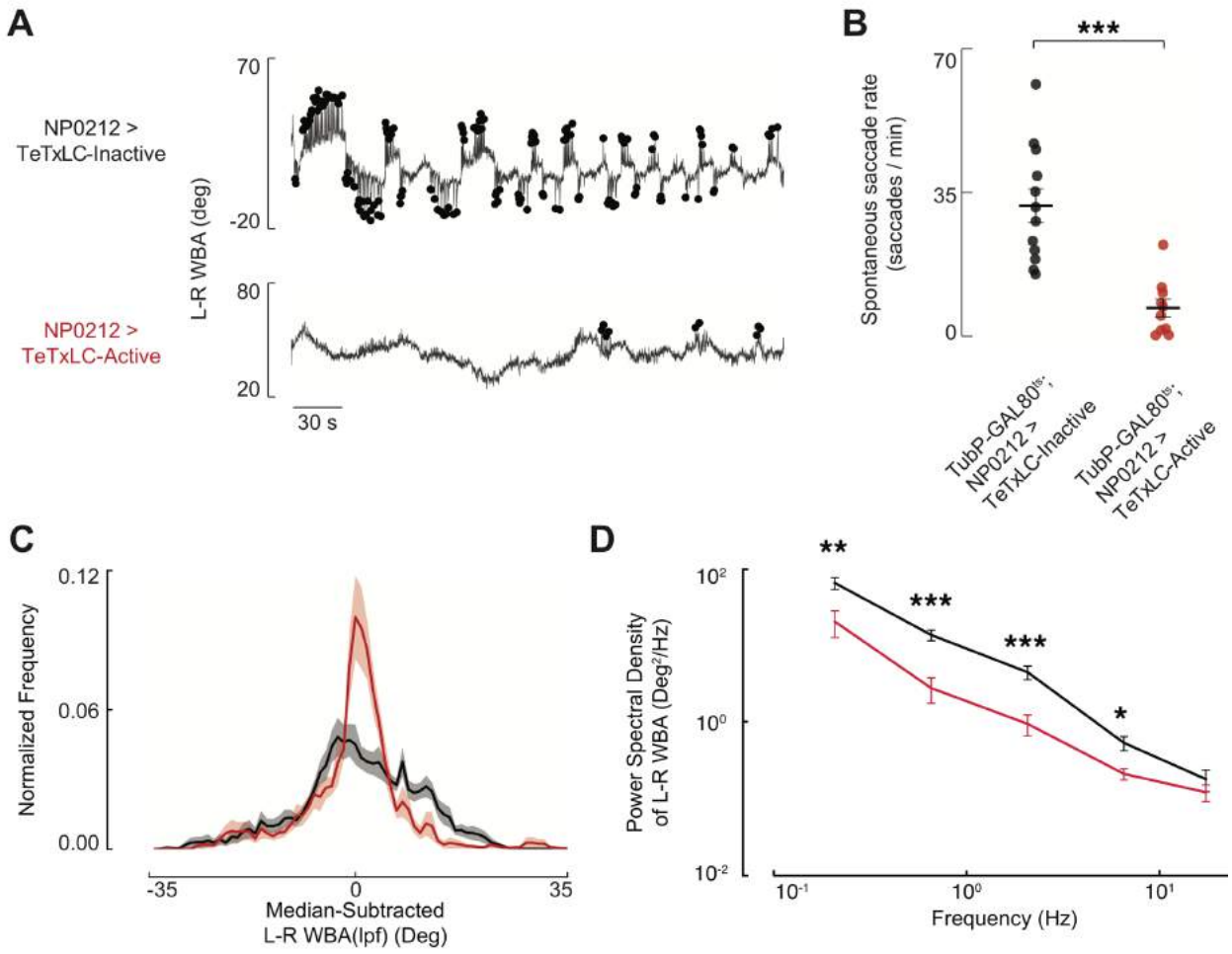
A
NP0212 >
TeTxLC-Inactive
NP0212 >
TeTxLC-Active
L-R WBA (deg)
70
-20
80
20
30 s
B
***
Spontaneous saccade rate
(saccades / min)
70
35
0
TubP-GAL80ts;
NP0212 >
TeTxLC-Inactive
TubP-GAL80ts;
NP0212 >
TeTxLC-Active
C
Normalized Frequency
0.12
0.06
0.00
-35
0
35
Median-Subtracted
L-R WBA(lpf) (Deg)
D
**
***
***
*
Power Spectral Density
of L-R WBA (Deg²/Hz)
10²
10⁰
10⁻²
10⁻¹
10⁰
10¹
Frequency (Hz)

Normal synaptic activity in cells targeted by *NP0212-GAL4* Is dispensable for visually evoked turns

Did inhibiting synaptic transmission in neurons targeted by *NP0212-GAL4* generally paralyze the flies' ability to steer with their wings? In *Drosophila*, the power muscles that generate the mechanical force necessary for flight are distinct from the muscles that drive steering maneuvers (Dickinson 2005), so one can easily imagine such a possibility. To test whether NP0212 > Shi^{ts} flies were still capable of making both rapid and persistent wing movements, we tested NP0212 > Shi^{ts} flies' responses to visual stimuli that elicit such responses: rapidly expanding (looming) discs and persistently rotating (optomotor) gratings, respectively.

Flies in both free and tethered flight typically respond to looming visual stimuli by performing a saccade away from the expanding stimulus (Tammero and Dickinson 2002b; Censi *et al.* 2013; Muijres *et al.* 2014). NP0212 > Shi^{ts} flies and parental controls responded to our expanding disc stimuli at a relatively consistent delay after the stimulus reached a critical size, and many flies responded bi-modally to looms from the center (data not shown), phenomena which are often considered to be characteristic of genuine loom responses (as opposed to, say, optomotor responses to the edge of the expanding disc) (Gabbiani, Krapp, and Laurent 1999; Bender and Dickinson 2006b). Notably, NP0212 > Shi^{ts} flies were able to execute these escape responses at the restrictive temperature of 34^{o}C (Figure 2.7a). The overall shape of the loom response seemed quite normal, even though these responses were assessed directly after a long period of flight with a uniformly lit screen at 34^{o}C, during which the same flies had

performed virtually no spontaneous saccades (Figures 2.7c-d replicate Figures 2.3b and 2.3e in flies that performed loom-evoked turns immediately afterward).

Moreover, the average size of the loom response in NP0212 > Shi^{ts} flies did not significantly decrease compared to the same genotype at 19ºC (Figure 2.7b; $p > 0.05$; Wilcoxon signed-rank test). NP0212 > Shi^{ts} flies also did not display significantly smaller loom responses than those of one of the parental controls at 34ºC (Figure 2.7b; $p > 0.05$; Mann-Whitney U test with a Bonferroni correction for NP0212 > Shi^{ts} and *NP0212-GAL4/+*), although their responses were significantly smaller than the other control (*UAS-Shi^{ts}/+*), which may indicate that genetic background may have a small effect on the magnitude of this behavioral response.

Figure 2.7 | Flies in which neurons targeted by *NP0212-GAL4* have impaired synaptic transmission can still perform loom-evoked saccades.

(**a**) Responses to looming discs expanding from the left (1st and 3rd rows) and right (2nd and 4th rows) of w^+; NP0212 > Shi^{ts} and parental controls (n = 8 flies, 10 trials per fly). In the top two rows, the thick line indicates the mean across trials and thin lines represent individual trials. In the bottom two rows, the thick line indicates the mean across flies and thin lines represent individual fly means. Arrowheads in 3rd column indicate trials with weak responses (see main text). (**b**) Average loom response in w^+; NP0212 > Shi^{ts} and parental controls (black bars: mean ± SEM) at 19ºC and 34ºC; each dot represents one fly. (**c**) Example traces of w^+; NP0212 > Shi^{ts} and parental control flies flying at 19ºC (blue) and 34ºC (orange) in the context of a uniformly lit screen immediately preceding the loom trials in (a). (**d**) Spontaneous turning rate of w^+; NP0212 > Shi^{ts} flies and parental controls at the 19ºC (blue) and 34ºC (orange) (black bars: mean ± SEM, n = 8, * $p < 0.05$, Wilcoxon signed rank test.

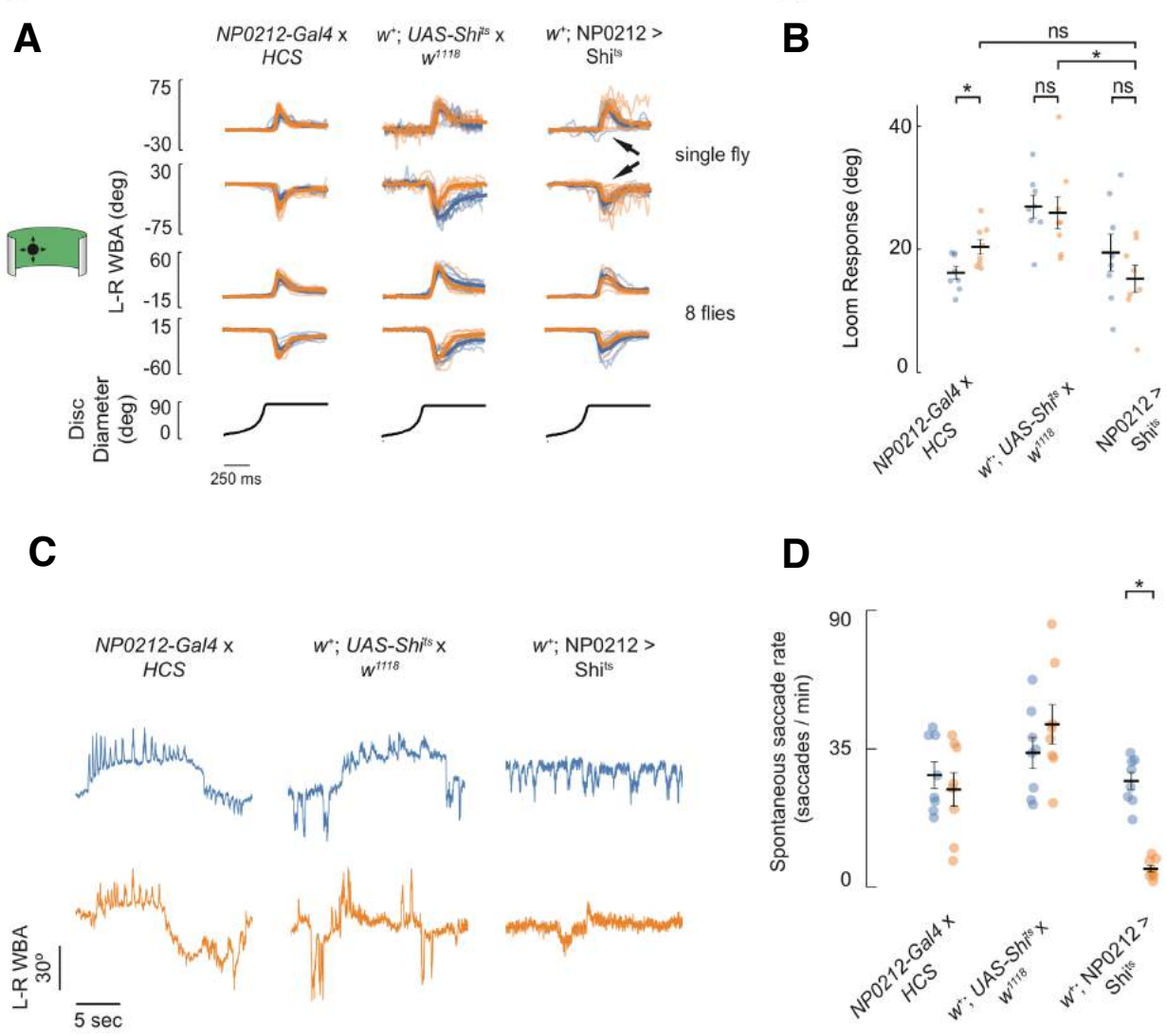
A
NP0212-Gal4 x HCS
w+; UAS-Shits x w1118
w+; NP0212 > Shits
75
-30
30
-75
60
-15
15
-60
L-R WBA (deg)
90
0
Disc Diameter (deg)
250 ms
single fly
8 flies
B
ns
*
ns
*
ns
40
20
0
Loom Response (deg)
NP0212-Gal4 x HCS
w+; UAS-Shits x w1118
NP0212 > Shits
C
NP0212-Gal4 x HCS
w+; UAS-Shits x w1118
w+; NP0212 > Shits
L-R WBA
30°
5 sec
D
*
90
35
0
Spontaneous saccade rate (saccades / min)
NP0212-Gal4 x HCS
w+; UAS-Shits x w1118
w+; NP0212 > Shits

Whereas NP0212 > Shi^{ts} flies showed grossly normal loom responses, we noticed that, on some trials, they did not seem to respond strongly to the loom (Figure 2.7a, arrows)—unlike control flies, which typically responded strongly on every trial. Analyzing this finding further, we found that, after ~10 loom trials at 34ºC, loom responses of NP0212 > Shi^{ts} flies began to weaken until there was almost no behavioral response by the 30th trial. Control animals showed strong responses throughout 30 loom trials. However, when we minimized *shibire^{ts}* expression in certain visual and central complex neurons by driving GAL80 expression under the control of the R83H12 enhancer fragment *R83H12-GAL80*) (Aso *et al.* 2014) (Figure 2.8a), we were able to rescue this depletion of the loom response while preserving the effect on spontaneous saccades (Figures 2.8b-c). That is, the spontaneous saccade rate of NP0212-GAL4, R83H12-GAL80 > Shi^{ts} flies was still markedly reduced at 34ºC, yet these flies responded reliably to looming stimuli for as long as we measured, even after 30 trials (Figure 2.8c). The spontaneous turn rate of NP0212-GAL4, R83H12-GAL80 > Shi^{ts} flies was barely but significantly higher than that of NP0212 > Shi^{ts} flies (Figure 2.8b), a difference that vanishes when a single outlier fly is excluded. However, even with the outlier included, the vast majority of the spontaneous turning deficit NP0212-GAL4, R83H12-GAL80 > Shi^{ts} is still evident. We note that the elimination of loom responses in NP0212 > Shi^{ts} flies was tied to the retinotopic location in which loom stimuli were repeatedly presented rather than to the direction in which the flies turned over and over again (data not shown). Taken together, we interpret these results to mean that the depletion of the loom response in NP0212 > Shi^{ts} flies is due to the expression of

shibire^{ts} in a retinotopic visual processing neuron class, which is involved in responding repeatedly to expansion, likely to be located in either the visual system or central complex.

Figure 2.8 | *83H12-GAL80* rescues the progressive loom response depletion in *NP0212* while minimally affecting the rate of spontaneous saccades.

(**a**) Immunofluorescence of mCD8-GFP (green) and *Brp* (purple) in the brain and thoracic ganglion of flies crossed to the indicated genotype. White arrows indicate path of haltere afferent neurons in the thoracic ganglion and their characteristic terminals in the subesophageal zone. (**b**) Spontaneous turning rate of flies of the indicated genotype at 19ºC (blue) and 34 ºC (orange) temperatures. (n = 9-15. Black bars: mean ± SEM. Within genotype: *** $p < 10^{-8}$, ** $p < 0.01$, Wilcoxon Signed Rank Test. Between genotypes: * $p < 0.05$, Mann-Whitney U Test of saccade rate at 34ºC). (**c**) Average response of flies of the indicated genotypes to expanding discs centered to the left (top row) or the right of the fly (bottom row) separated by block. Blocks of 10 trials are delineated by color (see legend upper right). Line and shaded region: mean ± SEM, n = 7-9 flies. Without the *R83H12-GAL80* transgene, NP0212 flies showed a gradual diminishment of loom-evoked behavioral responses over 30 trials. With the *R83H12-GAL80* transgene, flies responded to loom stimuli for as long as we could measure even though they showed very few spontaneous saccades.

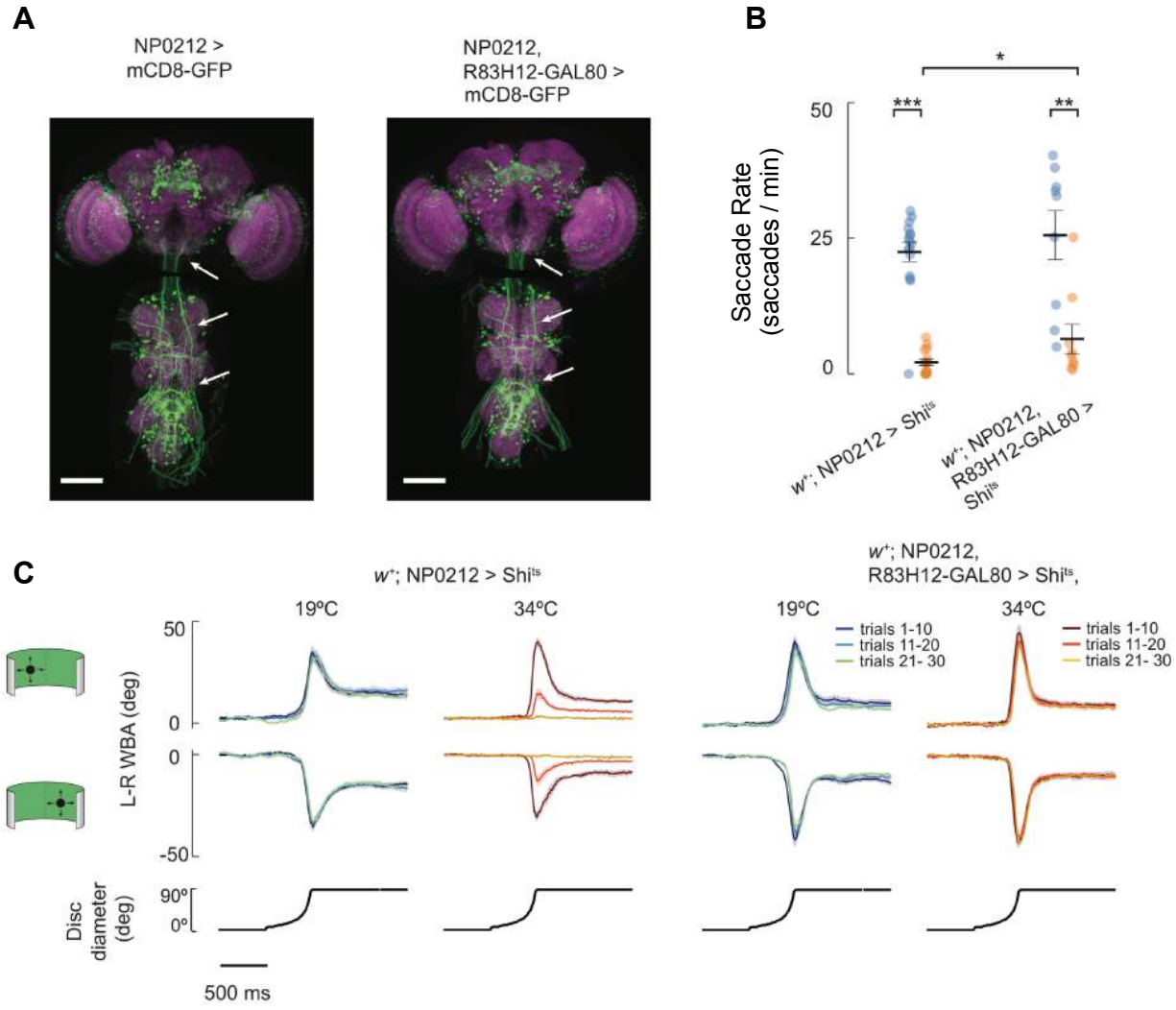
A
NP0212 >
mCD8-GFP
NP0212,
R83H12-GAL80 >
mCD8-GFP
B
Saccade Rate
(saccades / min)
50
25
0
***
**
*
w+; NP0212 > Shits
w+; NP0212,
R83H12-GAL80 >
Shits
C
w+; NP0212 > Shits
w+; NP0212,
R83H12-GAL80 > Shits,
19ºC
34ºC
19ºC
34ºC
trials 1-10
trials 11-20
trials 21- 30
trials 1-10
trials 11-20
trials 21- 30
L-R WBA (deg)
50
0
0
-50
Disc
diameter
(deg)
90º
0º
500 ms

In addition to rapid, spontaneous saccades, persistent turns were also affected in NP0212 > Shi^{ts} flies. To test whether this effect could be explained by a general inability of NP0212 > Shi^{ts} flies to tonically turn their wings, we tested classical, wing optomotor responses to coherent wide-field visual motion (in our experiment, a drifting vertically oriented square-wave grating) presented for 3 s. Flies generally respond to horizontally drifting gratings by turning tonically in the direction of motion. These responses were preserved in NP0212 > Shi^{ts} flies; indeed, the response to this optomotor stimulus increased with respect to the same flies at 19ºC and with respect to parental controls at 34ºC (Figures 2.9a-b). Whereas the cause for the increase in optomotor-response magnitude in NP0212 > Shi^{ts} is not clear, these observations demonstrate that the NP0212 > Shi^{ts} flies can perform strong, tonic wing steering responses even while they barely perform any spontaneous tonic turns. Together, these experiments demonstrate the existence of neural processes that are required for the execution of spontaneous tonic turns and high rates of spontaneous saccades but which are dispensable for generating loom-evoked and optomotor flight turns in *Drosophila*.

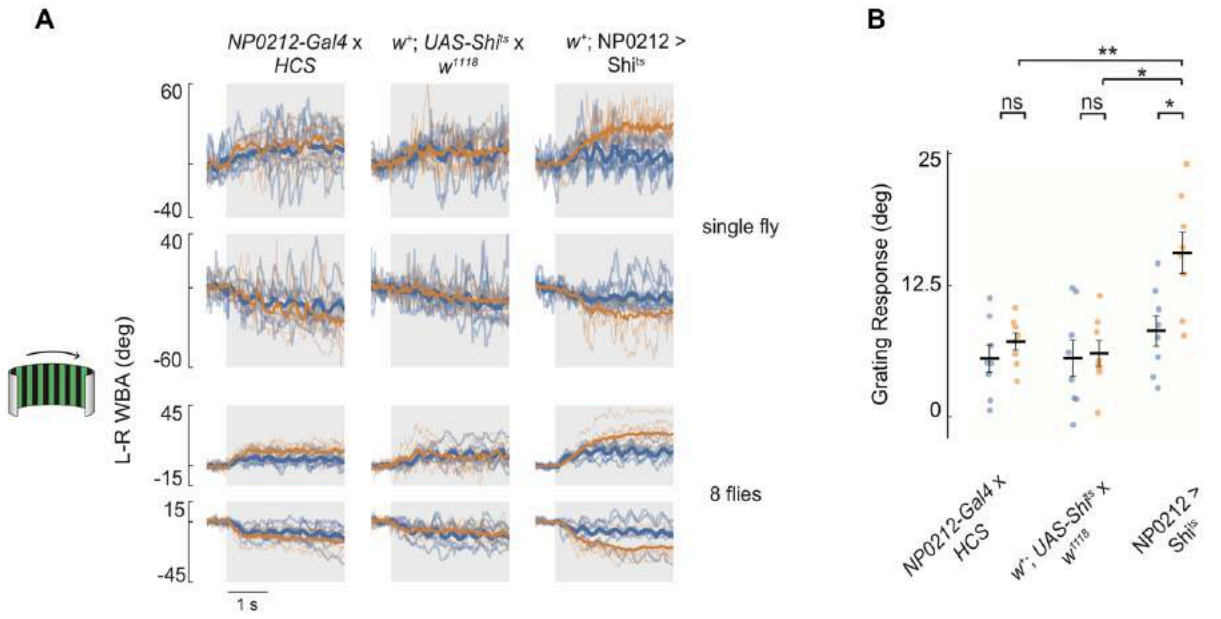

Figure 2.9 l Flies in which neurons targeted by *NP0212-GAL4* have impaired synaptic transmission can still perform optomotor responses.

(**a**) Average responses to horizontally drifting grating to the right (1st and 3rd rows) and left (2nd and 4th rows) in w^+; NP0212 > Shi^{ts} and parental controls (n = 8 flies, 10 trials per fly). In the top two rows, the thick line indicates the mean across trials and thin lines represent individual trials. In the bottom two rows, the thick line indicates the mean across flies and thin lines represent individual fly means. (**b**) Average grating response in w^+; NP0212 > Shi^{ts} and parental controls (black bars: mean ± SEM) at 19ºC and 34ºC; each dot represents one fly. Blue, 19ºC; orange, 34ºC. In all traces, gray rectangles denote periods in which the visual stimulus was displayed. * $p < 0.05$; ** $p < 0.01$; Mann-Whitney U test with a Bonferroni correction.

The NP0212 spontaneous turning phenotype is most likely mediated by Cha$^+$ neurons in the thoracic ganglion

NP0212-GAL4 drives expression in a large set of neurons spanning the visual lobes, the central complex, the mushroom bodies, and other regions of the brain and thoracic ganglion (Figure 2.3a). To gain a better handle on which cells in NP0212 might be required for the animal to execute spontaneous saccades, we co-expressed GAL80 transgenes driven by a variety of promotors, assessing the identity of the cells whose GAL4 expression was minimized or eliminated by crossing each GAL80 line to *NP0212-GAL4; UAS-mCD8-GFP* (NP0212 > GFP) (Figure 2.10a) and assessing the behavioral effect of minimizing the expression of GAL4 by measuring the spontaneous saccade rates of the NP0212, GAL80 > Shi^{ts} flies.

To test whether the spontaneous saccade defect in NP0212 was caused by neurons—rather than glia or muscles, for example—we crossed NP0212 > Shi^{ts} flies to *elav-GAL80*. *Elav* is a gene expressed ubiquitously in neurons (Yang *et al.* 2009) and, as expected, *elav-GAL80* eliminated transgene expression in the brain and thoracic ganglion while correspondingly rescuing the spontaneous saccade deficit rescuing the spontaneous saccade deficit (Figures 2.10a-b; 19ºC versus 34ºC; $p > 0.05$; Wilcoxon signed-rank test).

To ask whether the neurons targeted by NP0212-GAL4 required for spontaneous saccades reside in the brain or in the thoracic ganglion, we crossed NP0212 > Shi^{ts} to *tsh-GAL80*. *Tsh* (*teashirt*) is widely expressed by neurons in the thoracic ganglion, with nearly no expression in the head (Röder, Vola, and Kerridge 1992). As expected, in

NP0212, tsh-GAL80 > GFP flies, GFP was expressed strongly in the brain, whereas it was virtually eliminated from the thoracic ganglion (Figure 2.10a). *Tsh-GAL80* rescued the spontaneous saccade defect (Figure 2.10b; 19ºC versus 34ºC; $p > 0.05$; Wilcoxon signed-rank test), suggesting that the cells required for spontaneous turning in NP0212 reside in the thoracic ganglion. We note that the NP0212, *tsh-GAL80* > Shi^{ts} flies showed more fly-to-fly variability in saccade rates than wild-type animals. This observation suggests that neurons whose expression of the *teashirt* gene is variable across individuals might contribute to this phenotype. Because the number of neurons targeted by NP0212 is so large, it was not feasible to examine the brains of NP0212, *tsh-GAL80* > Shi^{ts} flies and to determine (by co-expression of GFP, for example) whether different cells were labeled in flies that did or did not exhibit the behavioral rescue.

Motor neurons in *Drosophila* are glutamatergic and express the vesicular glutamate transport protein gene *vglut* (Mahr and Aberle 2006). To test whether NP0212 > Shi^{ts} saccade silencing was due to the inhibition of a steering motor neuron specific for spontaneous saccades, we crossed NP0212 > Shi^{ts} flies to *vglut-GAL80* flies. As expected, NP0212, *vglut-GAL80* > GFP flies showed reduced fluorescence and fewer large cell bodies in the lateral metathoracic ganglion, a region known to contain flight motor neurons (Mahr and Aberle 2006) (Figure 2.10a). NP0212, *vglut-GAL80* > Shi^{ts} flies still showed significantly lower spontaneous turning rates at 34ºC than at 19ºC. However, the spontaneous turning rate at 34ºC was significantly higher in NP0212, *vglut-GAL80* > Shi^{ts} than in NP0212 > Shi^{ts} flies, although the effect size was

only 32% smaller than that of NP0212 > Shi^{ts} flies (61.2% versus 90.3% reduction in saccade rate) (Figure 2.10b). Such a mild rescue phenotype with GAL80 is difficult to interpret, as it may result from leaky expression of GAL80 in non-glutamatergic neurons or from partial contribution of glutamatergic neurons to the phenotype. However, these data suggest most of the NP0212 turning phenotype is not mediated by glutamatergic neurons.

In contrast, *cha-GAL80*, which drives expression in cholinergic neurons in *Drosophila* (Zhou, Rao, and Rao 2008), rescued the NP0212 spontaneous saccade defect in its entirety (Figure 2.10b; 19ºC versus 34ºC; $p > 0.05$; Wilcoxon signed-rank test). The precise identity of the Cha^{+} NP0212 neurons that most likely mediate the phenotype is ambiguous, because the majority of neurons labeled by NP0212 > GFP were subtracted by *cha-GAL80*, including all but the largest cells in the thoracic ganglion, which are putative glutamatergic motor neurons (Figure 2.10a).

We silenced neurons in 38 additional GAL4 lines that targeted subsets of the nervous system labeled in NP0212. Whereas an additional 3 out of 38 GAL4 lines showed significant decreases in saccade rates (Figures 2.11a-b; lines 2–4 from left; Student's t test; $p < 0.05$), none of these more specific driver lines fully recapitulated the nearly complete elimination of saccades associated with silencing cells targeted by NP0212.

Figure 2.10 l The neurons that mediate the spontaneous saccade phenotype in *NP0212 > Shi^{ts}* flies are likely to be *Cha^{+}* neurons in the thoracic ganglion

(**a**) Immunofluorescence of mCD8-GFP (green) and Brp (magenta) in the indicated driver lines in the brain and thoracic ganglion. (**b**) Mean spontaneous turning rate of flies of the indicated genotype at 19ºC (blue) and 34ºC (orange); each dot represents one fly. (Black bars: mean ± SEM; n = 7–18. Genotypes labeled with different letters have saccade rates that are significantly different at 34ºC; Mann-Whitney U test with Bonferroni correction. * $p < 0.05$; *** $p < 0.001$; Wilcoxon signed-rank test.) An outlier NP0212 > Shi^{ts}, *elav-GAL80* fly that had a spontaneous saccade rate of 91.6 turns/min and an outlier NP0212 > Shi^{ts}, *tsh-GAL80* fly that had a spontaneous saccade rate of 89.4 turns/min at 34ºC are not shown on the plot.

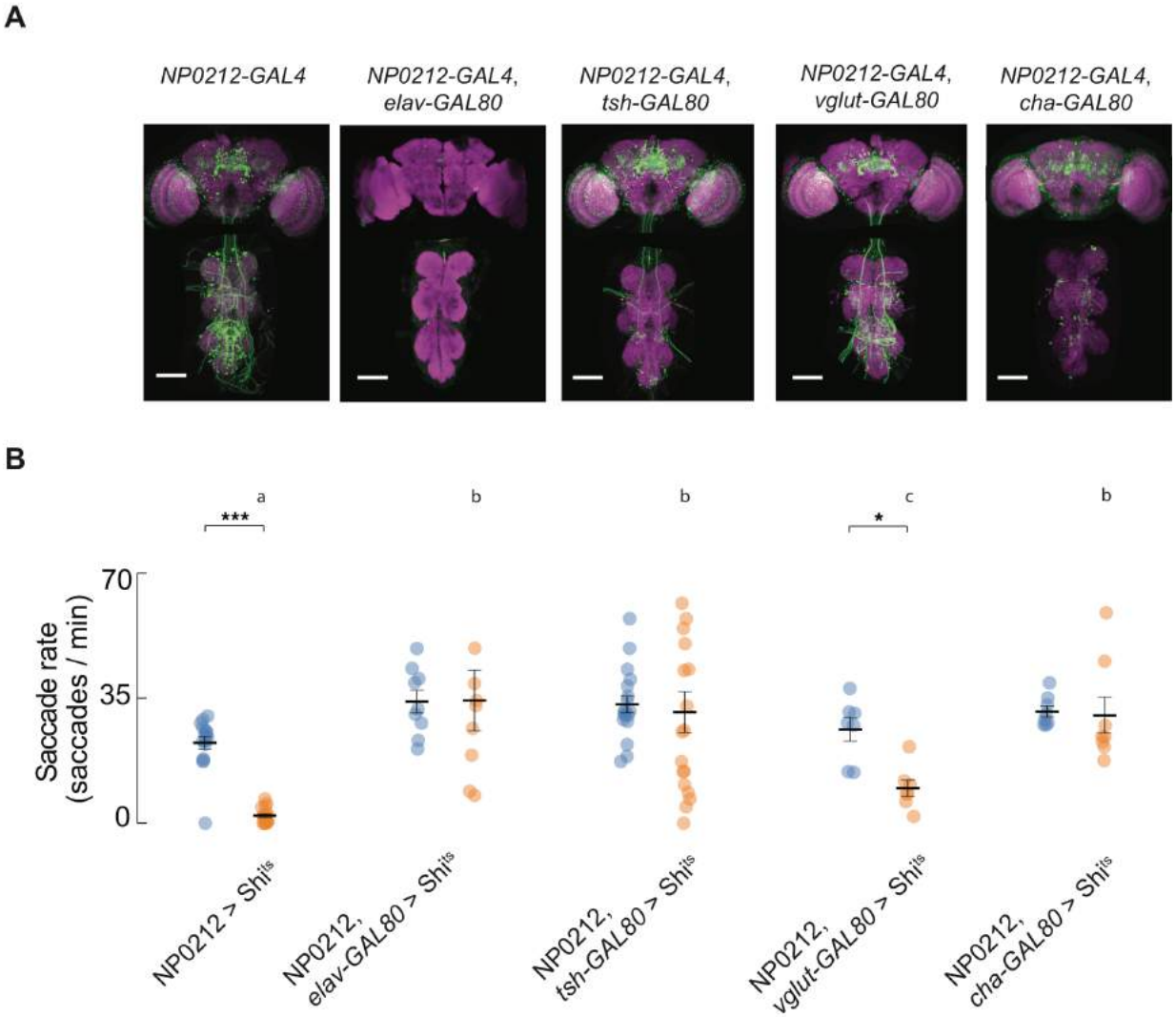
A
NP0212-GAL4
NP0212-GAL4, elav-GAL80
NP0212-GAL4, tsh-GAL80
NP0212-GAL4, vglut-GAL80
NP0212-GAL4, cha-GAL80
B
Saccade rate (saccades / min)
70
35
0
a
b
b
c
b
***
*
NP0212 > Shi^ts
NP0212, elav-GAL80 > Shi^ts
NP0212, tsh-GAL80 > Shi^ts
NP0212, vglut-GAL80 > Shi^ts
NP0212, cha-GAL80 > Shi^ts

Figure 2.11 | Expressing *shibire^{ts}* in 38 additional *GAL4* lines does not recapitulate the abolishment of spontaneous saccades observed in NP0212 > Shi^{ts} flies.

(**a**) Box plots showing the spontaneous turning rate at 34ºC as a percentage of the turning rate at 19ºC. The genotype median is indicated by the thick black horizontal line. Box boundaries show the first and third quartiles. Whiskers are 1.5 times the length of the inter-quartile range. (**b**) Bars indicate average turning rates of NP0212 > Shi^{ts} and the other 38 GAL4 lines at 19ºC (blue) and 34ºC (orange). Black bars indicate SEM. Genotypes are sorted by the median relative turning rate.

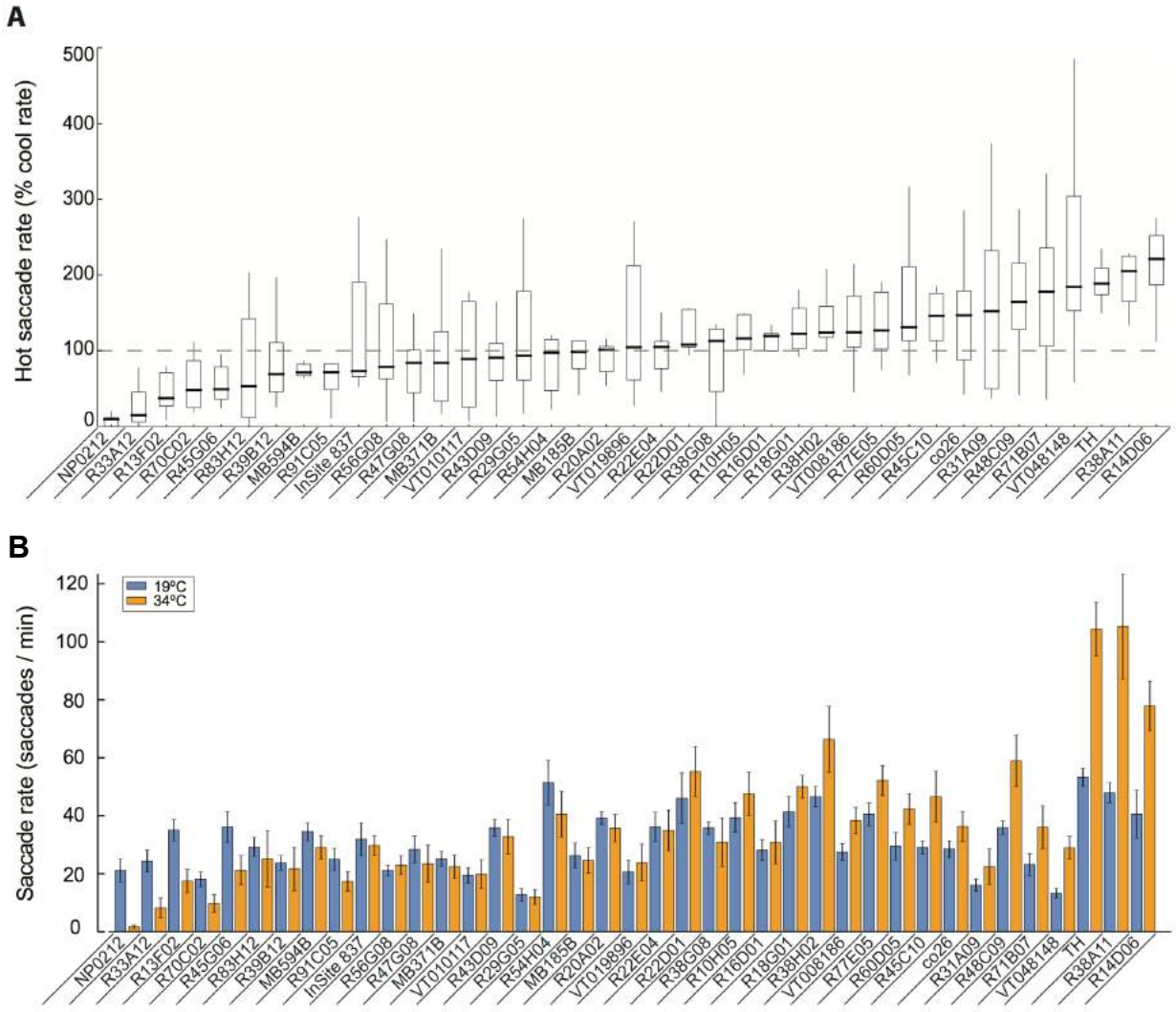
A
Hot saccade rate (% cool rate)
500
400
300
200
100
0
NP0212
R33A12
R13F02
R70C02
R45G06
R83H12
R39B12
MB594B
R91C05
InSite 837
R56G08
R47G08
MB371B
VT010117
R43D09
R29G05
R54H04
MB185B
R20A02
VT019896
R22E04
R22D01
R38G08
R10H05
R16D01
R18G01
R38H02
VT008186
R77E05
R60D05
R45C10
co26
R31A09
R48C09
R71B07
VT048148
TH
R38A11
R14D06
B
Saccade rate (saccades / min)
19ºC
34ºC
120
100
80
60
40
20
0
NP0212
R33A12
R13F02
R70C02
R45G06
R83H12
R39B12
MB594B
R91C05
InSite 837
R56G08
R47G08
MB371B
VT010117
R43D09
R29G05
R54H04
MB185B
R20A02
VT019896
R22E04
R22D01
R38G08
R10H05
R16D01
R18G01
R38H02
VT008186
R77E05
R60D05
R45C10
co26
R31A09
R48C09
R71B07
VT048148
TH
R38A11
R14D06

Chapter 3 | The angular resolution of the E-PG heading signal approaches that of the early visual system, and the E-PG heading signal in darkness can show a persistent offset from the E-PG heading estimate in the context of a visible landmark.

When a fly walks on an air cushioned ball in a virtual environment or in the dark, E-PG neurons show 2-3 equally spaced bumps of calcium activity along the protocerebral bridge that can be visualized by 2-photon imaging of GCaMP and whose position along the bridge correlates with the fly's angular heading (Figure 1.1d-f). In other words, the phase of this periodic signal changes in concert with left/right rotations of the fly on the ball. The E-PG phase moves at times and is stable at others. For example, when the fly rotates on the ball, as it does in Figure 1.1e, the E-PG phase moves smoothly along the protocerebral bridge. Conversely, when the fly stands still on the ball, as in Figure 1.1f, the E-PG phase can remain constant for minutes (i.e., the bumps in the bridge stay at a stable location for minutes), even in the absence of any visual input (Seelig and Jayaraman 2015). It has been hypothesized that E-PG neurons can be modeled as a ring attractor network (Kim *et al.* 2017). The resolution of this neural population to represent angular shifts in a visual landmark and/or the number of stable states in which E-PG activity can reside may have some bearing on the network's ability to represent the fly's heading with accuracy and precision.

In this chapter, I show two things. First, I use the E-PG phase response to abrupt shifts in the position of visual landmarks to show that the E-PG phase can resolve changes in heading as small as 5.625º in the context of a visual landmark, the finest resolution which our experiments allowed us to detect.

Second, I show that there is a latent heading angle stored in the E-PG system. This angle becomes evident when one turns off all visual input while the fly stands completely still. In such an experiment, one observes, surprisingly, that the E-PG phase signal relaxes to an angle that differs, often quite substantially, from the one carried by E-PGs when the visual landmark was present in front of the stably standing fly. This darkness-specific angle acts as a stable point in the system for as long as we have measured (at least tens of seconds) and seems to function like a simple working memory in the system.

As a framework for understanding this second result, I mention here one possible interpretation (which I also elaborate upon in the Discussion). E-PGs are known to make use of both angular velocity cues (e.g., proprioceptive cues) and positional visual cues (e.g., a bright bar) to inform their angular heading estimate (Seelig & Jayaraman, 2015; Green and Maimon 2018). It seems likely that the positional and integrating input streams to the E-PGs need not always agree on their assessment of which way the fly is currently heading. How might the E-PGs arbitrate which stream to attend to in the case of such a disagreement? When a visual input that rotates in lock step with the fly's rotational behavior is available (such as the sun or moon), it seems sensible that this input would dominate the E-PG heading estimate; if one can see which way one is

heading, one ought to trust one's sight. However, strong visual inputs are not always informative of one's heading in the world, for example when a fly locomotes in a swarm of conspecific insects that rapidly move this way and that on the retina. In this case, the E-PG heading estimate might be more accurate if it integrates the fly's own turning movements, rather than anchor this estimate to the azimuthal position of any one object. Thus, when I turn the visual input off in my experiments, the E-PG system might be reverting to a best guess of the animal's heading from the integration process. My results on the latent angle, which I describe in more depth below, suggest – if this interpretation is correct – that the integration-system's estimate of the fly's heading may be preserved as a persistent angular value in the central complex, *independently* of the E-PGs current calcium dynamics, for at least a few seconds. In this interpretation, when I turn off the visual bar presented to a standing fly, the E-PG heading signal relaxes to the integrator's angular estimate, which is close to, but not always exactly the same as, the visual-position based estimate. Other interpretations of the data are also possible, but I hope that this exposition might help calibrate the reader to one way of thinking about the results to follow.

Abruptly shifting the position of an angular landmark while the fly stands still causes the E-PG phase to rotate

When a tethered fly walks in our experimental apparatus with closed-loop control of the angle of a visual landmark (a tall bright bar), opening the loop briefly and abruptly rotating that landmark leads to a rotation in the E-PG phase (Green *et al.* 2018). To test

the sensitivity of the E-PG phase to small perturbations of such a visual stimulus, I expressed GCaMP6m in E-PGs and imaged calcium activity in the protocerebral bridge during closed loop control of a bright bar. Periodically I jumped the bar ±10º, ±20º, and ±30º. I should note that the resolution of the fly's visual display is 1.875º, which does not divide evenly into 10 and 20, and so when I commanded a shift of 10º the visual stimulus shifted either 9.375º or 11.25º, and when I commanded a shift of 20º this led to a shift of 18.75º or 20.625º on the display, which, on the aggregate, averaged out to 10º and 20º bar jumps, respectively. I will refer to these displacements as ±10º, ±20º, and ±30º bar jumps, (although, in the context of determining the resolution of the E-PG heading signal, I will discuss these displacements in terms of their maximum values ±11.25º, ±20.625º, and ±30º). I only jumped the bar to and from positions where it was fully visible. To ensure a stable baseline phase, I only jumped the bar when the fly had stood still for at least one second (Figure 3.1a) – I call this epoch the *stable-bar-1* period. After jumping the bar, I held the bar in place for five seconds – I call this epoch the *stable-bar-2* period. After this, I turned off the bar for five seconds – I call this epoch the *dark* period.

For ± 20º and ± 30º jumps, the E-PG phase changed significantly from the stable-bar-1 period to the stable-bar-2 period, rotating in the direction of the new bar position (Figs. 3.1b-e, 16.9º ± 5.61º, 22.3º ± 8.78º). While ±10º jumps did not elicit significant rotations of the E-PG phase at the population level, a few high quality recordings did show E-PGs rotating in response to ±10º bar jumps (Figure 3.1c).

Figure 3.1 | The E-PG phase relaxes after a visual stimulus is jumped and subsequently removed.

(**a**) Trial Structure. (**b**, **c**) Example recordings of E-PG neurons during a trial. The first column shows the fluorescent activity in each glomerulus over time. The second column shows the bar angle (black) and phase angle (blue) overlaid, 0º indicating the bar is directly in front of the fly). The E-PG phase is offset by a constant value so that the phase and bar position overlap. Gray vertical bars indicate where the bar is behind the fly. The third and fourth columns show the fly's yaw rotation and forward rotation of the ball, respectively. The bar jump is indicated by a white arrow on the GCaMP fluorescence plot and a red arrow on the phase plot. When the bar is removed, the entire arena is colored gray. (**b**) A 30º bar jump. (**c**) A 10º bar jump. Note how the E-PG phase relaxes past its position during the stable-bar-1 period (yellow arrow). (**d**) E-PG phase triggered on the moment the bar was jumped. Vertical gray dashed line indicates the moment the bar was jumped. Red dotted lines indicate the position to which the bar was jumped relative to baseline. Gray rectangle indicates when the visual stimulus was removed. Plots are separated by the size of the bar jump (n = 10, 19, 10). Trials for counterclockwise bar jumps (-10º, -20º, etc.) are flipped. Thick line: circular mean of trials. Thin lines: individual trials. Flies were static throughout all trials. Arena icons above the leftmost plot indicate the stable-bar-1 period, the stable-bar-2 period, and the dark period. (**e**) Circular mean of E-PG phase rotation in response to different jump sizes: stable-bar-2 period minus stable-bar-1 period. (**f**) Circular mean of E-PG phase rotation after the bar was removed: stable-bar-2 period minus dark period. (**g**) Circular mean of E-PG phase rotation over the course of the entire trial: dark period minus stable-bar-1 period. Blue dots: individual trials. Black lines and error bars: circular mean ± circular 95% confidence intervals. Stars indicate significance (circular median test, $p < 0.05$). The red dashed lines are plotted along y=x.

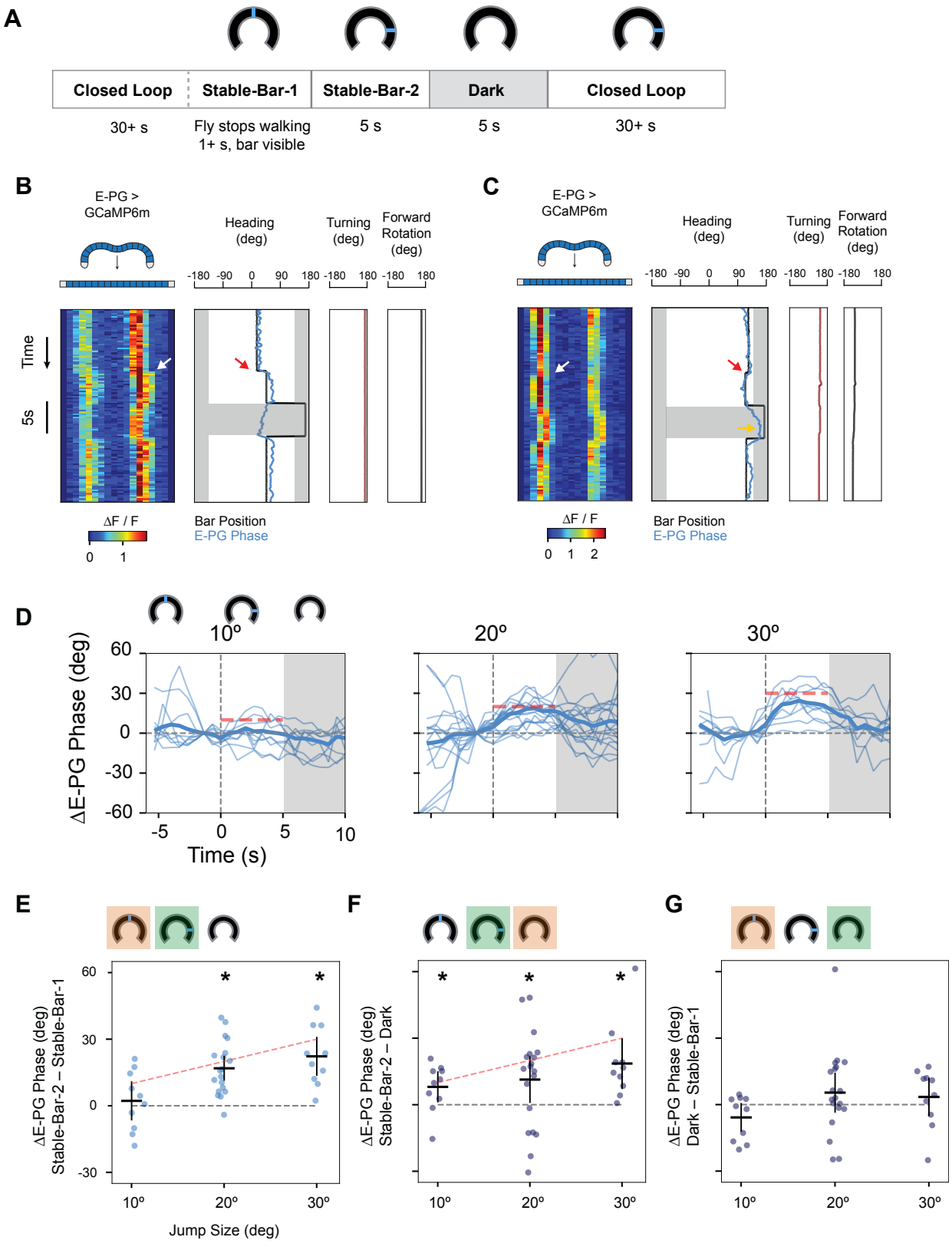
A
Closed Loop
Stable-Bar-1
Stable-Bar-2
Dark
Closed Loop
30+ s
Fly stops walking
1+ s, bar visible
5 s
5 s
30+ s
B
C
E-PG >
GCaMP6m
Heading
(deg)
Turning
(deg)
Forward
Rotation
(deg)
-180 -90 0 90 180
-180 180
-180 180
Time
5s
ΔF / F
0 1
0 1 2
Bar Position
E-PG Phase
D
10°
20°
30°
ΔE-PG Phase (deg)
60
30
0
-30
-60
-5 0 5 10
Time (s)
E
F
G
ΔE-PG Phase (deg)
Stable-Bar-2 – Stable-Bar-1
ΔE-PG Phase (deg)
Stable-Bar-2 – Dark
ΔE-PG Phase (deg)
Dark – Stable-Bar-1
*
10° 20° 30°
Jump Size (deg)

Abrupt removal of visual stimuli elicits a E-PG phase relaxation towards the phase in the stable-bar-1 period that sometimes overshoots this value

During the dark period – i.e., when I turned off the visual stimulus after the stable-bar-2 period – the E-PG phase tended to rotate back toward the value it occupied during the stable-bar-1 period (Figure 3.1f, stable-bar-2 phase minus dark phase: 8.05º ± 7.01, 11.34º ± 10.53, 18.57º ± 11.49 in the direction of the stable-bar-1 phase for 10º, 20º, and 30º bar jumps respectively). As a consequence of this relaxation, the difference in E-PG phase between the dark period and the stable-bar-1 period did not differ significantly from zero (Figure 3.1g).

The fact that, during the dark period, the E-PG phase relaxed to its phase in the stable-bar-1 period was consistent with a model wherein the E-PG phase in the stable-bar-1 period resided in an attractor state, and the relaxation in the dark represented a relaxation back toward that attractor state. But the results also raised a few questions. As mentioned in chapter 1, assuming an equal distribution of stable states and symmetric energy landscape around the ring, the maximum size of a relaxation ought to be half the distance between attractor states. A conservative estimate of 8 stable points in the E-PG ring attractor network – as all data suggest is the case because the phase does not appear to ever jump by more than 45º around the central complex when the fly walks in closed loop or in the dark – would predict a maximum relaxation size of 22.5º. However, 23% of relaxation magnitudes were greater than 22.5º. (Figs. 3.1c, e, f) How are such large relaxations possible if the E-PG ring attractor contained at least 8 stable points? Moreover, in some trials, the E-PG phase in the dark period relaxed past the

phase's position during the stable-bar-1 period (Figure 3.1c, yellow arrow). These trials are inconsistent with the assumption that the E-PG phase had been sitting in an energy minimum during the stable-bar-1 period.

The phase should not relax past its value in the stable-bar-1 period if the phase was at a stable point during that period. If, however, the E-PG phase during the stable-bar-1 period was 10º clockwise of the nearest stable point, one would expect the E-PG phase to relax 10º counter-clockwise of this value during the dark period. It might seem strange to assume that the E-PG phase was not resting in a stable state during the stable-bar-1 period. But of course the whole premise of the experiment was that jumping the bar could move the E-PG phase away from a stable state, propping it up on the energy landscape. If the bar is able to hold the phase away from an attractor state when it is abruptly moved, there is no reason that the bar would not be able to do the same thing in the stable-bar-1 period, before the bar was jumped.

Abrupt removal of visual stimuli causes the E-PG phase to relax to a stable point

I conducted a similar experiment, but I changed the trial structure to ensure that I always jumped the phase from an attractor state (Figure 3.2a). Once again, I began a trial when the fly had stood still for at least one second – the *stable-bar-1* period (Note that our visual display only covers 270˚ of azimuthal space and thus I only moved forward with the next epochs of the experiment if the bar was visible on the display during the stable-bar-1 period). I then shut off the visual stimulus – I call this the *dark-1 period*. After five seconds, I made the bar reappear on the screen, but at a new

azimuthal angle, holding it there for five seconds – I call this *stable-bar-2* period. Then I turned the bar off for a second time for five seconds – the *dark-2 period*. After the dark-2 period, I turned the bar on again in angular closed-loop mode (Figure 3.2a). In all subsequent analyses I only analyzed trials during which the fly stood completely still for the duration of the analysis period.

On 316 trials, the flies stood still through the stable-bar-1 and dark-1 period. Even though in this experiment I did not jump the bar prior to making the screen go dark, the E-PG phase nevertheless often rotated to a new angle upon the disappearance of the bar. Examples of such relaxations are shown in Figure 3.2b-c. On 70% of these trials, the E-PG phase relaxed more than 11.25º, the theoretical maximum relaxation size if the E-PG phase can reside in 16 equally distributed stable states (Figure 3.2d-e). On 42% of trials, the E-PG phase relaxed more than 22.5º, the maximum relaxation size which would correspond to 8 stable points. On 16% of trials the E-PG phase relaxed more than 45º, a maximum relaxation size which would correspond to 4 stable points. The E-PG phase clearly has more than 4 stable points. Individual flies can have dozens of standing events that uniformly cover 360º of phase (data not shown). It follows, then, that at least in the case of these large relaxations, and likely for all relaxations, the attractor state to which the E-PG phase relaxes in the dark-1 period is not the nearest attractor state of the E-PG system in general (which is likely much closer to the position of the phase at the moment the screen went dark), but instead some other, latent, stable angular value in the system.

This value is not random. In the dark-1 period the E-PG phase tends to relax to an angular position close to the phase in the stable-bar-1 period. While some relaxations from the stable-bar-1 phase angle are large, the relaxation sizes are not uniformly distributed (Figure 3.2d, Rayleigh test of uniformity, $p <<< 1x10^{-10}$), and are instead unimodally distributed about a value close to 0º (4.63º ± 4.31, circular mean ± 95% circular confidence interval). The phase position during the stable-bar-1 period has a circular correlation of 0.700 with the phase during the dark-1 period (Figure 3.2f).

The E-PG phase does not appear to relax to a consistent anatomical position. The distribution of E-PG phases appears uniform in the stable-bar-1 period and in the dark-1 period, example epochs during which the fly is standing still and in which we can measure the distribution of E-PG phases around the ring (Figure 3.2f**,** x- and y-axis histograms, $p > 0.1$ for both, Rayleigh test of uniformity).

When the fly walks in closed loop, the angular position of the E-PG phase tracks the position of the bar. One possibility is that the phase relaxes not to a consistent anatomical position (e.g. glomerulus 5 in the bridge), but instead to a position corresponding to a particular heading orientation (such as, for example, the glomeruli whose activation indicates the fly is facing directly away from the bar). This is a tempting explanation because, when the fly walks in closed loop, the screen is dark when the bar is in the 90˚ window behind the fly (because our arena only covers 270˚). Seeking to control for this possibility, we made a histogram of the bar positions on the LED display signaled by the E-PG phase at the end of the dark-1 period. This histogram suggested that bar positions behind the fly were not overrepresented at the end of the dark-1

period. In fact, the most common position for the phase to relax to corresponded to the bar being directly in *front* of the fly (Figure 3.2g**,** y-axis histogram). However, the direction of the phase relaxation did depend somewhat on the angular position of the bar when it disappeared. Note that data points in the -75º to 75º central range in Figure 3.2g tend to be slightly below the y=x equivalence red-dotted line to the right of zero and slightly above the y=x equivalence red-dotted line to the left of zero. While this trend is noisy, these data would suggest that when the bar turns off in front (-75˚ to 75˚) the phase has a weak tendency to drift further to the front. Conversely, when the bar is in the rear before it disappears (-180º to -75º or 75º to 180º) then the phase shows a weak tendency to drift further to the rear in the dark-1 period. This trend is evident by points being below the red dotted line in Fig. 3.2g in the -180º to -75º x-range and above the red line in the 75º to 180º x-range.

Figure 3.2 l The E-PG phase relaxes in the dark to a nearby angle, whose distance is consistently greater than the maximum relaxation one would predict in a perfectly tuned ring attractor with at least 8 stable points

(**a**) Trial structure. Note differences from 3.1. (**b**, **c**) Example recordings of E-PG neurons during a trial. Gray horizontal bars indicate the periods in which the bar was removed. The bar was jumped to a new location in the intervening period. (**b**) 43º dark-1 relaxation, -30º bar jump. (**c**) -55º dark-1 relaxation, 10º bar jump (**d**) Histogram of changes in E-PG phase: dark-1 minus stable-bar-1 (n=316; 11.25º bin size; 4.63º ± 4.32º circular mean ± circular 95% confidence interval) (**e**) Cumulative sum of the absolute value of the changes in E-PG phase upon the first removal of the bar: dark-1 minus stable-bar-1. Vertical gray lines indicate absolute change in phase of 11.25º, 22.5º, and 45º. (**f**) E-PG phase after at the end of the dark-1 period scattered against phase during the stable-bar-1 period. Histograms of these values are plotted along their respective axes. ±180º indicates a phase position wherein the most active glomeruli are on the edges and the very middle of the protocerebral bridge (glomeruli L8, L1, R1, and R8). (**g**) Bar position represented by the E-PG phase at the end of the dark-1 period scattered against the actual bar position during the stable-bar-1 period. Histograms of these values are plotted along their respective axes. 0º Indicates the bar directly in front of the fly.

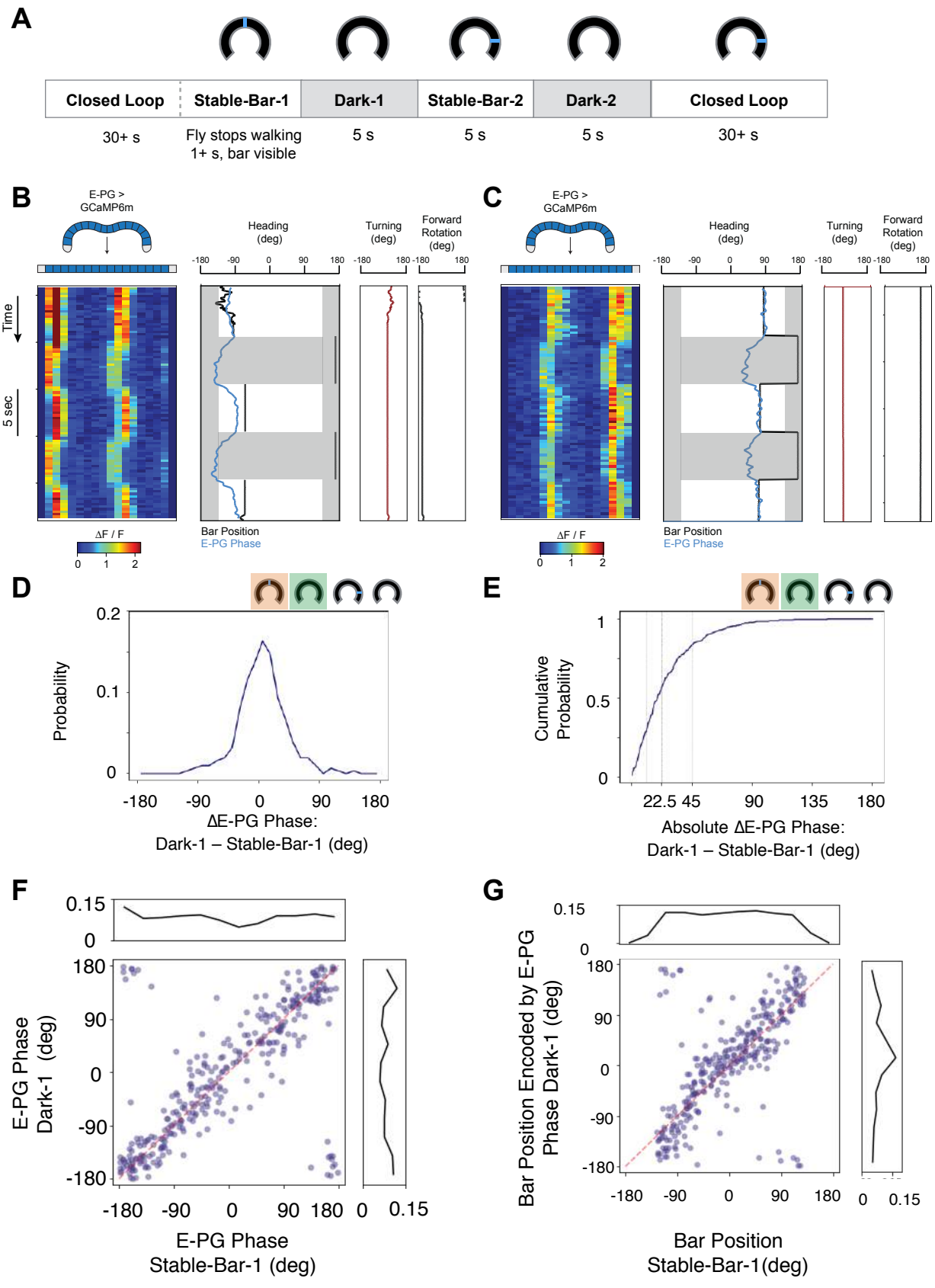
A
Closed Loop
Stable-Bar-1
Dark-1
Stable-Bar-2
Dark-2
Closed Loop
30+ s
Fly stops walking
1+ s, bar visible
5 s
5 s
5 s
30+ s
B
C
E-PG >
GCaMP6m
Heading
(deg)
Turning
(deg)
Forward
Rotation
(deg)
Time
5 sec
ΔF / F
Bar Position
E-PG Phase
D
Probability
ΔE-PG Phase:
Dark-1 – Stable-Bar-1 (deg)
E
Cumulative
Probability
Absolute ΔE-PG Phase:
Dark-1 – Stable-Bar-1 (deg)
F
E-PG Phase
Dark-1 (deg)
E-PG Phase
Stable-Bar-1 (deg)
G
Bar Position Encoded by E-PG
Phase Dark-1 (deg)
Bar Position
Stable-Bar-1(deg)

E-PG phase responses to abrupt shifts in the angular position of a visual landmark correspond to a resolution of 5.625º

The E-PG phase relaxed to a putative attractor state in the dark-1 period. To test for the presence of other attractor states, I perturbed the phase away from this dark-1 stable point by turning the bar on for five seconds during the stable-bar-2 period at one of the following angles offset from the stable-bar-1 bar position: ±5º, ±10º, ±20º, ±30º, ±45º, 60º, ±90º, ±180º.[5] I then made the bar disappear for five seconds a second time during the dark-2 period and tracked where the E-PG phase relaxed. Because the bar reappearances during the stable-bar-2 period were offset from the bar position in the stable-bar-1 period by fixed angles, this allowed me to assess the ability of the E-PG phase to signal visual angles at specific levels of resolution with a relatively large number of trials.

On 173 trials, the flies stood stationary through the entire stable-bar-1, dark-1, stable-bar-2, and dark-2 periods. As in previous reports in the literature (Green *et al.* 2018), the bar jumps between the stable-bar-1 and stable-bar-2 epochs led to a rotation of the E-PG phase in the expected direction, even after the 5s period in which the fly could not see the bar. This median E-PG phase displacement was significantly different from zero, even in the case of ±5.625º bar jumps between the stable-bar-1 and stable-

[5] ±5º shift commands shifted the visual stimulus ±3.75º or ±5.625º, ±10º shift commands shifted the visual stimulus ±9.375º or ±11.25º, and ±20º shift commands shifted the visual stimulus ±18.75º or ±20.625º. These, on the aggregate, averaged out to ±5º, ±10º, and 20º shifts, respectively. When I discuss the resolution of the E-PG compass I will refer to the maximum values of these displacements.

bar-2 periods (Figure 3.3a-b), corresponding to an estimated E-PG resolution of at most 5.625º.

After the E-PG phase relaxed to its stable point in the dark-1 epoch, does a bar jump of, say, 45º relative to the stable-bar-1 bar position perturb the phase 45º away from the phase position during the stable-bar-1 epoch, or 45º away from the stable point the phase settled into during the dark-1 epoch (which are often very similar, but, as noted above, not identical)? The data suggests the former option. The E-PG phase rotation from the stable-bar-1 period to the stable-bar-2 period was more correlated with the jump size than was the E-PG phase rotation between the dark-1 and stable-bar-2 periods (circular correlation of 0.458 vs 0.342, data not shown). This result suggests that the mapping between the visual stimulus and the E-PG phase was preserved during the trial, in spite of the phase relaxing to an odd stable point in the intervening dark period.

Figure 3.3 l The E-PG phase can resolve abrupt jumps in the angular position of a visual landmark as small as 5.625º

(**a**) E-PG phase triggered on the moment the bar disappeared. Gray bars indicate when the visual stimulus was removed. Plots are separated by the size of the bar jump (N = 173, n = 28, 28, 24, 24, 14, 21, 15, 19). Trials for counterclockwise bar jumps (-5º, -10º, etc.) are flipped. Red dotted lines indicate the position to which the bar was jumped. Thick line: circular mean of trials. Thin lines: individual trials. Flies were static throughout all trials. (**b**) Circular mean E-PG phase rotation in response to different jump sizes: stable-bar-2 minus stable-bar-1. Blue dots: individual trials. Black line and error bars: circular mean ± circular 95% confidence interval. For 180º bar jumps a 95% confidence interval could not be determined, so error bars span 90º in either direction. Stars indicate significance (circular median test, $p < 0.05$).

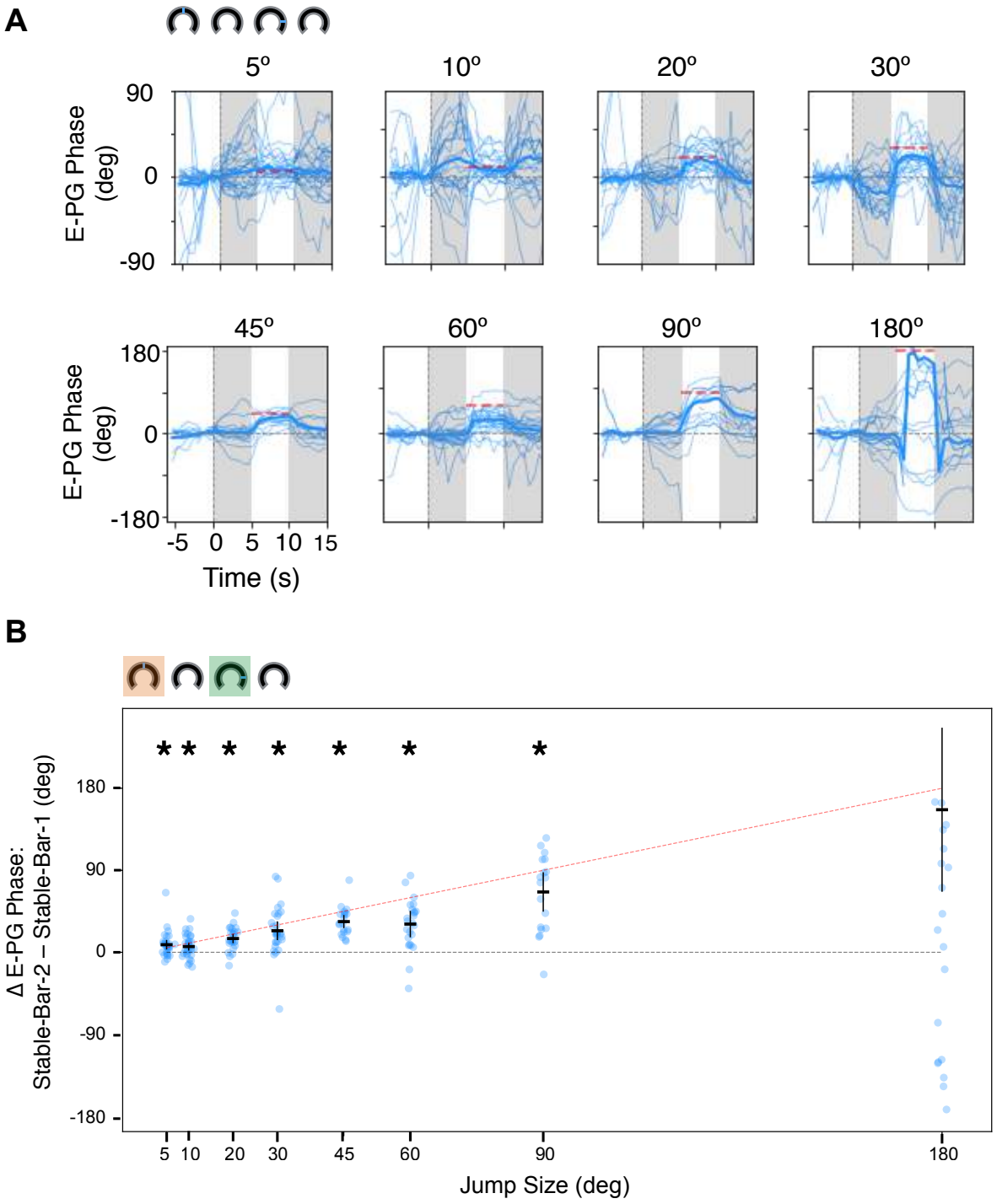
A
5°
10°
20°
30°
45°
60°
90°
180°
E-PG Phase (deg)
90
0
-90
180
-180
-5 0 5 10 15
Time (s)
B
Δ E-PG Phase: Stable-Bar-2 – Stable-Bar-1 (deg)
180
90
0
-90
-180
5 10 20 30 45 60 90 180
Jump Size (deg)

The phase to which E-PG relaxes when visual stimuli are removed is consistent over a short period of time when the fly stands still

After the stable-bar-2 epoch, the bar disappeared a second time (the dark-2 epoch) and I measured how the phase relaxed. If the phase to which the E-PG heading signal relaxes during the dark-2 epoch represents the nearest stable point on a ring attractor, then the size of the relaxation from the stable-bar-2 period to the dark-2 period should be small (a few degrees, depending on the number of stable points in the ring attractor). If, however, the E-PG phase tends to relax all the way back to the same value it held during the dark-1 period, that would suggest that the E-PG phase in both dark periods signals a consistent global attractor state in the system, which would be a new finding for the *Drosophila* central complex and E-PG literature. Plotting the E-PG phase position over time, and calling the E-PG phase position at the end of the dark-1 period zero, reveals that the E-PG phase typically returns to zero during the dark-2 period, independently of which direction it rotated during the intervening stable-bar-2 period (Figure 3.4a). This result suggests that the nearest stable point during the dark-2 epoch is the exact same stable point in which the E-PG phase resided during the dark-1 period. That is, there appears to be a consistent, latent, stable angle in the system, which is revealed in standing flies when one removes all visual input.

If one were to plot the amount the E-PG phase rotated between the stable-bar-2 and dark-2 epochs versus the amount the phase rotated between the stable-bar-1 and stable-bar-2 epochs, every zero-crossing point on this graph with negative slope would indicate a stable point in the system. In other words, on trials where the bar

reappearance during the stable-bar-2 epoch moved the phase to exactly to such a stable point, the phase would not relax clockwise or counterclockwise when the bar was removed a second time. If the bar reappearance perturbed the E-PG phase just clockwise of a stable point, one would expect a counter-clockwise relaxation when the bar was removed, and vice versa.

A binned average fit to these data only crosses the x-axis once (at $x < 0.1^{o}$). The data for relaxations with a magnitude less than 90^{o} are fit well by a line with a slope of -0.8 (Figure 3.4b). While dispersion about the line increases as the x-values become more extreme, note that, if x=0 represents the graph's only stable point, a symmetric system might be expected to have an unstable point at $\pm 180^{o}$. In addition, examining the margins of the graphs reveal extreme examples wherein the bar jump perturbed the phase close to 180^{o} from its stable point, and the phase relaxed all the way back. Relaxations of this magnitude are inconsistent with a system with more than one stable point.

In principle this stable point might be located at the energy minimum that the E-PGs relaxed to in the dark-1 period, or it might be the angular position indicated by the system the last time the fly was in closed loop, or other options. Example traces suggest the first option is correct (Figure 3.4a). In addition, the dark-1 and dark-2 E-PG phase angles are more correlated than the dark-2 and stable-bar-2 phases (Figure 3.4b, circular correlation between stable-bar-2 phase – dark-1 phase versus dark-2 phase – stable-bar-2 phase: -0.828. Figure 3.4c, circular correlation between stable-bar-2 phase – stable-bar-1 phase vs dark-2 phase – stable-bar-2 phase: -0.453).

Within a trial, the E-PG phase relaxes to approximately the same position in the dark-1 and dark-2 periods, which are ten seconds apart. Could the angular position to which the E-PG phase relaxes potentially be constant over a longer period of stasis? To test this, I computed the circular distance separating the position to which the E-PG phase relaxed in dark periods between trials separated by different amounts of time, comparing events during which the fly walked in the intervening period to events when the fly stood still between two dark periods (Figure 3.5a). If two dark periods were separated by less than 20s, flies always remained static between them (data plotted in blue). If two dark periods were separated by more than 40s, flies invariably moved between these two events (data plotted in red). In the 20-40s window, however, events of both type occurred. I could therefore compare these two categories of pairs of events in this time bin. Doing so revealed that, if dark periods were separated by a period of stasis, the circular distance separating the angles to which the E-PG phase relaxed in these two periods is smaller than if the fly walked in the intervening period (Figure 3.5a).

When a fly walked between two dark periods, this changed the position to which the E-PG phase relaxed in the subsequent dark period. Preliminary evidence suggests that the *direction* in which the fly rotated the ball in the intervening period affects the new position to which the E-PG phase relaxes. In 30 pairs of dark periods separated by 20-40s during which flies walked in the intervening period, the direction the fly rotated on the ball in the intervening period was weakly but significantly correlated to the change in angular position to which the E-PG phase relaxed in the subsequent dark period (Figure 3.5b, circular correlation $= -0.251$, $p < 0.001$).

In summary, when a fly stands still and the visual stimulus is removed, the E-PG phase relaxes to a new angle with a median relaxation magnitude of ~20º. The angle to which the system relaxes is remembered, at least on a short timescale of five seconds, since the phase relaxes to the same position again after being yoked to a new position by visual input. The E-PGs do not relax to a random anatomical position, tending to rest close to where the E-PG phase initially resided prior to the removal of the bar. Sometimes, however, relaxation magnitudes are quite large – larger than values consistent with the known minimum number of stable points. We cannot detect multiple attractor states in the system. To a first approximation, no matter how far the E-PGs are jumped away from the relaxation position in which they resided during the first dark period, the relaxation makes it all the way back to that position during the second dark period.

Again, one interpretation for the latent angle in the E-PG system is that it represents a short-term memory of the angular-velocity integration system's heading estimate, revealed once positional-visual input is removed. If this interpretation is correct, it is surprising that there is any memory of the integrator's heading estimate that is independent of the E-PG signal itself, suggesting a second mechanism of latching a memory in the system, independent of E-PGs, an idea I describe further in the discussion.

Figure 3.4 | The E-PG phase relaxes to a single stable point in both dark periods

(**a**) Same data as in Figure 3.3a, but aligned to the position of the E-PG phase at the end of the dark-1 period. Each line represents a single trial. Trials for counterclockwise bar jumps (-5º, -10º, etc.) are flipped. (**b**) E-PG phase rotation: dark-2 minus stable-bar-2 scattered against the E-PG phase rotation: stable-bar-2 minus dark-1. In the dark-2 period, the E-PG phase relaxed toward the position it adopted during the dark-1 period, no matter how fare the phase rotated during the stable-bar-2 period. Blue line: a binned average of these data (circular mean ± circular 95% confidence interval). Circular correlation: -0.828. (**c**) E-PG phase rotation: dark-2 minus stable-bar-2 scattered against E-PG phase rotation: stable-bar-2 minus stable-bar-1. Circular correlation: -0.453.

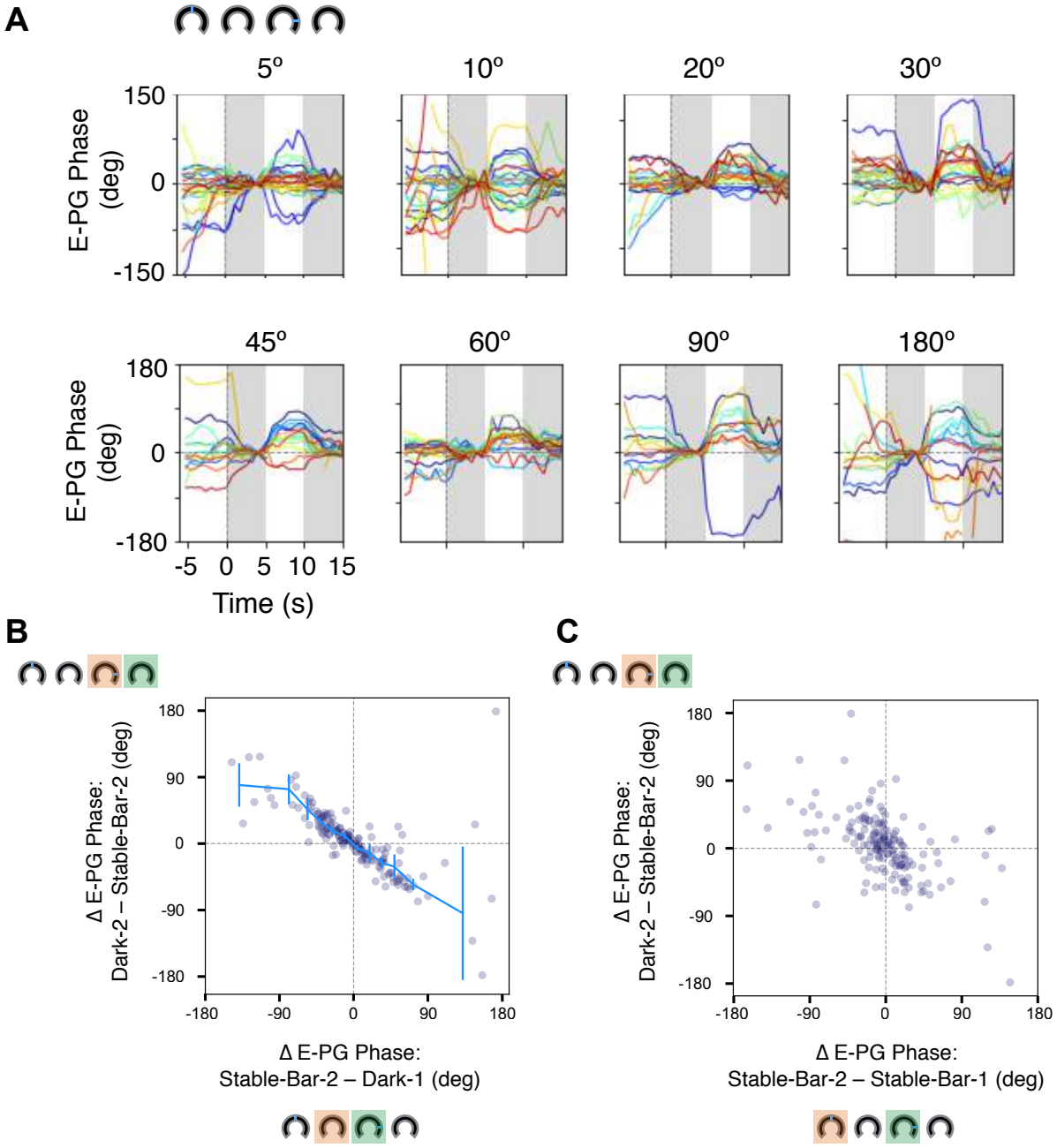
A
5°
10°
20°
30°
45°
60°
90°
180°
E-PG Phase (deg)
150
0
-150
180
-180
-5 0 5 10 15
Time (s)
B
C
Δ E-PG Phase: Dark-2 – Stable-Bar-2 (deg)
Δ E-PG Phase: Stable-Bar-2 – Dark-1 (deg)
Δ E-PG Phase: Stable-Bar-2 – Stable-Bar-1 (deg)
180
90
0
-90
-180

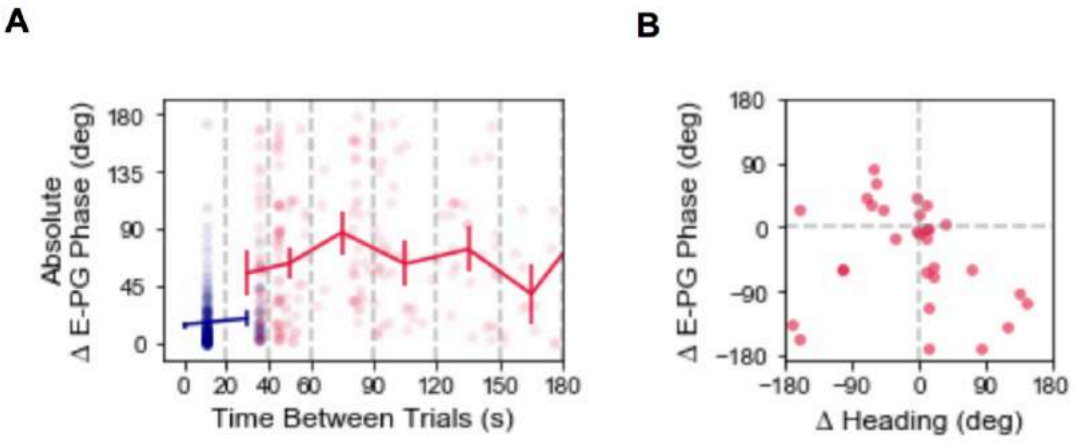

Figure 3.5 | The position to which the E-PG phase relaxes in the dark depends the fly's turning behavior between trials.

(**a**) Absolute circular distance between the E-PG phase extracted from two 5-second long dark periods during which the fly stood still, plotted against the time separating those two dark periods. Data plotted in red represent two events between which the fly moved in the intervening period. Data plotted in blue represent two events between which the fly did not move in the intervening period. Dots represent the change in phase between two dark periods. Lines represent circular mean ± circular 95% confidence interval of time-binned data. Time bins limits are indicated by grey vertical dotted lines. (**b**) Change in E-PG phase plotted against change in ball heading. The data shown are the red data (i.e. data for which the fly moved between standing events) in the 20-40s bin from (a). Events between which the absolute unwrapped change in ball heading exceeded 180^{o} were excluded. Circular correlation: -0.251, $p < 0.001$.

Chapter 4 | Discussion

By inactivating synaptic transmission in a large, genetically defined set of neurons, almost all spontaneous saccades in tethered flying *Drosophila* were abolished. The observed suppression of spontaneous saccades spares loom-evoked saccades and optomotor responses. This demonstrates that the mechanisms underlying the execution of spontaneous turns and these two types of visually evoked turns are, at some level, dissociable. Conversely, it has been previously shown that flies blinded with a prolonged depolarization afterpotential continue to perform spontaneous saccades (Kim, Fitzgerald, and Maimon 2015). Together, these results argue that spontaneous turning is doubly dissociable from both loom responses and optomotor responses in *Drosophila*; whereas certain neural processes that contribute to both classes of behaviors are likely to exist, it is possible to inhibit each one without abolishing the other.

Spontaneous saccades are defined here as saccades whose precise time of initiation cannot be easily linked to any abrupt external event. However, environmental stimuli are known to affect the rate of saccades that would still fall within this definition of spontaneous. For example, the first paper describing spontaneous saccades in tethered flight noted that flies perform saccades of unpredictable timing (i.e., spontaneous) much less frequently in the dark (Heisenberg and Wolf 1979). Also, it has recently been shown that magnetically tethered flies (which are free to rotate about their yaw axis) perform saccades in the direction of yaw optic flow or toward a visual object

(Mongeau and Frye 2017). These saccades can be considered stimulus driven in that their average onset times can be predicted by a model that integrates optic-flow velocity, or visual-object position, over time. However, unlike saccades driven by loom stimuli, these stimulus-driven turns show considerable onset-time variability relative to the mean, suggesting that there exists a stochastic component to their initiation times, akin to spontaneous turns. It will be interesting to determine whether NP0212 > Shi^{ts} flies can perform optic-flow- and visual-object-associated saccades, which are stimulus driven in one sense and yet spontaneous (or stochastic) in another. The answer to this question may help to further refine the definition of a spontaneous action.

It should be noted that expressing *shibire^{ts}* in neurons targeted by *NP0212-GAL4* does not eliminate absolutely all measurable, non-stimulus-locked flight maneuvers. NP0212 > Shi^{ts} flies at 34ºC continued to make some sharp turns during optomotor stimuli (see single-trial NP0212 > Shi^{ts} example traces in Figure 2.9a). Such turns, whose rate seems to be increased by optomotor stimuli and which have been noted previously (Lindsay, Sustar, and Dickinson 2017; Kim, Fitzgerald, and Maimon 2015; Schnell, Ros, and Dickinson 2017), represent a potentially different class of flight maneuver from those blocked in NP0212 > Shi^{ts} flies.

Whereas we did not present any overt stimuli to elicit spontaneous saccades, the flies could almost certainly sense stimuli that we did not control, such as the air currents generated by their own flapping wings (Mamiya and Dickinson 2015). We therefore cannot fully exclude the possibility that every seemingly spontaneous turn in our tethered preparation represents an immediate or integrated response to an

environmental stimulus that we do not measure. However, flies that have been blinded (Kim, Fitzgerald, and Maimon 2015) or that have had their antennae glued (data not shown)—blocking smell and mechanosensation in these organs—still saccade. Furthermore, if spontaneous saccades represent responses to subtle environmental stimuli, these stimuli would have to change on a timescale commensurate with the structure of the turning behavior. Namely, spontaneous saccades in tethered flight typically occur in bursts (Heisenberg and Wolf 1979; Mayer *et al.* 1988), all in the same direction, lasting tens of seconds. These bursts switch from a set of turns to the left, then a set of turns to the right, and back to the left, and so on (see Figures 2.1c**,** 2.3b-c, 2.6a, and 2.7c), and this pattern is recapitulated in magnetically tethered flies that rotate about their yaw axis (Figure 2.2). It seems to us unlikely that uncontrolled environmental stimuli would always show this structure across different preparations and experimental days.

It has been reported that the rate and direction of 93% of apparently spontaneous turns could be explained by the amount of visual expansion a freely flying fly experiences at any given moment in a 2-m-diameter cylindrical arena (Censi *et al.* 2013). In our experiments, flies that did not perform spontaneous turns still performed loom-evoked turns. These results might mean that neurons in NP0212 are required to execute the ~7% of saccades that could not be explained by visual expansion in the free-flight experiments. It is also possible that, in free-flight conditions where flies do not encounter an arena wall as often, more than 7% of saccades would be internally initiated. Intriguingly, in the free-flight study, flies performed spontaneous saccades at a

rate of ~0.4 saccades/s (~24 saccades/min), which is almost exactly the same as the rates detected in rigidly tethered flies (Censi *et al.* 2013).

It is possible that the causal neurons in NP0212 are necessary for both spontaneous and loom-evoked turns, but chemical synaptic transmission is essential for executing spontaneous saccades, whereas electrical transmission—which is not expected to be affected by *shibire*^{ts}—governs the loom-triggered behavior. *Drosophila's* giant fiber neuron is an example of a cell in which chemical and electrical transmission serve different output functions (von Reyn *et al.* 2014). In this scenario, the two behaviors can still be considered dissociable, but the dissociation would take place at a sub-cellular locus.

It may be that the NP0212 enhancer drives transgene expression in neurons where bursts of action potentials normally occur as an early step in driving a spontaneous turn to initiate and that these initiator neurons are cholinergic cells in the thoracic ganglion. However, it is important to note that this is not the only option or even the most parsimonious one. Work by Schnell et al. (Schnell, Ros, and Dickinson 2017) has identified a descending neuron, AX, whose calcium activity and membrane voltage are tightly correlated to fast wing steering maneuvers in tethered flight and whose exogenous activation induces directional steering responses. AX, or neurons like it in the brain, might initiate a spontaneous saccade or relay such an initiation signal from neurons even further upstream (i.e., closer to the sensory periphery) and thoracic ganglion neurons in NP0212 may act as a downstream gate of such initiation signals, originating in the brain. In this scenario, silencing NP0212 cells would yield a phenotype

of markedly reduced spontaneous saccades, even though this driver line would not include neurons that participate in the process of initiation *per se*. Indeed, AX could further drive loom-evoked turns, and perhaps even optomotor turns, via coupling to a different thoracic-ganglion interneuron system than that targeted by the NP0212 enhancer.

Motor-related signals that precede wing steering maneuvers exist in brain cells beyond AX. For example, the optic-flow responsive horizontal-system (HS) neurons in the fly visual lobe show modulations of their membrane voltage that correlate with rapid flight steering maneuvers, and these membrane voltage changes in HS cells precede spontaneous wing-steering changes (Kim, Fitzgerald, and Maimon 2015). Furthermore, exogenous activation of HS cells is sufficient to drive flies to turn during flight and walking (Haikala *et al.* 2013; Fujiwara *et al.* 2017). Because HS cells are located in the visual system and because these neurons receive antagonistic visual and motor-related inputs, their wing-steering-related modulations have been interpreted as efference copies rather than as motor commands (Kim, Fitzgerald, and Maimon 2015). AX cells, on the other hand, respond strongly to wing steering behavior, and the variation in their responses to visual stimuli covaries with the strength of the fly's behavioral response. In addition, AX neurons have a prominent projection to the wing-steering neuropil in the thoracic ganglion. Thus, AX's wing-steering-related signal has been interpreted as a motor command (Schnell, Ros, and Dickinson 2017). As such, one might imagine that silencing synaptic transmission in AX cells might impair wing-steering behavior. We expressed *shibire*^{ts} in two different driver lines that target AX neurons but were not able

to detect a defect in saccade rate at 34ºC (*R91C05-GAL4* and *R56G08-GAL4* in Figure 2.11). We note that it is possible that AX neurons drive rapid turns through gap junctions, which are not impaired by *shibire^{ts}*, or that our *shibire^{ts}* transgene was not expressed strongly enough in these *GAL4* driver lines to inhibit the labeled neurons. That said, our inability to abolish spontaneous saccades with *shibire^{ts}* in AX cells or over 30 other Gal4 lines is generally consistent with the possibility that a relatively widespread network of neurons in the fly nervous system is involved in initiating or otherwise processing saccadic commands and that silencing any one component may not impair the fly's ability to initiate action. *NP0212-GAL4* may target a large swath of the initiating network or a downstream gate of such a network. Future work will be needed to tease apart these varying hypotheses.

Recent work by Lindsay et al. (Lindsay, Sustar, and Dickinson 2017) has argued that the direct flight-steering muscles in *Drosophila* fall into two main categories: tonic muscles, whose calcium activity scales linearly with the strength of flight turns and which are preferentially recruited during graded changes in wing steering, and phasic muscles, which are recruited preferentially during very strong, sharp saccades. In our experiments, both sharp and graded spontaneous turns were depleted in NP0212 > Shi^{ts} flies (Figures 2.3 and 2.5), whereas sharp and graded turns induced by looming (Figures 2.7a-b and 2.8c) and optic flow stimuli, respectively (Figure 2.9), were preserved. Thus, our results add another dimension to the categorization of flight turns in *Drosophila*; spontaneous turns and both loom and optomotor visual responses should

be considered to have a neural distinction outside of the steering motor-neuron system, much like graded and sharp turns do within it.

The precise identity of the neurons labeled by NP0212 that mediate spontaneous turning remains unclear. We hypothesize that the locus of NP0212 inhibition of spontaneous flight turns is upstream of steering motor neurons, because NP0212 > Shi^{ts} flies that could not execute spontaneous saccades were still capable of responding to visual stimuli (Figures 2.7, 2.8, 2.9), because average saccade size did not measurably change in NP0212 > Shi^{ts} compared to the *UAS-Shi^{ts}* parental control (Figure 2.4), and because *vglut-GAL80* did not fully rescue the NP0212 spontaneous saccade deficit (Figure 2.10). Because *tsh-GAL80* and *cha-GAL80* rescued the deficit, we hypothesize that the causal neurons in NP0212 are cholinergic and in the thoracic ganglion. This result is intriguing in light of results from Berni et al., who show that, in *Drosophila* larvae, synaptic transmission in neurons in the thoracic ganglion are required for high rates of turning during an exploratory routine but that synaptic transmission in the brain lobes is dispensable for this behavior (Berni *et al.* 2012).

One class of cholinergic neurons in the thoracic ganglion that express *GAL4* in the NP0212 driver line is the afferent fibers from the halteres (Figure 2.8c, white arrows) (Trimarchi and Murphey 1997), which are mechanosensory balance organs involved in dipteran flight control (Dickinson 1999). The halteres regulate wing steering (Dickinson 1999) and are monosynaptically coupled to the b1 wing-steering motor neuron in Drosophilids (Trimarchi and Murphey 1997. To test the hypothesis that the NP0212 > Shi^{ts} saccade phenotype arises from silencing synaptic transmission in haltere afferent

neurons, we inhibited neurons in seven GAL4 lines that target subsets of haltere afferents. However, inhibiting synaptic transmission in these cells with *shibirets* did not lead to a consistent drop in the rate of spontaneous saccades (R33A12, R70C02, R39B12, R29G05, R22E04, R31A09, and R71B07 in Figure 2.11), suggesting that these are not the causal neurons for the NP0212 saccade phenotype (though this conclusion is tentative because, without further anatomical experiments, one cannot be 100% certain that the seven GAL4 lines we tested targeted the identical haltere afferents in NP0212 with a similar level of GAL4 expression).

We impaired synaptic transmission in smaller subsets of neurons that are targeted by the *NP0212-GAL4* driver line by using other, more specific, GAL4 lines (Figure 2.11). Whereas the majority of lines we tested showed no significant depletion in spontaneous saccade rate when crossed to *UAS-Shi^{ts}*, this does not mean that these driver lines do not target cells necessary for the generation of spontaneous saccades, because Shibire inhibits only chemical synapses, not electrical ones (Koenig, Saito, and Ikeda 1983). In addition, Shibire may not get expressed at sufficient levels to elicit a complete phenotype in all GAL4 lines that target a cell class of interest. Still, because none of these other GAL4 drivers yielded a full spontaneous-saccade-silencing phenotype, it remains possible that more than one anatomically defined neuronal class must be silenced to fully eliminate spontaneous turning. Further work will be needed to definitively prove this idea.

The fact that the neurons that mediate spontaneous saccades can be genetically dissociated from those neurons necessary for other visually-mediated flight turns

suggests that flies may be able to adjust the rate of spontaneous turning to suit their needs without affecting the gain of their responses to visual stimuli. One might imagine that this ability to adjust the rate of one's stochastic exploratory behavior might prove adaptive. While turning away from a looming predator, it may make sense for the fly to suppress spontaneous saccades, which might otherwise lead the fly to blithely wander back toward the threat it just avoided.

One striking example of fruit flies modulating their rate of spontaneous turns was inferred on the basis of results of mark-and-capture experiments performed in the heat of Death Valley. Jerry Coyne and colleagues released 100,000 fluorescently labeled *Drosophilids* in Death Valley National Park and set up insect traps 7 and 15 km away from the release site. The next day, dozens of fluorescently labeled flies were captured between the two sites (Coyne *et al.* 1982). Based on the metabolic rate of flying flies, it has been argued that it might barely have been possible for the flies to have made the trip across the desert without stopping for food – but only if the flies had flown relatively straight and had made few spontaneous turns (Dickinson 2014). In the laboratory, flies saccade every few seconds (Bender and Dickinson 2006b, Censi *et al.* 2007). Flies that dithered to that extent in the Death Valley experiment could never have made the 7-15 km journey without starving to death (Dickinson 2014). A conclusion one could draw from this experiment is that flies perform spontaneous saccades when they have the luxury of doing so. However, when a harsh environment requires that flies make a quick getaway, some flies are capable of suppressing their own spontaneous turns for hours at a stretch – perhaps by suppressing the activity of neurons that, like the causal

neurons labeled by *NP0212-GAL4*, are functionally tuned to generating spontaneous flight turns. Interestingly, flies exhibit a fictive version of this dispersal behavior on the tether, in which flies fly with a fixed angle relative to a bright angular landmark that is remembered over hours. Normal physiological activity in E-PG neurons is necessary for observing this fictive flight dispersal behavior (Giraldo *et al.* 2018), implying an antagonistic interaction between circuits that generate spontaneous, exploratory flight turning (which are likely to reside in the thoracic ganglion, at least in part) and E-PG and E-PG-related signals in the central complex, which are used to guide more precise, goal-directed trajectories (Green *et al.* 2018).

In chapter three of this thesis I attempted to quantify the angular resolution of the orientation estimate of E-PG neurons, a central-complex cell class implicated in goal-directed navigation. I found that when a visual landmark is abruptly shifted a small amount while the fly stands still, the E-PG phase rotates in that direction. The circular median changes of the phase angle are significantly different from 0º in the direction in which the bar was jumped, even for bar jumps as small as 5.625º, which is approximately the angular resolution limit of the fly visual system (Heisenberg and Wolf 1984). Note that while 5.625º and 11.25º bar jumps elicited a significant rotation of the E-PG phase in the *second* set of experiments (in which the second stable bar period was preceded by a period of darkness), in the first set of experiments, an immediate 11.25º bar jump, with no intervening dark period, did *not* measurably change the E-PG phase. I currently do not have a good explanation for why this might be, and that

negative result may cast doubt upon the claim that the E-PG heading estimate can resolve even smaller angular discrepancies. I should note, however, that the number of trials for both the 5.625º and 11.25º jumps were roughly three times as large in the second set of experiments as the number of trials in the 11.25º bar jump condition in the first set of experiments.

Since the E-PG phase moved in the expected direction to bar jumps as small as of 5.625º, one might naturally conclude that the E-PG ring-attractor network comprises at least 64 stable points separated by at most 5.625º. However, the previous result only demonstrates that when the system is dominated by feed-forward visual inputs that it can resolve 5.625º angle changes; in the absence of an unambiguous angular landmark, the E-PGs might signal heading in a coarser (or finer) way.

I attempted to determine the resolution of the E-PG heading direction estimate by removing visual input while the fly stood still and quantifying the resulting phase relaxation that accompanied the transition to darkness. I will focus this discussion on the set of experiments quantified in Figures 3.2–3.5, in which the first stable bar period was immediately followed by a five second dark period, after which I made the bar reappear for a second time, five seconds in duration, at a new position, followed by a second dark period, also five seconds in duration (Figure 3.2a). The principal result is that, when the visual stimulus was initially removed, the E-PG phase often rotated to a new stable location in the first dark period. 42% of relaxation magnitudes in this first dark period were greater than 22.5º. Theoretically, the maximum sizes of these relaxations should be related to the number of stable states in the network. Under the assumption that the

E-PG attractor states in darkness are equally distributed from one another, the largest relaxation should be half of the distance between each attractor state, or 360º / (2 * n-states). An exceedingly conservative estimate for the number of attractor states is 8; E-PGs project to 8 glomeruli in each half of the protocerebral bridge and all of azimuthal space is mapped onto those 8 glomeruli. If the E-PG ring attractor network contains 8 stable states, this would correspond to a maximum relaxation size of 22.5º. However, during the first dark period, relaxations that exceeded this value were routinely observed. It is even possible that I have *under*estimated the amount by which the system relaxes. During the first dark period, for a relaxation of a given size, around 75% of the change in phase occurred in the first 2.5s of the dark period, and the remaining 25% in the remaining 2.5s (data not shown, for examples see Figures 3.2b-c). While the change in phase slowed considerably as the dark period progressed, it is possible that, given a longer dark period, the phase would have continued to relax even further, and that the histogram in Figure 3.2d would be even broader. Even having potentially cut short some subset of the first-dark-period relaxations I observed, there seemed to be no limit on the size of relaxations; in a few rare cases, the E-PG phase relaxed almost 180º away from its value in the baseline period, the maximum possible displacement. The size of many of the relaxations prevented me from assigning an angular resolution to the putative E-PG ring attractor network in the absence of a visual landmark.

While the size of the relaxations was larger than expected for a well-tuned ring attractor, on average the phase during the dark period remained close to the position it held in the first stable bar period (Figure 3.2d). This result implies that, when a visual

stimulus is abruptly removed, the E-PGs adopt a network state similar to a single point attractor, and the location of this energy minimum is in some way related to the time history of the E-PG phase when the fly walked in closed loop with a bright bar.

We know the position to which the E-PG phase relaxed in the first dark period was retained in a working memory that lasts at least five seconds because the phase relaxed to a very similar location during the second dark period (Fig. 3.4b). Moreover, it seems that only one stable point is unmasked when visual input is removed when the fly stands still. That is, the data points in Fig. 3.4b cross the x-axis only once; however far the phase was perturbed from the stable point when I jumped the bar, the E-PG phase tended to rotate that far in the *other direction* when the visual stimulus was removed a second time. If other stable points existed, and if the bar jump had landed the phase anywhere near these other energy minima, the E-PG phase ought to have remained closer to the new phase location when I made the bar disappear the second time. I did not observe this result. That the single, unmasked, attractor state is remembered over a five second landmark-visible period and that it is unique argues that abruptly removing visual stimuli while flies are standing still converts the E-PGs' putative ring attractor network into a single point attractor network whose energy minimum lies somewhere near the E-PGs' heading estimate at the moment the visual input is abruptly removed.

What does this latent attractor state of the network, only evident after visual stimuli are abruptly removed, mean functionally about the fly's angular heading system? The least glamourous option is that it means little about the normal function of the system. Unless the ring attractor is tuned to create a perfectly flat energy minimum

(which is almost impossible to create in biological systems), removing feed-forward input to a ring attractor network should cause the network state to relax to some stable point or other. I lean against this interpretation for a couple of reasons. The simplest mechanism that would explain the presence of a non-functional bias in the system is some non-uniformity in the connection strengths between E-PG neurons, perhaps fixed over my half hour experiments. The stable point I observed, however, shifted around over time if the fly walked between dark periods (Figure 3.5) and was typically centered on the last bar position (Figure 3.2d). More importantly, perhaps, when a fly walking in complete darkness stops walking and stands still, we have not observed the heading signal to relax to new positions from the one it occupied at the moment the fly stopped walking. The heading signal tends to stay parked where it was whenever the fly stopped, consistent with the idea that the heading signal need not drift in a standing fly that experiences no external visual input. Rather, it only drifts so at the abrupt *removal* of visual input. This latter result is inconsistent with most forms of the model where the drift represents an unavoidable consequence of imperfect synaptic weights in the system. If so, one would have to explain why the consequences of these odd synaptic weights that lead to non-functional drift are somehow not evident in a fly that stands still in continuous darkness.

Another possibility is that this latent angle represents the angular direction in which the fly wishes to be heading (the *goal heading*), as to be differentiated from the angle at which it is currently heading (*current heading*). When hot, hungry flies walk in our virtual environment with a bright visual landmark in angular closed loop, they walk

very fast along a consistent, but arbitrarily chosen, direction for tens of minutes, a behavior we call *arbitrary angle fixation* or *menotaxis*. (Green *et al.* 2018, and see Giraldo *et al.* 2018 for a flight version of a similar task). Work in our lab by Green *et al.* has argued that E-PG neurons function, at least in part, to represent the fly's current heading during menotaxis (as opposed to the goal heading or current-minus-goal heading). Because this behavioral work reveals that flies have at least two relevant angles encoded somehow in their brain during navigation – a current heading angle, whose signal is carried, at least in part, by E-PGs, and a goal heading angle, whose nature is not known – it is attractive to imagine that the latent angle revealed in my experiments may represent the goal heading angle of the fly rather than its current heading. One reason that this model has some appeal is that the two angles, current heading and goal heading, are usually aligned in the fly's life (when they are not, the fly would be expected to turn its body to make them aligned) and, likewise, the bright-bar-visible phase angle and the latent phase angle (revealed when the bar disappears) are typically aligned, but not perfectly so (Figure 3.2d). If I could get flies to briefly stop walking as they perform menotaxis – perhaps achievable by turning off airflow to the floating ball – I could potentially both measure the fly's goal angle (based on the trajectory of the animal over minutes during menotaxis) and the latent angle (via bar jumps in stationary flies) to see if these two angles are one and the same.

A third possibility, which I lean toward, mentioned already in chapter 3, is that the position to which the E-PG phase relaxes in the dark represents a second estimate of angular heading – one that is more influenced by integration of self-motion cues than by

the current position of visual landmarks. This idea is supported by (1) the observation that the angular position to which the E-PG phase relaxed remained consistent between the first and second dark period, through which I required that flies remain static, (2) that, for dark periods separated by larger amounts of time, the E-PG phase tended to relax to more similar positions if the fly had stood still than if she had walked in the intervening period, (3) if the fly did walk between two bar disappearances, the direction that the fly rotated on the ball weakly correlated with the direction the relaxation position of the E-PG phase rotated, and (4) that the E-PG phase tends to be co-aligned with the heading angle in the system driven by the current bar position, but not perfectly so (consistent with a different "vote", from a non-visual modality, on which direction the fly is heading). Another observation that supports the model in which the latent angle represents an angle estimated by a neural integrator is that the position to which the E-PG phase relaxed often changed *between* trials in a given fly, and flies often moved around between trials. An integrator's estimate of the fly's heading in the world would be expected to change if the fly moved. Indeed, when I examined a subset of dark periods between which the fly had turned on the ball only a little (± 180^{o}), the direction the fly had turned on the ball was weakly correlated to the change in the position to which the E-PG phase relaxed. With more data, one could more precisely describe the magnitude and directionality of such shifts in the latent angle contingent on the movements of the fly between trials.

A final possibility worth considering is that the latent angle might represent a of working memory of the fly’s recent heading orientation. Perhaps this signal interacts

with or shares features in common with the working memory flies exhibit when performing the “detour paradigm”. As a reminder, in this paradigm, a fly walking between two dark stripes is briefly distracted, whereupon all positional visual cues are removed. Most of the time the fly resumes the trajectory on which it was headed (Strauss and Pichler 1998). Kuntz *et al.* have recently advanced a model wherein the fly’s remembers which direction to proceed following distraction because the animal’s previous heading angles have been marked in the ellipsoid body by Nitric Oxide release. Perhaps the glomeruli to which the E-PG phase relaxed during bar-to-dark transitions had previously been “marked” by Nitric Oxide – or perhaps this stored heading angle is actually the more foundational phenomenon on which a fly’s directional working memory is based (Kuntz, Poeck, and Strauss 2017).

During bar-to-dark transitions the E-PG bump often relaxes to a previously inactive glomerulus of the protocerebral bridge. What is the mechanism of this process? While I have not yet imaged the ellipsoid body (only the bridge, to date) during this task, it is possible that, when the fly stops walking, there are two bumps in the ellipsoid body: one mediated by feed-forward visual input and one “stored” bump. Inhibition in the protocerebral bridge may potentially reshape this two-bump signal in the ellipsoid body into a single-bump signal in the bridge, centered around the visually-mediated bump. If the visual input vanishes, however, the only remaining, “stored”, bump in the ellipsoid body might begin to dominate the E-PG signal in both the ellipsoid body and the bridge.

If there is a second bump in the ellipsoid body, why has it not been previously reported (Seelig and Jayaraman 2015, Green *et al.* 2017)? One possibility is that this

second bump might be signaled with a much lower calcium peak in E-PGs as compared to the “main” bump when the fly has access to visual-positional cues. If the two bumps resided close enough to one another they would not be easily resolved. It is also possible that a different cell class altogether carries a second heading signal and that this other heading signal is not evident in E-PG GCaMP fluorescent signal when positional-visual input is present.

Which cells might carry, and store in working memory, a heading signal above and beyond the E-PG heading signal in the central complex? Two appealing candidate cell classes are the P-EGs and P-ENs, which are two columnar cell classes that project from the protocerebral bridge to the ellipsoid body (Wolff, Iyer, and Rubin 2015) and show excitatory functional connectivity to E-PG cells (Franconville, Beron, and Jayaraman 2018). The recurrent circuitry of the central complex suggests that E-PGs provide positional visual input to P-EGs and P-ENs. However, if the strength of that visual input were gated by movement, then when the bar is jumped while the fly is standing still, the E-PG phase would update, while the P-EGs and/or the P-ENs may not. Then, when visual input vanished, the stored angular state of the P-EGs and/or P-ENs could outcompete the visual bump, bringing the entire recurrent circuit into sync. Careful two-color imaging experiments of the heading signal carried by E-PGs alongside a second cell type (starting with P-ENs and P-EGs) may allow me to ultimately find a neural correlate of the latent heading signal suggested by my current experiments.

The above explanation of latent-phase storage would challenge the model of how a head direction signal is stored in the *Drosophila* central complex. Current models suggest that heading angles are stored in these recurrent circuits through persistent activity, and this persistent activity is maintained in via excitatory coupling between E-PG, P-EG, and P-EN neurons (Green *et al.* 2017; Green and Maimon 2018). The activity of these cell classes are thought to resemble coupled ring attractor networks of the sort modeled by Redish *et al.* (Redish, Elga, and Touretzky 1996) whose heading direction estimates are consistent with one another. While the logic of cell-type A being upstream or downstream of cell-type B is not straightforward in recurrent neural circuits, E-PGs are the only known class of neurons with dendrites in the ellipsoid body and axons in the bridge (Wolf, Iyer, and Rubin 2015), implying that, if the E-PG phase shifts in the bridge, all three heading signals should shift in concert. Instead, I propose that, in the P-ENs, P-EGs, or E-PGs, the glomerulus or ellipsoid body wedge that stores the "latent" phase signal – which, in many cases, is quite disparate from the E-PG glomerulus with the highest calcium activity – maintains some form of persistent activity or a persistent conductance that can be situated away from peak of the activity bump in E-PGs. Perhaps this persistent activity is even maintained in a manner which cannot be visualized with GCaMP. For instance, a cation channel may remain persistently open at the location of the latent phase, but, while visual input is present, shunting inhibition could prevent voltage-gated Ca^{2+} channels from opening at this location. This latent phase would only be unmasked when visual input – and, with it, lateral inhibition – was removed. Whatever the mechanism of this persistent activity may be, the results of

chapter three of this thesis raise the possibility that coupled ring attractor networks may store multiple variables in a hierarchical manner via disparate circuit and molecular mechanisms.

Conclusions

This thesis demonstrates the existence of neurons in the *Drosophila melanogaster* central nervous system whose normal synaptic activity is specifically required for the performance of spontaneous flight turns. Further experiments in walking flies allow me to estimate the resolution of a heading signal represented by neurons in the central complex whose normal synaptic activity is necessary for flies to maintain a straight heading; this resolution approaches that of the early visual system. This work also shows that these heading direction-tuned neurons store a second, latent angle that manifests when visual input is removed. The properties of this stored, latent angular signal are consistent with the notion that, alongside a positional estimate of its heading, the *Drosophila* central complex stores an integrated self-motion estimate of this variable which is brought to bear when positional information becomes unavailable.

Varying environmental conditions and internal states may call upon animals to employ diverse navigational strategies to meet their changing needs. This work highlights the neural substrates in *Drosophila melanogaster* underlying the performance of a spontaneous behavior on the one hand and the maintenance of a precise internal estimate of heading on the other. Further work will be needed to show the mechanisms by which these neural substrates help the fly's central nervous system achieve these aims, and whether these mechanisms correspond to those that underlie stochastic and goal-directed locomotor strategies in other organisms.

Methods

Fly Stocks

We studied female, *Drosophila melanogaster*, 1-4 days post-eclosion. Flies were reared with standard corn-meal agar, in 25ºC incubators with a 12 hour light/dark cycle. The following lines were used: pJFRC99-20XUAS-IVS-Syn21-Shibire-ts1-p10 inserted at VK00005 (Bloomington Drosophila Stock Center, BDSC # 66599), tubP-GAL80^{ts} (BDSC # 7017), UAS-TeTxLC active (Sweeney *et al.* 1995), UAS-TeTxLC inactive (Sweeney *et al.* 1995), UAS-mCD8-GFP, Elav-GAL80 (Nilay Yapici), Tsh-GAL80 (Nilay Yapici), Cha-GAL80 (Nilay Yapici), vGlut-GAL80 (Nilay Yapici), *w^{1118},* Heisenberg Canton S (HCS). In spontaneous turning experiments, unless otherwise indicated, *w-* experimental flies and parental controls were used (i.e. *w-; GAL4* and *w-; UAS-Shi^{ts}* flies were crossed each other or to *w^{1118}* flies to generate parental controls). For imaging experiments I used w-; + UAS-GCaMP6m flies. (Bloomington Drosophila Stock Center, BDSC #42748). E-PG neurons were labeled by w- ; + ; 60D05-Gal4 (BDSC #39247). In visual response experiments (Figures 2.7-2.9) and imaging experiments (Figures 3.1-3.5) flies carried a single wild type copy of the *white* gene (*w+*) derived from the HCS wild type strain.

Transgenic Flies

The R83H12 fragment was amplified from genomic DNA (y; cn bw sp) using the same primers as in (Jenett *et al.* 2012) (forward: gaaaggacctctgcccctagttaaa, reverse:

gatatgaagacaacaaggggcgtg). This R83H12 fragment was first cloned into pCR8/GW/TOPO (Invitrogen), and then recombined into pBPGal80Uw (Nilay Yapici) using Gateway cloning as in (Pfeiffer *et al.* 2008). pBPGal80Uw contains attR1 and attR2 sequences upstream of the *Drosophila* Synthetic Core Promoter (DSCP), the Gal80 sequence, the Woodchuck Hepatitis Virus (WHP) Posttranscriptional Regulatory Element (WPRE), and the SV40 terminator sequence. The plasmid also contains mini-white. This R83H12-Gal80 vector was then integrated into VK00027 using PhiC31 recombinase (Genetic Services, Inc), and transformants selected as in (Pfeiffer *et al.* 2008).

Immunohistochemistry

We dissected fly brains in 19ºC S2 medium, and fixed them in 1% paraformaldehyde at 4ºC overnight. Fixed brains were washed 3 times for 30-60 min with PAT3 (0.5% Triton X-100 and 0.5% Bovine Serum Albumin (BSA) in PBS), then blocked with 3% NGS in PAT3 for 1.5 hours at room temperature. We incubated brains with primary and secondary antibodies as previously described (Nern, Pfeiffer, and Rubin 2015), and mounted them in VectaShield (Vector Labs). We stained with anti-GFP (Rockland) at a dilution of 1:1000 along with nc82 antibody (DSHB) at 1:50 to label neuropil. We imaged brains using a 20x 1.0 NA objective on an Inverted Leica DMI 6000 confocal microscope with 1 or 1.5 µm separating each optical slice.

Behavioral Data Acquisition

In tethered flight experiments, we estimated wingbeat amplitudes of the left and right wings in real time, as previously described (Maimon, Straw, and Dickinson 2010). Video data were collected at 50 Hz with an AVT-GE680 camera with an Infinistix lens (94 mm working distance). Data were digitized at 10 kHz using a Digidata 1440 (Axon Instruments). In imaging experiments, data were also digitized at 10 kHz using a Digidata 1440 (Axon Instruments). Two-photon scanning images were acquired with PrairieView (Bruker). Behavioral image triggers, two-photon image acquisition triggers, and visual stimulus triggers were collected on a single Digidata 1440.

Ball tracking and closed-loop

The tethered-walking preparation was similar to that of Green *et al.* 2017. In imaging experiments, the fly walked on an air cushioned ball shaped from Last-a-Foam FR-4618 (General Plastics) with a diameter of ~6.35 mm and a mass ranging between 42 and 46 mg. The ball rested in an aluminum base with a concave hemisphere with a 6.75 mm diameter. A 1 mm channel was drilled through the bottom of the hemisphere and air was flowed through it at a rate of approximately 260 mL/min. The ball was painted with irregular black spots so that its rotations could be imaged. For all walking experiments, I imaged the fly and ball from the front under 850 nm illumination with a Prosilica GE680 camera (Allied Vision Technologies) externally triggered at 50 Hz. The ball's rotations in yaw, pitch, and roll were tracked using FicTrac software. Older versions of FicTrac would accumulate slight delays over time. I used a modified version of FicTrac,

"FicTrac_noqueue", that did not accumulate these delays. A plastic square with a circular hole cut in it was fitted around the ball holder, and sat a few mm underneath the ball, orthogonal to the ball holder, with its side edges parallel to the fly's body axis. The edges of this plastic square were used to calibrate FicTrac so that the program tracked rotations of the ball in the fly's frame of reference. FicTrac outputted analog voltages corresponding to the angular position of the ball along the yaw, pitch, and roll (heading, forward walking, sideways walking) axes through a digital to analog converter (USB-3101, Measurement Computing). In closed loop, the heading axis output voltages were fed into MATLAB at 50 Hz, which integrated these voltages to control the azimuthal position of a bar displayed on the LED arena with a frame rate of 20 Hz. When the fly turned left, the bar rotated right, and vice versa, simulating the natural visual input a rotating fly would experience from a stationary, visual landmark at infinity.

Visual stimuli

In tethered flight experiments, we used a cylindrical visual display (Reiser and Dickinson 2008) covering 216º and 90º in azimuth and elevation, respectively (IORodeo) with each pixel (570 nm LEDs) subtending ~2.25º on the fly's retina. For behavioral genetic experiments we tilted the arena ~45º downward from upright so as to roughly match the fly's pitch-down head angle. Expanding disk stimuli, whose ratio of radius to expansion velocity (l/v) were held constant, were projected on the visual display as dark spots against a bright background. The stimuli were centered 45º to the left or right of the fly and expanded to a radius of 90º in 482 ms with a pixel update rate of 56 frames/sec.

The angular size of the spot in degrees varied according to the function $\theta(t) = 2*\arctan((l/v) / -t)$ for an $(l/v) = 22$, for $22 \leq t \leq 503$, where t represents time in ms prior to collision (i.e. $\theta(0) = 180^o$). Grating stimuli were square waves with an 18^o spatial wavelength. Smooth gratings rotated about the fly with a temporal frequency of 2.5 cycles/s. Both the looming disk and the grating had a nominal contrast of 100%, though reflections likely reduced this value. In imaging experiments we used a similar cylindrical visual display to that described above covering 270^o and 81^o in azimuth and elevation, respectively with each pixel subtending ~1.875^o on the fly's retina. LEDs in the calcium imaging arena were blue (BM-10B88MD, Betlux Electronics). The arena was covered by five sheets of blue filter (Tokyo Blue, Rosco) to minimize the number of photons absorbed by the PMTs during imaging experiments. In closed loop experiments, the fly's rotations controlled the azimuthal position of a bright bar 6 pixels wide x 40 pixels high (11.25^o x 81^o).

Tethered flight behavioral experiments

Females were collected 1-4 days after eclosion and tethered to a custom holder in a manner similar to that previously described (Maimon, Straw, and Dickinson 2010). For Shi^{ts} experiments, tethered flies were placed in front of a uniform, bright visual display. Water was perfused onto the chamber above the fly's head, and the water's temperature was controlled by an in-line peltier device (Harvard Apparatus) connected to a CL-100 bipolar temperature controller (Harvard Apparatus). We took images with an A655sc thermal camera (FLIR) calibrated to a BB701 blackbody radiator (Omega) to

confirm that the fly's thorax and head equilibrated above the restrictive temperature of shibire (30-34ºC) less than 20 seconds after the bath temperature reached 34ºC. Flies always flew in the context of a blank screen for at least 3.5 minutes with the temperature held at 19º. If the experiment included visual stimuli, these were presented after this period. The temperature was then increased to 34ºC, and the process was repeated. Time zero was set to when the bath hit 26ºC on its way from 19ºC to 34ºC. The period one minute before and one minute after this heating transition was not taken into consideration when calculating the spontaneous saccade rate. For TeTxLC; $GAL80^{ts}$ experiments, flies were collected 1-3 days after eclosion and incubated at 31ºC for 24 hours prior to tethering. Flies' spontaneous flight behavior was assayed less than 2 hours after removal from 31ºC.

Visual response quantification during tethered flight

Loom response amplitude of average fly traces was calculated by subtracting the average L-R WBA in a window 560-800 ms after expansion began from the average during a 200 ms window prior to expansion (Figure 2.7). Grating response amplitude was calculated by subtracting the average L-R WBA in a window 1-1.5 s after the visual stimulus began to move from the average during a 500 ms period beforehand (Figure 2.9). Single fly average traces were composed of the average of the first 10 trials for loom, and all trials for gratings (up to a maximum of 10) in which the fly was flying for at least 95% of the time in both the baseline period and the duration of the stimulus.

Saccade detection

Spontaneous saccades were detected using an algorithm which worked by comparing the raw L-R WBA signal to a low-pass filtered "baseline" signal (cutoff frequency = 0.5 Hz). The baseline signal, L-R WBA(lpf), was computed by linearly interpolating regions of the filtered L-R WBA signal that were both relatively flat (absolute slope < 4 deg/s) and had a low magnitude second derivative (absolute acceleration < 200 deg/s^2). If the raw signal crossed at least 8º above or below this calculated baseline and remained beyond this threshold for at least 60 ms, then the algorithm classified this event as a saccade.

Calcium imaging behavioral experiments

1-4 day old female w+ / w-; +; *60D05-Gal4* / *UAS-GCaMP6m* flies were anesthetized at 4ºC. Flies' were tethered to a custom holder as in Green *et al.* 2017. Their proboscis was glued with blue light-curable glue (Bondic) such that it could not be extended. Glue was place on the dorsal surface of the head and the tip of the thorax, and these points of contact were glued to the holder. The head was tilted downward such that the posterior surface of the head was visible through a hole in the bottom of the custom holder. Once tethered, flies rested in a cool dark room for 4-9 hours. Flies rested in a clear plastic box, in which was placed a wet paper towel to maintain humidity. Images were acquired over a 20-30 minute-long imaging session. Before imaging, the cuticle covering the posterior surface of the fly's head was dissected away. To do this, a window was cut with a 30G x ½ syringe needle, and trachea were removed with sharp

forceps, taking care not to damage the glial sheath beneath. The fly was placed on the microscope in such a way that the fly could walk comfortably on the foam ball and so that its head sat beneath the objective. At this point extracellular saline was perfused over the fly's head at 21ºC – 24ºC and imaging began.

Calcium imaging

I used a two-photon microscope with a movable objective (Bruker) and custom built stage (ThorLabs, Siskiyou). The laser used for two-photon excitation was a Chameleon Ultra II Ti:Sapphire femtosecond pulsed laser (Coherent) tuned to 925 nm for imaging GCaMP6m. I used a 40x 0.8 NA objective (Olympus) to image the brain. Emitted light was split by a 575 nm dichroic mirror and was then filtered by a 490-560 nm bandpass filter (Chroma). Signals were detected with GaAsP detectors (Hamamatsu). During experiments, the brain was perfused with extracellular saline with an osmolarity of 280±5 mOsm. The concentration of the constituent solutes in mM were: NaCl 103, KCl 3, N-Tris(hydroxymethyl) methyl-2-aminoethanesulfonic acid (TES) 5, trehalose 10, glucose 10, sucrose 2, $NaHCO_3$ 26, NaH_2PO_4 1, $CaCl_2$ 1.5, and $MgCl_2$ 4. The saline was bubbled with a gas mixture composed of 95% O_2 and 5% CO_2. The saline temperature was controlled with the same peltier device described above, and the temperature was held between 21ºC and 24ºC. To image the protocerebral bridge, I selected a region of interest containing the entire bridge, about 150 x 60 pixels in size. The power of the excitation laser was between 40 and 60 mW as measured at the sample. The dwell time per pixel was approximately 2.8 μs. I scanned through 3-5 z-

planes separated by 6-9 μm using a piezo motor at a volumetric scanning rate of 3-5 Hz.

Imaging experiment trial structure

In imaging experiments in Chapter 3, flies walked in closed loop control of the angular position of a bright bar. MATLAB tracked flies' translational speed on the ball, and the angular position of the bright bar. Flies walked in closed loop control of the angular position of a bright bar for 30+ seconds until the following criteria all were met: all 11.25º of the bar had to be visible, and the average translational speed over the previous three seconds had to be below a threshold value. In figures 3.2-3.4, trial triggering had the additional criteria that the average absolute turning speed of the fly had to be below 15ºs for 1 s and that the bar had to have been fully visible for at least 1s (to prevent trials from triggering abruptly as soon as the bar moved into view). If these criteria were met, MATLAB triggered a trial. The trial structures for flies in Figure 3.1 and Figures 3.2-3.4 are listed in Figures 3.1a and 3.2a, respectively. In Figure 3.1, a trial consisted of a period of stasis (stable-bar-1), followed by a bar jump of ±10º, ±20º, or ±30º (stable-bar-2). The bar was held in these positions for 5s. This was followed by a 5s dark period, before flies were returned to closed loop. In Figures 3.2-3.4, a trial consisted of a period of stasis lasting 1s (stable-bar-1), followed by a 5s dark period (dark-1), followed by a 5s period during which the bar was jumped to a position ±5º, ±10º, ±20º, ±30º, ±45º, ±60º, ±90º or 180º from the bar's position during the stable-bar-1 period, and the bar was held here for 5s (stable-bar-2), after which the bar was removed a second time for 5s (dark-

2), after which the fly was returned to closed loop. In all experiments, once the fly met the behavioral criteria for a trial, a jump size was chose than would render the bar fully visible during the stable-bar-2 period. Flies often started walking in the middle of a trial. During periods when the bar was held behind the fly or at a fixed visible angle (in the dark-1, dark-2, and stable-bar-2 periods in Figures 3.1-3.4), if the fly began to walk, MATLAB continued to store the fly's yaw rotations on the ball, and these yaw rotations were integrated to generate an appropriate new bar position when the fly was returned to closed loop.

Image analysis

Images were analyzed in python 2.7. Images were registered by translating every z-slice at every time point so as to best match it with the time-averaged image of that z-slice. Regions of Interest (ROIs) were drawn manually in Fiji (Schindelin *et al.* 2012) for the 16 glomeruli of the protocerebral bridge innervated by E-PG neurons. E-PGs do not innervate the outer two glomeruli of the bridge (Wolff, Iyer, and Rubin 2015), so no region was defined for these glomeruli. ROIs for a single bridge glomerulus could span multiple z-slices. These ROIs were colored in Photoshop according to their anatomical position on the protocerebral bridge. For every time point, I calculated the mean pixel intensity inside each ROI. I calculated the $\Delta F/F$ (with the formula $(F-F_0 / F_0)$, where the F_0 baseline represents the average fluorescence of each ROI in the dimmest 5% of frames) for each glomerulus separately. At this point, at every time point, I had a 16-element vector representing the $\Delta F/F$ value at every glomerulus. In E-PG neurons,

these vectors exhibit a relatively constant power spectrum peak at 8 glomeruli (Green *et al.* 2017). I extracted the E-PG phase from every time point by taking the Fourier Transform of every time point independently and extracting the phase of Fourier component with an 8 glomerulus period. The rotation of this phase tracks the rotation of a the bar when the fly walks in closed loop (Green *et al.* 2017). To plot the E-PG phase aligned with the bar position (Figures 1.1e-f, 2.1b-c, 2.2b-c), I added an offset to the E-PG phase (the circular difference between the bar position and the E-PG phase 5 seconds into the subset of the recording I wished to plot), and then I wrapped this sum. To calculate the bar position represented by the E-PG phase (Figure 3.2g), I added the offset between the bar and the phase over the last 20 seconds of closed loop. This offset was calculated by taking the circular mean of the circular difference between the bar position and the phase position over the last 20 seconds of closed loop.

Aligning imaging data collected at different frame rates

Frame trigger outputs from Prairie indicated the precise time frames were acquired, allowing behavioral data and imaging data to be aligned. In Figures 3.1d and 3.3a, I had to average E-PG phases from different flies. Because different flies were imaged at slightly different frame rates depending on the size of the region of interest and the number of z-slices collected, when averaging the stimulus-triggered phase response across trials, I binned data into 0.67 second-long time bins, which is more than twice the length of the frame collection period in my slowest imaging session. That is, in Figures 3.1d, 3.3a, and 3.4a, every point in every trial represents the circular mean of 2-3 phase

measurements. When plotting averages across trials I simply took a circular mean of these binned trials.

Selection criteria for trials to analyze

While during imaging a trial was *triggered* by a brief period of stasis, I only analyzed data for which the fly stood still throughout the indicated analysis period. My criteria for stillness were that the fly's absolute turning speed could at no point exceed 40 deg/s, nor could the fly's forward velocity exceed 2.5 mm/s. These thresholds proved sufficiently low that they weeded out trials wherein the fly started walking, but sufficiently high that I was not eliminating trials due to noise. I had one additional criterion for ruling out a trial: the E-PG phase estimate could not look too noisy by eye. If the envelope of E-PG phases oscillated wildly with an envelope >= ~45º (as sometimes occurs when the fly stands still, because the E-PG signal becomes dim and the signal-to-noise ratio decreases), I did not include this trial in my analyses. 9 trials from the experiments schematized in Figure 3.1 and 62 trials from the experiments schematized in Figures 3.2-3.4 were excluded on this basis.

E-PG phase response quantification

For the data in Figure 3.1, the E-PG phase of the stable-bar-1 period was calculated by taking the circular mean of the E-PG phase in the 1 second before the bar was jumped. The E-PG phase of the stable-bar-2 period was calculated by taking a circular mean of the E-PG phase in the window 3-5 seconds after the bar was jumped. The E-PG phase

of the dark period was calculated by taking the circular mean of the E-PG phase in the 8-10 second window after the bar was jumped (i.e. 3-5 seconds after the bar was removed. For the data in Figures 3.2-3.4, the stable-bar-1 period phase was calculated by taking the circular mean of the E-PG phase in the 1 second before the bar was turned off the first time. The dark-1 period phase was calculated by taking a circular mean of the E-PG phase in the window 3-5 seconds after the bar was turned off the first time. The stable-bar-2 period phase was calculated by taking the circular mean of the E-PG phase in the 3-5 seconds after the bar reappeared (8-10 seconds after the bar was initially turned off). The dark-1 period phase was calculated by taking a circular mean of the E-PG phase in the window 3-5 seconds after the bar was turned off the *second* time (13-15 seconds after the bar was initially turned off). To calculate the ΔE-PG phase between any of these two periods, I simply subtracted the values and then wrapped them so the value fell between -180º and 180º. Because bar jumps of different sizes were presented pseudo-randomly and because flies sometimes interrupted trials by walking in the middle, I collected a different number of completely static trials in each category from different flies. As such, when I plotted event-triggered average E-PG phases (Figures 3.1d and 3.3a) , I computed the circular mean phase response across *trials*, not across flies.

Statistical analysis

The statistical tests used are mentioned in the text. In Chapter 2 I used the SciPy.stats python module. In Chapter 3, circular correlation values, circular 95% confidence

intervals were calculated using functions in the circstats.py python module (Jessica B. Hamrick, Peter W. Battaglia, 2013). I wrote the code for the circular median test myself using an algorithm described by Berens (2009).

References

Aksay, E., R. Baker, H.S. Seung, and D.W. Tank. 2000. “Anatomy and Discharge Properties of Pre-Motor Neurons in the Goldfish Medulla That Have Eye-Position Signals During Fixations”. *J Neurophysiol* 84 (2):1035-49.

Aksay, Emre, Guy Major, Mark S. Goldman, Robert Baker, H. Sebastian Seung, and David W. Tank. 2000. “History Dependence of Rate Covariation between Neurons during Persistent Activity in an Oculomotor Integrator”. *Cerebral Cortex* 13: 1173–84.

Aksay, Emre, Itsaso Olasagasti, Brett D Mensh, Robert Baker, Mark S Goldman, and David W Tank. 2007. “Functional Dissection of Circuitry in a Neural Integrator” *Nat Neurosci* 4(10): 494 – 504.

Alexander G.E., DeLong M.R., Strick P.L. 1986. “Parallel organization of functionally segregated circuits linking basal ganglia and cortex”. *Annu Rev Neurosci*, 9*,* 357–381.

Arleo, Angelo, Cyril Déjean, Pierre Allegraud, Mehdi Khamassi, Michael B. Zugaro, and Sidney I. Wiener. 2013. “Optic Flow Stimuli Update Anterodorsal Thalamus Head Direction Neuronal Activity in Rats” *J Neurosci* 33(42): 16790 – 95.

Aso, Y., D. Sitaraman, T. Ichinose, K.R. Kaun, K. Vogt, G. Belliart-Guerin, P.Y. Placais, A.A. Robie, N. Yamagata, C. Schnaitmann, *et al.* 2014. “Mushroom Body Output Neurons Encode Valence and Guide Memory-Based Action Selection in *Drosophila*.” *eLife* 3: e04580.

Bassett JP and JS Taube. 2001. “Neural Correlates for Angular Head Velocity in the Rat Dorsal Tegmental Nucleus”. *J Neurosci* 21: 5740–51.

Bassett JP, Tullman ML, Taube JS. 2007. “Lesions of the Tegmento-Mammillary Circuit in the Head Direction System Disrupt the Head Direction Signal in the Anterior Thalamus”. *J Neurosci.* 27 (28): 7564–77.

Becker, W., and H.M. Klein. 1973. “Accuracy of Saccadic Eye Movements and Maintenance of Eccentric Eye Positions in the Dark” *Vision Res* 13: 1021–34.

Bender, J.A. and M.H. Dickinson. 2006a. “A Comparison of Visual and Haltere-Mediated Feedback in the Control of Body Saccades in *Drosophila melanogaster*” *J Exp Biol* 209: 4597–4606.

Bender, J.A., and M.H. Dickinson. 2006b. “Visual Stimulation of Saccades in Magnetically Tethered *Drosophila*” *J Exp Biol* 209: 3170–82.

Ben-Yishai, R, Bar-Or RL, Sompolinsky H. 1995. “Theory of Orientation Tuning in Visual Cortex.” *Proc Natl Acad Sci USA* 92: 3844–48.

Berg, H C, and D A Brown. 1972. “Chemotaxis in Escherichia Coli Analysed by Three-Dimensional Tracking.” *Nature* 239 (5374): 500–4.

Berens, Phillip. 2009. “CircStat: A MATLAB Toolbox for Circular Statistics” *Journal of Statistical Software* 31(10): 1–21.

Berni, J., S.R. Pulver, L.C. Griffith, and M. Bate. 2012. “Autonomous Circuitry for Substrate Exploration in Freely Moving *Drosophila* Larvae” *Curr Biol* 22: 1861–70.

Bertrand S, A Bertrand, R Guevara-Carrasco, and F Gerlotto. 2007. “Scale-invariant Movements of Fishermen: the Same Foraging Strategy as Natural Predators”. *Ecological Applications : A Publication of the Ecological Society of America* 17: 331–37.

Blair HT and PE Sharp. 1998. “Role of the Lateral Mammillary Nucleus in the Rat Head Direction Circuit: a Combined Single-unit Recording and Lesion Study”. *Neuron* 21: 1387–97.

Block, Steven M, Jeffrey E Segall, and Howard C Berg. 1982. “Impulse Responses in Bacterial Chemotaxis.” *Cell* 31 (1): 215–26.

Bostock, Elizabeth, Robert U. Muller, and John L. Kubie. 1991. “Experience-dependent Modifications of Hippocampal Place Cell Firing”. *Hippocampus* 1(2): 193–206.

Boyden Jr., S. E. 1962. “The Chemotactic Effect of Mixtures of Antibody and Antigen on Polymorphocellular Leucocytes” 1962. *J Exp Med* 115 (3): 453–66.

Brody, Carlos D, Ranulfo Romo and Adam Kepecs. 2003. “Basic Mechanisms for Graded Persistent Activity: Discrete Attractors, Continuous Attractors, and Dynamic Representations.” *Curr Opin Neurobiol* 13:204–211.

Brower, L. P. 1996., *J Exp Biol* 199, 93-103.

Buchanan SM, Kain JS, and de Bivort BL. 2015. “Neuronal Control of Locomotor Handedness in *Drosophila*”. *PNAS* 112(21): 6700–05.

Butler, William N., Kyle S. Smith, Matthijs A.A. van der Meer, and Jeffrey S. Taube. 2017. “The Head-Direction Signal Plays a Functional Role as a Neural Compass during Navigation” *Curr Biol* 27, 1259–67.

Carli, M., Evenden M.L., Robbins, T.W. 1985. “Depletion of Unilateral Striatal Dopamine Impairs Initiation of Contralateral Actions and not Sensory Attention”. *Nat Lett* 313: 679–681.

Censi, A., A.D. Straw, R.W. Sayaman, R.M. Murray, and M.H. Dickinson. 2013. “Discriminating External and Internal Causes for Heading Changes in Freely Flying *Drosophila*”. PLoS Comput. Biol. *9*, e1002891.

Collett, T.S. and M.F. Land. 1975. “Visual Control of Flight Behavior in the Hoverfly *Syritta pipiens L.” J Comp Physiol* 99: 1–66.

Coyne, Jerry A., Ian A. Boussy, Timothy Prout, Stephen H. Bryant, J. S. Jones and John A. Moore (1982). “Long-Distance Migration of *Drosophila*” *The American Naturalist* 119(4): 589–595.

Dickinson, M.H. 1999. “Haltere-mediated Equilibrium Reflexes of the Fruit Fly, *Drosophila melanogaster*” *Philos Trans R Soc Lond B Biol Sci* 354: 903–916.

Dickinson, Michael H. 2004. “Death Valley, *Drosophila*, and the Devonian Toolkit” *Annu Rev Entomol* 59: 51–72.

Dickinson, M.H. 2005. “The Initiation and Control of Rapid Flight Maneuvers in Fruit Flies” *Integr Comp Biol* 45: 274–281.

Dickinson, M.H., F.-O. Lehmann, and W.P. Chan. 1998. “The control of Mechanical Power in Insect Flight” *Am Zool* 38: 718–728.

Dittman, Andrew H. and Thomas Quinn. 1996. “Homing in Pacific Salmon: Mechanisms and Ecological Basis” *J Exp Biol* 199, 83–91.

Dudchenko, P.A., and J.S. Taube. 1997. “Correlation Between Head Direction Cell Activity and Spatial Behavior on a Radial Arm Maze”. *Behav Neurosci* 111: 3–19.

Dunn, T.W., Y. Mu, S. Narayan, O. Randlett, E.A. Naumann, C. Yang, A.F. Schier, J. Freeman, F. Engert, M.B. and Ahrens. 2016. “Brain-wide Mapping of Neural Activity Controlling Zebrafish Exploratory Locomotion”.*eLife* 5:e12741.

Eichenbaum, Howard, Caroline Stewart, and R.G.M. Morris. 1990. “Hippocampal Representation in Place Learning”. *J Neurosci*, 10 (11): 3531–42.

Finkelstein, A, D Derdikman, A Rubin, JN Foerster, L Las, and N Ulanovsky. 2015. "Three-dimensional Head-direction Coding in the Bat Brain". *Nature*. 517 (7533): 159–164.

Fouad, K., Rathmayer, W., and Libersat, F. (1996). Neuromodulation of the escape behavior of the cockroach *Periplaneta americana* by the venom of the parasitic wasp *Ampulex compressa*. J. Comp. Physiol. A *178*, 91–100.

Franconville, Romain, Celia Beron, and Vivek Jayaraman 2018. “Building a functional connectome of the *Drosophila* central complex”. eLife 2018;7:e37017. DOI: 10.7554/eLife.37017

Fujiwara, T., T.L. Cruz , J.P Bohnslav, and M.E.Chiappe. 2017. “A Faithful Internal Representation of Walking Movements in the *Drosophila* Visual System” *Nat Neurosci* 20: 72–81.

Gabbiani, F., H.G. Krapp, and G. Laurent. 1999. “Computation of Object Approach by a Wide-Field, Motion-Sensitive Neuron” *J Neurosci* 19: 1122–41.

Gal, R. F. Libersat. 2008. “A Parasitoid Wasp Manipulates the drive for walking of its cockroach prey.” *Curr Biol* 18: 877–882.

Gordus, Andrew, Navin Pokala, Sagi Levy, Steven W. Flavell, and Cornelia I. Bargmann. 2015. “Feedback from Network States Generates Variability in a Probabilistic Olfactory Circuit” *Cell* 161: 215–27.

Götz, K. G. 1968. “Flight Control in *Drosophila* by Visual Perception of Motion” *Kybernetik* 4: 199–208.

Götz, K.G. “Visual guidance in *Drosophila*.” in *Development and Neurobiology of Drosophila* (eds. Siddiqi, O., Babu, P., Hall, M.L. & Hall, J.C.) 391–407 (Plenum Press, New York, 1980).

Green, Jonathan and Gaby Maimon. 2018. “Building a heading signal from anatomically defined neuron types in the *Drosophila* central complex” *Curr Opin Neurobiol* 52:156–164.

Hafting, T., M. Fyhn, S. Molden, M.-B. Moser, E. I. Moser. 2005. “Microstructure of a spatial map in the entorhinal cortex.” *Nature* 436: 801–806.

Haikala, V., Joesch, M., Borst, A., and Mauss, A.S. (2013). Optogenetic control of fly optomotor responses. J. Neurosci. *33*, 13927–34.

Harland, Bruce, Roddy M. Grieves, David Bett, Rachael Stentiford, Emma R. Wood, and Paul A. Dudchenko. 2017. “Lesions of the Head Direction Cell System Increase Hippocampal Place Field Repetition” *Curr Biol* 27: 2706–2712.

Heinze, S, and U Homberg. 2007. “Maplike Representation of Celestial E-Vector Orientations in the Brain of an Insect.” *Science* 315 (5814): 995–97.

Heinze, Stanley and Steven M. Reppert. 2011. “Sun Compass Integration of Skylight Cues in Migratory Monarch Butterflies” *Neuron* 69: 345–358.

Heisenberg, M. and R. Wolf. 1979. “On the Fine Structure of Yaw Torque in Visual Flight Orientation of *Drosophila melanogaster*”. *J Comp Physiol* 130: 113–130.

Heisenberg, M. and Wolf, R. 1984. “Vision in *Drosophila*: Genetics of Microbehavior” (Springer).

Homberg, Uwe. 2008. “Evolution of the Central Complex in the Arthropod Brain with Respect to the Visual System.” *Arthropod Structure & Development* 37 (5): 347–62.

Ilius, M., R. Wolf, and M. Heisenberg. 1994. “The Central Complex of *Drosophila melanogaster* is involved in flight control: Studies of Mutants and Mosaics of the Gene *Ellipsoid Body Open*” *J Neurogenet*, 21: 321–338.

Jakobson, R. 1968. “Child Language: Aphasia and Phonological Universals”. The Hague: Mouton.

Janovic, J. 2008. “Parkinson’s Disease: Clinical Features and Diagnosis”. *J Neurol Neurosurg Psychiatry* 79*,* 368–376.

Jenett, A. *et al.* 2012. “A GAL4-driver Line Resource for *Drosophila* Neurobiology” *Cell Rep* 2: 991–1001.

Kaada, B.R., E.W. Rasmussen, and O. Kveim. 1961. “Effects of hippocampal lesions on maze learning and retention in rats”. *Exp Neurol* 3: 333-55.

Kim, Irene and Michael H. Dickinson. 2017. “Idiothetic Path Integration in the Fruit Fly *Drosophila melanogaster*” *Curr Biol* 27, 2227–38.

Kim, A.J., L.M. Fenk, C. Lyu, and G. Maimon. 2017. “Quantitative Predictions Orchestrate Visual Signaling in *Drosophila*” *Cell* 168: 280–294.

Kim, A.J., J.K Fitzgerald, and G. Maimon. (2015). “Cellular Evidence for Efference Copy in *Drosophila* Visuomotor Processing” *Nat Neurosci* 18: 1247–55.

Koenig, J.H., K. Saito, and K. Ikeda. 1983. “Reversible Control of Synaptic Transmission in a Single Gene Mutant of *Drosophila melanogaster*” *J Cell Biol* 96: 1517–22.

Knierim, James J., Hemant S. Kudrimoti, and Bruce L. McNaughton. 1995. “Interactions Between Idiothetic Cues and External Landmarks in the Control of Place Cells and Head Direction Cells” *J Neurosci* 15: 1648–1659.

Knierim, James J. and Kechen Zhang. 2012. “Attractor Dynamics of Spatially Correlated Neural Activity in the Limbic System”. *Annu Rev Neurosci* 35: 267–285.

Kuntz, Sara, Burkhard Poeck, and Roland Straus. 2017. “Visual Working Memory Requres Permissive and Instructive NO/cGMP Signaling at Presynapses in the *Drosophila* Central Brain” *Curr Biol* 27(5): 613-623.

Lindsay, T.H., A. Sustar, and M.H. Dickinson. 2017. “The Function and Organization of the Motor System Controlling Flight Maneuvers in Flies”. *Curr Biol* 27: 345–358.

Mahr, A., and H. Aberle. 2006. “The Expression Pattern of the *Drosophila* Vesicular Glutamate Transporter: a Marker Protein for Motoneurons and Glutamatergic Centers in the Brain” *Gene Expr Patterns* 6: 299–309.

Maimon, G., A.D. Straw, and M.H. Dickinson. 2008. “A Simple Vision-Based Algorithm for Decision Making in Flying *Drosophila*”. *Curr Biol* 18: 464–470.

Maimon, G., A.D. Straw, and M.H. Dickinson. 2010. “Active Flight Increases the Gain of Visual Motion Processing in *Drosophila*” *Nat Neurosci* 13: 393–399.

Mamiya, A. and M.H. Dickinson. 2015. “Antennal mechanosensory neurons mediate wing motor reflexes in flying *Drosophila*” *J Neurosci* 35: 7977–91.

Maye, A., C.-H. Hsieh, G. Sugihara, and B. Brembs. 2007. “Order in Spontaneous Behavior”. *PLoS ONE* 2, e443.

Mayer, M., K. Vogtmann, B. Bausenwein, R. Wolf, and M. Heisenberg. 1988. “Flight Control During ‘Free Yaw Turns’ in *Drosophila melanogaster*” *J Comp Physiol A* 163: 389–399.

McGuire, S.E., P.T. Le, A.J. Osborn, K. Matsumoto, and R.L Davis. 2003. “Spatiotemporal Rescue of Memory Dysfunction in *Drosophila*” *Science* 302: 1765–68.

Milner, B., S. Corkin, and H.-L Teuber. 1968. “Further analysis of the hippocampal amnesic syndrome: 14 year follow-up study of H.M.”. *Neuropsychologia* 6: 215-34.

Miri, Andrew, Kayvon Daie, Aristides B Arrenberg, Herwig Baier, Emre Aksay, and David W Tank. 2011. “Spatial gradients and multidimensional dynamics in a neural integrator circuit”. *Nat Neurosci* 14(9): 1151–59.

Mizumori, SJ, and JD Williams. 1993. “Directionally Selective Mnemonic Properties of Neurons in the Lateral Dorsal Nucleus of the Thalamus of Rats.” *J Neurosci* 13 (9): 4015–28.

Mongeau, J.-M. and M.A. Frye. 2017. “*Drosophila* Spatiotemporally Integrates Visual Signals to Control Saccades” *Curr Biol* 27: 2901–14.

Moser, May-Britt, David C Rowland, and Edvard I Moser. 2015. “Place Cells, Grid Cells, and Memory.” *Cold Spring Harbor Perspectives in Biology* 7 (2). Cold Spring Harbor Lab: a021808. doi:10.1101/cshperspect.a021808.

Mouritsen, Henrik and Barrie J. Frost. 2002. “Virtual migration in tethered flying monarch butterflies reveals their orientation mechanisms” *PNAS*, 99 (15): 10162–10166.

Muijres, F.T., M.J. Elzinga, J.M. Melis, and M.H. Dickinson. 2014. “Flies Evade Looming Targets by Executing Rapid Visually Directed Banked Turns” *Science* 344: 172–177.

Muijres, F.T., M.J. Elzinga, N.A. Iwasaki, and M.H. Dickinson. 2015. “Body Saccades of *Drosophila* Consist of Stereotyped Banked Turns.” *J Exp Biol* 218: 864–875.

Muller, Martin and Rudiger Wehner. 1988. “Path Integration in Desert Ants, *Cataglyphis fortis*” *Proc Natl Acad Sci USA* 85: 5287-5290.

Nadel, L. 1968. “Dorsal and ventral hippocampal lesions and behaviour”. *Physiol Behav* 3: 891-900.

Nern, A., B.D. Pfeiffer, and G.M. Rubin. 2015. “Optimized Tools for Multicolor Stochastic Labeling Reveal Diverse Stereotyped Cell Arrangements in the Fly Visual System”. *Proc Natl Acad Sci USA* 112: E2967-E2976.

Neuser, Kirsa, Tilman Triphan, Markus Mronz, Burkhard Poeck, and Roland Strauss. 2008. “Analysis of a spatial orientation memory in *Drosophila*” *Nat Lett* 453: 1244-48.

Ofstad, Tyler A, Charles S Zuker, and Michael B Reiser. 2011. “Visual Place Learning in *Drosophila Melanogaster*.” *Nature* 474 (7350): 204–7.

O'Keefe, J, and J Dostrovsky. 1971. “The Hippocampus as a Spatial Map: Preliminary Evidence From Unit Activity in the Freely-Moving Rat.” *Brain Research* 34 (1): 171–75.

O’Keefe, John and Lynn Nadel. 1978. “The Hippocampus as a Cognitive Map” (Clarendon Press).

Ölveczky, B.P., Andalman A.S., Fee, M.S. 2005. “Vocal Experimentation in the Juvenile Songbird Requires a Basal Ganglia Circuit”. *PLOS Biology* 3:e153.

Peyrache, Adrien, Marie M Lacroix, Peter C Petersen & György Buzsáki. 2015. “Internally Organized Mechanisms of the Head Direction Sense” *Nat Neurosci* 18 (4): 569–75.

Pfeiffer, B.D. *et al.* (2008). “Tools for Neuroanatomy and Neurogenetics in *Drosophila*” *Proc Natl Acad Sci USA* 105: 9715–20.

Pierce-Shimomura, Jonathan T., Thomas M. Morse and Shawn R. Lockery. 1999. “The Fundamental Role of Pirouettes in *Caenorhabditis elegans* Chemotaxis”. *J Neurosci* 19 (21): 9557-69.

Quirk, Gregory J., Robert U. Muller, and John L. Kubie. 1990. “The Firing of Hippocampal Place Cells in the Dark Depends on the Rat’s Recent Experience” *J Neurosci* 10(6): 2008–17.

Reppert, Steven M., Haisun Zhu, and Richard H. White. 2004. “Polarized Light Helps Monarch Butterflies Navigate” *Curr Biol* 14: 155–158.

Ranck, JB Jr. 1984. “Head Direction Cells in the Deep Cell Layer of Dorsal Presubiculum in Freely Moving Rats”. *Soc Neurosci Abstr.*

Redish, A David, Adam N Elga, and David S Touretzky. 1996. “A Coupled Attractor Model of the Rodent Head Direction System” *Network: computation in neural systems.* 7(4): 671–685.

Reiser, M.B., and M.H. Dickinson. 2008. “A Modular Display System for Insect Behavioral Neuroscience” *J Neurosci Methods* 167: 127–139.

Reynolds, A.M., and M.A. Frye. 2007. “Free-flight Odor Tracking in *Drosophila* is Consistent with an Optimal Intermittent Scale-free Search”. *PLoS ONE* 2: e354.

Riley, J.R., U. Greggers, A.D. Smith, D.R. Reynolds and R. Menzel. 2005. “The Flight Paths of Honeybees Recruited by the Waggle Dance” *Nature* 435: 205-207.

Roberts *et al.* 2016. *eLife* 5:e12572.

Röder, L., C. Vola, and S. Kerridge. 1992. “The Role of the *Teashirt* Gene in Trunk Segmental Identity in *Drosophila*” *Development* 115: 1017–33.

Robertson, RG, ET Rolls, P Georges-François, and Panzeri S. 1999. "Head Direction Cells in the Primate Pre-subiculum". *Hippocampus* 9 (3): 206–19.

Schnell, B., I.G. Ros, and M.H. Dickinson. 2017. “A Descending Neuron Correlated with the Rapid Steering Maneuvers of Flying *Drosophila*” *Curr Biol* 27: 1200–05.

Schindelin, Johannes *et al.* 2012. “Fiji: an Open-Source Platform for Biological-Image Analysis.” *Nature Methods* 9 (7): 676–682.

Seung HS. 1996. “How the Brain Keeps the Eyes Still.” *Proc Natl Acad Sci USA* 93:13339–44.

Seung, H.S., D.D. Lee, B.Y. Reis, and D.W. Tank. 2000. “Stability of the Memory of Eye Position in a Recurrent Network of Conductance-Based Model Neurons”. *Neuron* 26: 259–71.

Sharp PE, A Tinkelman, and J Cho. 2001. “Angular Celocity and Head Direction Signals Recorded from the Dorsal Tegmental Nucleus of Gudden in the Rat: Implications for Path Integration in the Head Direction Cell Circuit”. *Behav Neurosci* 115: 571–88.

Sims, David W. *et al.* 2008. “Scaling Laws of Marine Predator Search Behaviour” *Nature* 451: 1098–1102.

Skaggs, WE, JJ Knierim, HS Kudrimoti, and BL McNaughton. 1995. “A Model of the Neural Basis of the Rat's Sense of Direction.” *Advances in Neural Information Processing Systems* 7: 173–80.

Sommer, Stefan and Rüdiger Wehner. 2005. “Vector Navigation in Desert Ants, *Cataglyphis fortis*: Celestial Compass Cues are Essential for the Proper Use of Distance Information” *Naturwissenschaften* 92: 468–471.

Stackman RW, Golob EJ, Bassett JP, Taube JS. 2003. “Passive Transport Disrupts Directional Path Integration by Rat Head Direction Cells”. *J Neurophysiol* 90:2862–74.

Stackman, Robert W, and Jeffrey S Taube. 1997. “Firing Properties of Head Direction Cells in the Rat Anterior Thalamic Nucleus: Dependence on Vestibular Input.” *J Neurosci* 17 (11): 4349–58.

Stackman RW, and JS Taube. 1998. “Firing Properties of Rat Lateral Mammillary Single Units: Head Direction, Head Pitch, and Angular Head Velocity.” *J Neurosci* 18: 9020–37.

Stowers, John R *et al.* 2017. “Virtual Reality for Freely Moving Animals” *Nature Methods* 14: 995–1002.

Strauss, R, and J Pichler. 1998. “Persistence of Orientation Toward a Temporarily Invisible Landmark in Drosophila Melanogaster.” *J Comp Physiol A: Sensory, Neural, and Behavioral Physiology* 182(4): 411–423.

Strauss, Roland and Martin Heisenberg. 1993. “A Higher Control Center of Locomotor Behavior in the *Drosophila* Brain” *J Neurosci* 13(5): 1852-1861.

Straw, A.D., and M.H. Dickinson. 2009. “Motmot, an Open-source Toolkit for Realtime Video Acquisition and Analysis”. *Source Code Biol Med* 4: 5.

Suster, M.L., L. Seugnet, M. Bate, and M.B. Sokolowski. 2004. “Refining GAL4-driven Transgene Expression in *Drosophila* with a GAL80 Enhancer-Trap”. *Genesis* 39: 240–245.

Sweeney, S.T., K. Broadie, J. Keane, H. Niemann, and C.J. O’Kane. 1995. “Targeted Expression of Tetanus Toxin Light Chain in *Drosophila* Specifically Eliminates Synaptic Transmission and Causes Behavioral Defects”. *Neuron* 14: 341–351.

Tammero, L.F. and M.H. Dickinson. 2002. “The Influence of Visual Landscape on the Free Flight Behavior of the Fruit Fly *Drosophila melanogaster*.” *J Exp Biol* 205: 327–343.

Tammero, L.F. and M.H. Dickinson. 2002. “Collision-avoidance and Landing Responses are Mediated by Separate Pathways in the Fruit Fly, *Drosophila melanogaster*” *J Exp Biol* 205: 2785–98.

Tammero, L.F., M.A. Frye, and M.H Dickinson. 2004. “Spatial Organization of Visuomotor Reflexes in *Drosophila*” *J Exp Biol* 207: 113–122.

Taube JS. 1995. “Head Direction Cells Recorded in the Anterior Thalamic Nuclei of Freely Moving Rats” *J Neurosci* 15: 1953–71.

Taube JS and RU Muller. 1998. "Comparison of Head Direction Cell Activity in the Postsubiculum and Anterior Thalamus of Freely Moving Rats.” *Hippocampus* 8:87–108.

Taube, JS, RI Muller and JB Ranck. 1990. “Head Direction Cells Recorded from the Postsubiculum in Freely Moving Rats. I. Description and Quantitative Analysis” *J Neurosci* 10: 420–35.

Taube, JS, RI Muller and JB Ranck. 1990. “Head Direction Cells Recorded from the Postsubiculum in Freely Moving Rats. II. Effects of Environmental Manipulations” *J Neurosci* 10: 436–47.

Terao, Y. Fukuda, H., Ugawac, Y., Hikosaka, O. 2013. "New Perspectives on the Pathophysiology of Parkinson's Disease as Assessed by Saccade Performance: A Clinical Review." *Clinical Neurophysiology*, 124: 1491–1506.

Tervo, Dougal G.R., Mikhail Proskurin, Maxim Manakov, Mayank Kabra, Alison Vollmer Kristin Branson, and Alla Y. Karpova. 2014. "Behavioral Variability through Stochastic Choice and its Gating by Anterior Cingulate Cortex". *Cell* 159: 21–32.

Biased random walk leukocyte -Tranquillo, RT, DA Lauffenburger, and SH Zigmond. 1988. "A Stochastic Model for Leukocyte Random Motility and Chemotaxis Based on Receptor Binding Fluctuations." *J Cell Biol* 106: 303-09.

Trimarchi, J.R. and R.K. Murphey. 1997. "The *shaking-B2* Mutation Disrupts Electrical Synapses in a Flight Circuit in Adult *Drosophila*" *J Neurosci* 17: 4700–10.

Turner-Evans, Daniel B., and Vivek Jayaraman. 2016. "The insect central complex" *Curr Biol* 26: R445–R460.

Varga, Adrienn G, and Roy E Ritzmann. 2016. "Cellular Basis of Head Direction and Contextual Cues in the Insect Brain." *Curr Biol* 26 (14): 1816–28.

Von Frisch, K. 1967. "The Dance Language and Orientation of Bees" (Havard University Press).

von Reyn, C.R., P. Breads, M.Y. Peek, G.Z. Zheng, W.R. Williamson, A.L. Yee, A. Leonardo, A., and G.M. Card. 2014. "A Spike-Timing Mechanism for Action Selection." *Nat Neurosci* 17: 962–970.

Ward S. 1973 "Chemotaxis in the nematode *Caenorhabditis elegans*: identification of attractants and analysis of the response by use of mutants". *Proc Natl Acad Sci USA* 70 (3): 817–21.

Wehner, R., and M. Müller. 2006. "The Significance of Direct Sunlight and Polarized Skylight in the Ant's Celestial System of Navigation". *Proc Natl Acad Sci USA* 103: 12575–79.

Williams, F.X. (1942). *Ampulex compressa* (Fabr.), a cockroach-hunting wasp introduced from New Caledonia into Hawaii. Proc Haw Ent Soc *11*, 221–233.

Winter, S.S., B.J. Clark, and J.S. Taube. 2015. "Disruption of the head direction cell network impairs the parahippocampal grid cell signal". *Science* 347: 870 – 874.

Wittlinger, M., R. Wehner, and H. Wolf. 2006. "The Ant Odometer: Stepping on Stilts and Stumps". *Science* 312: 1965–67.

Yang, C.-H., S. Rumpf, Y. Xiang, M.D. Gordon, W. Song, L.Y. Jan, and Y.-N. Jan. 2009. “Control of the Postmating Behavioral Switch in *Drosophila* Females by Internal Sensory Neurons” *Neuron* 61: 519–526.

Yoganarasimha, D. and James J. Knierim. 2005. “Coupling Between Place Cells and Head Direction Cells During Relative Translations and Rotations of Distal Landmarks” *Exp Brain Res* 160: 344–359.

Zhang K. 1996. “Representation of Spatial Orientation by the Intrinsic Dynamics of the Head-Direction Cell Ensemble: a Theory”. *J Neurosci* 16: 2112–26.

Zhou, C., Y. Rao, and Y. Rao. 2008. “A Subset of Octopaminergic Neurons are Important for *Drosophila* Aggression” *Nat Neurosci* 11: 1059–67.